Extended semiclassical approximations for systems with mixed phase-space dynamics

Dissertation

zur Erlangung des Doktorgrades
der Naturwissenschaften (Dr. rer. nat.)
der Naturwissenschaftlichen Fakultät II – Physik
der Universität Regensburg

vorgelegt von
Jörg Kaidel
aus Bad Kissingen

Dezember 2003

Die Arbeit wurde von Prof. Dr. Matthias Brack angeleitet.
Das Promotionsgesuch wurde am 23. Dezember 2003 eingereicht.
Das Promotionskolloquium fand am 28. Januar 2004 statt.

Prüfungsausschuss:

Vorsitzender:	Prof. Dr. Dieter Weiss
1. Gutachter:	Prof. Dr. Matthias Brack
2. Gutachter:	Prof. Dr. Klaus Richter
Weiterer Prüfer:	Prof. Dr. Milena Grifoni

"So in the limiting case in which Planck's constant $\hbar$ goes to zero, the correct quantum-mechanical laws can be summarized by simply saying: Forget about all these probability amplitudes. The particle does go on a special path, namely, that one for which S does not vary in the first approximation."

(R. P. Feynman)

Contents

Chapter 1

Introduction

Every approximation to quantum mechanics belongs to one of the following three categories: perturbation theory, variational principles, and semiclassical approaches [Ber 72]. Any of those approximative methods yields good results only if special circumstances are given, but cannot be applied in general. For the quantities which are of interest perturbation theory yields power series in a variable which indicates the variation of the given problem from an exactly solvable case. Variational methods yield the best estimate from a given class of trial functions. Semiclassical approximations work well in the limit in which the reduced Planck's constant $\hbar$ is small compared to the action functions of the corresponding classical problem. Furthermore it is characteristic of a semiclassical approximation that one is able to use information about the classical system in order to make predictions about the corresponding quantum-mechanical one.

In the framework of his model of the atom, N. Bohr in 1913 introduced the first semiclassical approximation which later was extended to the so-called Bohr-Sommerfeld rule. It represents a full quantization of a system's energies which is solely based on the interpretation of the classical action integrals of periodic orbits as integer multiples of $\hbar$. Later this quantization procedure was extended by the works of A. Einstein [Ein 17], M. Brillouin [Bri 26] and J. B. Keller [Kel 58] to the so-called *EBK quantization* in order to take into account zero point energies. However in the above work by A. Einstein it was emphasized that the theory can only be applied to classically integrable systems and not to systems with irregular trajectories which are today called *chaotic*. This problem as well as the invention of wave mechanics by E. Schrödinger, W. Heisenberg et al. were the two main reasons why semiclassical methods were more and more forgotten. Today this first phase in the development of quantum mechanics is often called "Old quantum theory".

In 1971 M. Gutzwiller, influenced by the studies of van Vleck, Dirac and Feynman on the path integral formalism, realized that in the semiclassical limit quantum mechanics is constrained to classical trajectories. The famous result he obtained is called the *Gutzwiller trace formula* which approximates the quantum-mechanical density of states by quantities related to classical periodic orbits [Gut 71]. In other words this means that one can predict, at least approximately, a fully quantum-mechanical property just using classical mechanics and without solving any Schrödinger equation whatsoever. Gutzwiller's work represented the starting point of a

renewed interest in semiclassical methods which lasts until today.

One reason for it is that exact calculations of quantum spectra are difficult to perform for systems with more than two interacting particles. If one is interested in large systems like quantum dots, metal clusters or highly excited atoms the usage of semiclassical methods in connection with a mean-field approximation is often very economic and at the same time accurate enough to reproduce qualitative features [Bra 03, Gut 90].

However the main reason why semiclassical approximations have gained interest in the last decades is due to the fact that together with the theory of random matrices [Meh 91] it represents the most successful theoretical approach to what is called *quantum chaos*. The goal of this kind of research is to find out whether the sensitive dependence of classical trajectories on their initial conditions (*chaos*) has a counterpart in the quantum world or at least influences the results of quantum calculations [Ric 01].

Full semiclassical quantizations can be performed for integrable systems using the EBK quantization and for fully chaotic systems using Selberg's trace formula which can be derived from the Gutzwiller trace formula [Cvi]. However, integrable and completely chaotic systems represent exceptions and typically dynamical systems possess regular as well as chaotic regions in phase space. Therefore those kind of systems are called *soft-chaotic* or *mixed*. For such systems the appearance and vanishing of periodic trajectories in dependence of external system parameters is characteristic. It turns out that exactly at those transitions Gutzwiller's trace formula diverges. This is the reason why the semiclassical description of mixed systems still remains an unsolved problem today. It represents the main topic of this work.

In chapter two the standard semiclassical approximations to the quantum level density are derived. In the case of integrable systems the main result is the so-called Berry-Tabor formula while for general systems it is the famous trace formula by Gutzwiller. It will be shown that both results rely on the so-called *stationary-phase approximation* which is an asymptotic approximation of an exact integral. Section 2.1 is written in more detail in order to introduce terminologies which are necessary for the understanding of the following chapters. Finally it will be explained that due to the stationary-phase approximation the standard semiclassical formulae diverge at periodic-orbit bifurcations, which seriously restricts the validity of the semiclassical standard formalism in the case of mixed as well as integrable systems.

In the third chapter it is shown how to improve the stationary-phase approximation in the vicinity of a periodic-orbit bifurcation by going to higher orders in the phase functions of the semiclassical trace integrals. The resulting generalized action functions are called *Birkhoff normal forms*. They depend on the type of the occurring bifurcation and can be classified according to catastrophe theory. It will be explained that the situations become more complicated if bifurcations lie very close and that therefore new normal forms have to be constructed.

In chapter four it is described how the normal forms can be used to overcome the divergence problem near periodic-orbit bifurcations. So-called *uniform approximations* will be derived which correspond to interpolations between the vicinity of bifurcations and the asymptotic region far away from it, where the standard semiclassical formulae hold. Uniform approximations constitute the final goal for the

semiclassical description of the density of states. At the end of the chapter uniform approximations for the breaking of global symmetries are introduced using semiclassical perturbation theory.

In the fifth chapter the well-known Hénon-Heiles system is studied. It represents a paradigm of a two-dimensional mixed Hamiltonian system. Its classical dynamics is examined with an emphasis on the bifurcations of the shortest periodic orbits. Afterwards the quantum-mechanical energy spectrum is calculated and semiclassical approximations to the density of states are applied. In particular for the first time the problem is treated as an open system, quantum-mechanically as well as semiclassically. The semiclassical approximations include several types of uniform approximations for bifurcations of codimension one and two. Furthermore a new type of codimension-two uniform approximation is developed, which is necessary to improve the semiclassical result. The agreement between the exact quantum results and the semiclassical approximations turns out to be very good, even in the energy regime where the classical phase space is non-compact.

In chapter six the Hénon-Heiles Hamiltonian is modified in such a way that it becomes separable and therefore integrable. The bifurcation scenarios of the periodic orbits are examined. For the bifurcations a new semiclassical uniform approximation can be constructed in analytical form, corresponding to the separable limit of the newly developed uniform approximation for the non-integrable codimension-two scenario of chapter five. The agreement with the exact quantum calculations again turns out to be very satisfying. Also for this case the spectral distribution will be considered as that of an open system. In the energy range where some classical trajectories can leave the potential, the density of the quantum resonances can be approximated semiclassically using real periodic orbits.

In a similar way as in the preceding chapters, in chapter seven a two-dimensional double-well potential is studied. It represents a closed system which shows bifurcation scenarios to which the newly constructed uniform approximation of chapter five can successfully be applied as well.

After giving a summary and an outlook, the appendix explains several mathematical and technical concepts which were important for this study.

Chapter 2

Standard semiclassical approximations

The spectral densities are approximated in first order of $\hbar$ for classically integrable as well as general systems. The final expressions depend only on quantities related to classical periodic orbits. At the end of the chapter it is explained why their application is seriously restricted in the case of bifurcations of periodic orbits.

2.1 EBK quantization and the formula of Berry and Tabor

One of the quantization rules which have been known before the advent of wave mechanics in the 1930s is called the *torus* or *EBK quantization* of classically integrable systems. It was developed by A. Einstein, M. Brillouin and J. B. Keller and is based on the fact that every trajectory of a classically integrable D-dimensional system with Hamiltonian function H lies on a D-dimensional, torus-shaped manifold of the full $2D$-dimensional phase space. In general a D-dimensional torus has D irreducible loops C_i ($i = 1, ..., D$) which can not be contracted to a single point and which can not be mapped onto each other. For each of these loops one quantizes the corresponding action variable I_i as

$$I_i \equiv \frac{1}{2\pi} \oint_{C_i} \mathbf{p}\, d\mathbf{q} = \hbar \left(n_i + \mu_i/4 \right) \qquad n_i \in \mathbb{N}_0 \quad i = 1, ..., D. \tag{2.1}$$

Here the *Maslov index* μ_i counts the number of conjugate points of the trajectory in configuration space with respect to the loop C_i (for the definition of conjugate points see e.g. section 1.6 of [Gut 90]). In the one-dimensional case it corresponds to the number of turning points $\mu_i = 2$. With the quantization of the energy dependent classical action variables, also the total energy E is quantized implicitly. It can be characterized by D quantum numbers n_i as

$$E = H\left(I_1, I_2, ..., I_D\right) = E_{(n_1, n_2, ..., n_D)}, \tag{2.2}$$

where it was used that for a classically integrable system the Hamiltonian function H depends on the action variables I_i only. In general equation (2.1) represents an

accurate approximation only for large quantum numbers n_i. Now because in an integrable system every classical trajectory ξ going from $\mathbf{r}$ to $\mathbf{r}'$ corresponds to a superposition of the elementary loops C_i in phase space, its action S_ξ in the limit of large quantum numbers n_i follows as

$$\boxed{S_\xi \equiv \int_{\mathbf{r}}^{\mathbf{r}'} \mathbf{p}\, d\mathbf{q} \gg \hbar.} \tag{2.3}$$

This relation which is not only given for integrable systems is generally called the *semiclassical limit*. It indicates the transition regime between classical and quantum physics.

The spectral density or density of states of a discrete quantum-mechanical energy spectrum $\{E_n\}$ is defined as

$$g(E) \equiv \sum_n \delta(E - E_n) \qquad n \in \mathbb{N}_0, \tag{2.4}$$

so that with (2.2) one can write in the case of a two-dimensional EBK spectrum:

$$g(E) = \sum_{n_1=0} \sum_{n_2=0} \delta(E - E_{n_1,n_2}). \tag{2.5}$$

Applying the *Poisson identity* [Tic 48]

$$\sum_{n=0}^{\infty} f(n) = \sum_{M=-\infty}^{\infty} \int_0^\infty f(n)\ \exp(2\pi i M n)\, dn + \frac{f(0)}{2}, \qquad M \in \mathbb{N}_0 \tag{2.6}$$

results in

$$\begin{aligned} g(E) \;=\; & \sum_{M_1,M_2=-\infty}^{\infty} \int_0^\infty dn_1 \int_0^\infty dn_2\ \delta(E - E(n_1,n_2))\ \exp(2\pi i (M_1 n_1 + M_2 n_2)) \\ & + \frac{1}{2} \sum_{M=-\infty}^{\infty} \int_0^\infty dn_1\ \delta(E - E(n_1,0)) \exp[2\pi i M n_1] \\ & + \frac{1}{2} \sum_{M=-\infty}^{\infty} \int_0^\infty dn_2\ \delta(E - E(0,n_2)) \exp[2\pi i M n_2] + \frac{\delta(E)}{4} \end{aligned} \tag{2.7}$$

with $M_1, M_2 \in \mathbb{N}_0$. The first term of (2.7) is called the *topological sum* over the two-dimensional grid points (M_1,M_2). Using (2.1) this term can be rewritten as

$$\begin{aligned} g^{(2)}(E) = \frac{1}{\hbar^2} \sum_{M_1=-\infty}^{\infty} \sum_{M_2=-\infty}^{\infty} & \exp\left[-i(M_1\mu_1 + M_2\mu_2)\frac{\pi}{2}\right] \\ & \times \int_{\hbar\mu_1/4}^\infty dI_1 \int_{\hbar\mu_2/4}^\infty dI_2\ \delta(E - H(I_1,I_2))\ e^{\frac{2\pi i}{\hbar}(M_1 I_1 + M_2 I_2)}. \end{aligned} \tag{2.8}$$

In (2.8) only the combination $M_1 = M_2 = 0$ gives a non-oscillatory function which, in leading order of $\hbar$, can be written as

$$\tilde{g}^{(2)}(E) = \frac{1}{(2\pi\hbar)^2} \int_0^\infty dI_1 \int_0^\infty dI_2 \int_0^{2\pi} d\phi_1 \int_0^{2\pi} d\phi_2\ \delta(E - H(I_1,I_2)). \tag{2.9}$$

It is called the *Thomas-Fermi term* which corresponds to a semiclassical approximation of the smooth average part $\tilde{g}(E)$ of the density of states. As can be seen from (2.9) it is calculated by a division of the whole energetically allowed phase-space volume by h^D. The separation

$$\boxed{g\left(E\right) = \tilde{g}\left(E\right) + \delta g\left(E\right)} \tag{2.10}$$

of the full density of states into a smooth part $\tilde{g}(E)$ and an oscillatory part $\delta g(E)$ is generally given, even for non-integrable systems [Bra 03].
Using

$$\delta\left(E - H\left(I_1, I_2\right)\right) = \frac{1}{2\pi\hbar}\int_{-\infty}^{\infty} \exp\left[i\tau\left(E - H\left(I_1, I_2\right)\right)/\hbar\right] d\tau \tag{2.11}$$

the oscillating part of the topological sum can be written as

$$\delta g^{(2)}\left(E\right) = \frac{1}{2\pi\hbar^2} \sum_{\substack{M_1, M_2 \\ (M_1, M_2) \neq (0,0)}} \exp\left(-i\mathbf{M}\cdot\mu\frac{\pi}{2}\right) \times \frac{1}{\hbar}\int_{-\infty}^{\infty} d\tau \int_{\hbar\mu_1/4}^{\infty} dI_1 \int_{\hbar\mu_2/4}^{\infty} dI_2 \; e^{\frac{i}{\hbar}\left[2\pi\mathbf{M}\cdot\mathbf{I} + \tau\left(E - H\left(I_1, I_2\right)\right)\right]} \tag{2.12}$$

where the vectors $\mathbf{M} \equiv (M_1, M_2)$, $\mathbf{I} \equiv (I_1, I_2)$ and $\mu \equiv (\mu_1, \mu_2)$ were introduced. The integrals over the action variables I_1 and I_2 can now be calculated in *stationary-phase approximation*. For this one defines the phase function

$$\Phi_{\mathbf{M}}\left(I_1, I_2, \tau\right) \equiv \left(2\pi\mathbf{M}\cdot\mathbf{I} + \tau\left(E - H\left(I_1, I_2\right)\right)\right) \tag{2.13}$$

and assumes that in the semiclassical limit $\Phi_{\mathbf{M}}/\hbar$ varies very strongly in I_1 and I_2 and that therefore only the stationary points of $\Phi_{\mathbf{M}}$ contribute essentially to the integrals over I_1 and I_2, respectively. Thus one replaces $\Phi_{\mathbf{M}}$ by its expansion in I_1 and I_2 up to second order around the stationary points. The remaining integrals are of Fresnel type and can be solved analytically using

$$\int_{-\infty}^{\infty} e^{iaq^2}\, dq = \sqrt{\frac{\pi}{|a|}}\; e^{i\,\mathrm{sign}(a)\,\pi/4}. \tag{2.14}$$

The stationary points $\tilde{I}_i$ of Φ_M are implicitly given by the formula

$$2\pi M_i = \tau\omega_i\left(\tilde{I}_1, \tilde{I}_2\right), \quad \text{where} \quad \omega_i \equiv \frac{\partial H\left(I_1, I_2\right)}{\partial I_i} \quad (i = 1, 2)\,. \tag{2.15}$$

Equivalently one can write

$$M_1 : M_2 = \omega_1 : \omega_2 \tag{2.16}$$

which means that only tori with commensurate frequencies ω_i play a role. The trajectories on tori with commensurate frequencies are always periodic, which causes

the final formula, the so-called *Berry-Tabor formula*, to be given by quantities which are related to periodic orbits only:

$$\begin{aligned}\delta g^{(2)}(E) \;\approx\; & \frac{1}{2\hbar^2} \sum_{\substack{M_1,M_2 \\ (M_1,M_2)\neq(0,0)}} \exp\left(-i\mathbf{M}\cdot\mu\frac{\pi}{2}\right) \exp\left(-i\frac{\pi}{4}\left(N_+ - N_-\right)\right) \\ & \times \int_{-\infty}^{\infty} \frac{1}{\tau\left|\kappa\right|^{1/2}}\, e^{\frac{i}{\hbar}\left[2\pi\mathbf{M}\cdot\check{\mathbf{I}}+\tau\left(E-H\left(\check{I}_1,\check{I}_2\right)\right)\right]}\, d\tau.\end{aligned} \tag{2.17}$$

Here κ is given by

$$\kappa(E,\tau) = \det\left(\frac{\partial^2 H}{\partial I_i \partial I_j}\right)_{\check{I}_1,\check{I}_2} \tag{2.18}$$

and N_+ and N_- indicate the number of positive and negative eigenvalues of the matrix of second derivatives appearing in (2.18) respectively. The expression (2.17) often represents a good approximation of the oscillating part $\delta g(E)$. The single sums in (2.7) give corrections in higher order of $\hbar$ and are thus often neglected. The remaining δ-function in (2.7) contributes only to the first integral of the density of states for spectra with energies $E > 0$ [Bra 03].

In the case of superintegrable systems with extra dynamical symmetries, like the harmonic oscillator, (2.17) cannot be applied due to the vanishing of κ.

2.2 Gutzwiller's trace formula

In an autonomous quantum system with a discrete energy spectrum $\{E_n\}$, the density of states (2.4) can be expressed by the Green function $G(\mathbf{r}', \mathbf{r}, E)$ as

$$g(E) = -\frac{1}{\pi}\,\Im m \int d\mathbf{r}'\, d\mathbf{r}\, \delta(\mathbf{r}' - \mathbf{r})\; G(\mathbf{r}', \mathbf{r}; E)\,. \tag{2.19}$$

The Green function corresponds to the probability amplitude of a particle with energy E to propagate from $\mathbf{r}$ to $\mathbf{r}'$. For the case of a two-dimensional system it can be approximated in the semiclassical limit (2.3) as [Gut 90]

$$G_{scl}(\mathbf{r}', \mathbf{r}; E) = \frac{1}{i\hbar\sqrt{2\pi i\hbar}} \sum_{\xi} \sqrt{|D_\xi|}\, \exp\left\{\frac{i}{\hbar} S_\xi(\mathbf{r}', \mathbf{r}; E) - i\frac{\pi}{2}\hat{\nu}_\xi\right\}. \tag{2.20}$$

The sum runs over all classical paths ξ from $\mathbf{r}$ to $\mathbf{r}'$ at energy E. D_ξ is the determinant of the matrix of second derivatives of the action S_ξ along the trajectory:

$$D_\xi(\mathbf{r}', \mathbf{r}; E) = \det\begin{pmatrix} \frac{\partial^2 S_\xi}{\partial \mathbf{r}'\partial \mathbf{r}} & \frac{\partial^2 S_\xi}{\partial \mathbf{r}'\partial E} \\ \frac{\partial^2 S_\xi}{\partial E\partial \mathbf{r}} & \frac{\partial^2 S_\xi}{\partial E^2} \end{pmatrix}. \tag{2.21}$$

The Morse index $\hat{\nu}_\xi$ counts the number of conjugate points along ξ. These are the points of the trajectory where one of the eigenvalues of the matrix in (2.21) becomes

zero and ξ touches a caustic in configuration space.
Using (2.19) the semiclassical approximation of the density of states can be written as

$$g_{scl}(E) = -\frac{1}{\pi}\,\Im m \int d^2r'\, d^2r\; \delta(\mathbf{r}' - \mathbf{r})\;\; G_{scl}(\mathbf{r}', \mathbf{r}; E)\,. \tag{2.22}$$

One recognizes that due to the calculation of the trace one has $\mathbf{r}' = \mathbf{r}$ so that only closed classical trajectories contribute. For the integration in (2.22) over the configuration space in the vicinity of ξ one goes over to a local coordinate system whose coordinate s goes along ξ while q lies perpendicular to ξ as sketched in figure 2.1.

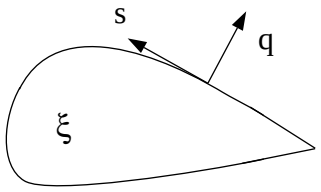

Figure 2.1: *Local coordinate system in the vicinity of a closed (not periodic) orbit ξ in coordinate space.*

Substituting in (2.22) the δ-function with respect to q by

$$\delta(q' - q) = \frac{1}{2\pi\hbar}\int_{-\infty}^{\infty} dp_q\; e^{\frac{i}{\hbar}p_q(q-q')} \tag{2.23}$$

and evaluating the integral over s' for an orbit ξ of length l_ξ at $s' = s + l_\xi$ the contribution of one orbit ξ to (2.22) becomes

$$\delta g_\xi(E) = -\frac{1}{\pi\hbar}\,\Im m\,\frac{1}{(2\pi i\hbar)^{3/2}}\int ds\; dq\; dq'\; dp_q\sqrt{|D_\xi|}$$
$$\times\,\exp\left\{\frac{i}{\hbar}S_\xi(s', q', s, q, E) + \frac{i}{\hbar}p_q(q - q') - i\frac{\pi}{2}\hat{\nu}_\xi\right\}\Bigg|_{s'=s+l_\xi}. \tag{2.24}$$

The integral over q can now be evaluated in stationary-phase approximation in the way it was described in section 2.1. One obtains

$$\delta g_\xi(E) = \frac{1}{2\pi^2\hbar^2}\,\Re e\;\int ds\; dq'\; dp_q\;\sqrt{\left|\widetilde{D}_\xi\right|}$$
$$\times\,\exp\left\{\frac{i}{\hbar}\tilde{S}_\xi(s', q', s, p_q, E) - \frac{i}{\hbar}q'p_q - i\frac{\pi}{2}\tilde{\nu}_\xi\right\}\Bigg|_{s'=s+l_\xi}. \tag{2.25}$$

Here $\tilde{S}_\xi$ is the Legendre transform of S_ξ

$$\tilde{S}_\xi(s', q', s, p_q, E) = S_\xi(s', q', s, q, E) + qp_q, \tag{2.26}$$

with the coordinate q evaluated at the stationary point which obeys

$$\frac{\partial S_\xi}{\partial q} + p_q = 0. \tag{2.27}$$

The determinant $\widetilde{D}_\xi$ keeps its form of (2.21) where here now $\mathbf{r}' = (s', q')$ and $\mathbf{r} = (s, p_q)$ have to be used [Sie 96]. After applying two more stationary-phase approximations for the integrals over q' and p_q the remaining s-integral gives an expression which is proportional to the time of one traversal of ξ [Gut 90, Bra 03]. Furthermore the stationary point in q' obeys

$$\frac{\partial S_\xi}{\partial q'} - p_q = 0. \tag{2.28}$$

Together with (2.27) this yields

$$\frac{\partial S_\xi}{\partial q'} + \frac{\partial S_\xi}{\partial q} = p_q' - p_q = 0. \tag{2.29}$$

Thus every contributing orbit ξ must obey $\mathbf{r} = \mathbf{r}'$ as well as $\mathbf{p} = \mathbf{p}'$ which means that the orbits ξ have to be periodic. The final result for the approximation of the trace integral (2.22) is the famous *Gutzwiller Trace Formula*, which in two dimensions takes the following form

$$\boxed{\delta g_{scl}(E) = \frac{1}{\pi\hbar} \sum_\xi \frac{T_\xi}{r_\xi \sqrt{\left|\mathrm{Tr}\widetilde{M}_\xi - 2\right|}} \cos\left(\frac{S_\xi}{\hbar} - \frac{\pi}{2}\nu_\xi\right).} \tag{2.30}$$

As is the case for a typical semiclassical approximation, in (2.30) only classical quantities play a role even though $\delta g_{scl}(E)$ is quantum-mechanical. The classical periodic orbits ξ appear, with the r_ξ-th repetition of a primitive orbit counted as own orbit. Furthermore one needs the orbit periods T_ξ and the actions S_ξ of the orbits. They can easily be calculated along with the numerical integration of the orbits. The phase correction ν_ξ is called *Maslov index*. It is related to the Morse index $\hat{\nu}_\xi$ of (2.20) and represents a topological constant which is not depending on the starting point on the periodic orbit. It is not the same quantity as the index μ_i appearing in (2.1) even though it carries the same name [Bra 03]. For the calculation of the Maslov index see appendix A. The matrix $\widetilde{M}_\xi$ is called *stability matrix*. It corresponds to the nontrivial part of the monodromy matrix M_ξ which in linear approximation describes the relation between initial variations $\delta\xi$ from the orbit ξ and the final variations $\Delta\xi$ after one orbital period T_ξ:

$$\Delta\xi = M_\xi \ \delta\xi. \tag{2.31}$$

While solving the Hamiltonian equations of motion, one additionally solves the following differential equation

$$\dot{X}(t) = J \ H''|_{\xi(t)} \ X(t) \tag{2.32}$$

with

$$J = \begin{pmatrix} 0 & I_{2\times2} \\ -I_{2\times2} & 0 \end{pmatrix} \qquad H'' = \frac{\partial^2 H(\xi)}{\partial\xi^\dagger \partial\xi} \qquad X(0) = I_{4\times4}. \tag{2.33}$$

The monodromy matrix is then the matrizant $X(t)$ evaluated after one period T_ξ. It can always be transformed into the following form

$$M_\xi = \begin{pmatrix} \begin{pmatrix} 1 & * \\ 0 & 1 \end{pmatrix} & * \\ 0 & \widetilde{M}_\xi \end{pmatrix}, \tag{2.34}$$

where $*$ stands for arbitrary entries [Eke 90]. One can now recognize the relation between the monodromy matrix M_ξ and the stability matrix $\widetilde{M}_\xi$ which appears in Gutzwiller's trace formula (2.30).

In two-dimensional Hamiltonian systems the eigenvalues of $\widetilde{M}_\xi$ always appear in pairs λ and λ^{-1} independent of the initial variation $\delta\xi$, so that $\mathrm{Tr}\widetilde{M}_\xi$ is uniquely determined independent of the starting point on the orbit ξ. The value of $\mathrm{Tr}\widetilde{M}_\xi$ indicates the stability of a periodic orbit:

- A periodic orbit is stable, if $\left|\mathrm{Tr}\widetilde{M}_\xi\right| < 2$
- A periodic orbit is unstable, if $\left|\mathrm{Tr}\widetilde{M}_\xi\right| > 2$.

The value $\mathrm{Tr}\widetilde{M}_\xi = 2$ represents a special case. Exactly in this case the trace formula (2.30) yields non-physical divergences, which will be the main subject of the following chapters.

While orbit period and action multiply for higher repetitions r of a primitive orbit, the stability trace obeys:

$$\mathrm{Tr}\widetilde{M}^r_\xi = 2 \cdot \mathrm{T_r}\left(\frac{\mathrm{Tr}\widetilde{M}^1_\xi}{2}\right), \tag{2.35}$$

where T_r is the Chebyshev polynomial with index r. The Maslov indices for higher repetitions can be calculated as in appendix A. Their changes due to bifurcations can always be uniquely predicted from the normal form of the bifurcation as will be explained in section 4.1.

In general Gutzwiller's trace formula does not converge to a reasonable function or to the exact density of states. In fact the evaluation of (2.30) diverges in the usual case if applied to physical systems. Furthermore the calculation of all periodic orbits and related quantities represents a difficult task especially in the case of chaotic systems where the number of periodic orbits increases exponentially with the system energy. Therefore if one is not interested in a full semiclassical quantization one can determine the *coarse-grained level density*

$$g_\gamma(E) = \frac{1}{\gamma\sqrt{\pi}} \sum_i \exp\left\{-\left[(E - E_i)/\gamma\right]^2\right\} \tag{2.36}$$

which results from a Gaussian convolution of the full density of states (2.4) over an energy range γ which should be smaller than the average level spacing. The coarse-grained level density (2.36) is very often enough to determine a system's gross-shell

effects which are e.g. responsible for the stability of finite fermion systems and for their deformation properties. The same convolution leading to (2.36) can also be applied to (2.30) and results in [Bra 03]

$$\delta g_{scl}(E) = \frac{1}{\pi\hbar} \sum_{\xi} \frac{T_\xi \cdot \exp\left\{-\left(\gamma T_\xi/2\hbar\right)^2\right\}}{r_\xi \sqrt{\left|\mathrm{Tr}\widetilde{M}_\xi - 2\right|}} \cos\left(\frac{S_\xi}{\hbar} - \frac{\pi}{2}\nu_\xi\right) \tag{2.37}$$

after evaluation of the convolution integral in stationary-phase approximation. In (2.37) the new exponential factor forces the periodic orbit sum to converge by letting the periodic orbits with large orbit periods contribute less than the ones with shorter periods.

2.3 Failure of Gutzwiller's trace formula

As explained in the previous section, Gutzwiller's trace formula is based on two approximations: the semiclassical approximation (2.20) of the Green function as well as the stationary-phase approximations of the trace integral (2.25) in the coordinates q, q' and p_q. The latter ones fail if not only the first derivative but at least also the second derivative vanishes at the stationary points because for the stationary-phase approximation the second derivatives appear in the denominator as can be seen from equation (2.14). Therefore in the case of stationary points with vanishing second derivative the trace formula diverges. In general this problem appears if the stationary points come so close that a parabolic description of the phase function is not enough. One says that the periodic orbits belonging to those kind of stationary points cannot be considered as *isolated* anymore. Periodic orbits are isolated and the stationary-phase approximation certainly works, if the classical actions of the periodic orbits differ by a large multiple of $\hbar$. The range of validity of the stationary-phase approximation is difficult to estimate, though, so that it can happen that in special cases it works very well even if the actions of the periodic orbits participating in the bifurcation differ just by a small multiple of $\hbar$. In figure 2.2 (lower row) one can see two stationary points in q which lie very close to each other for a certain external parameter, so that $S_\xi(q;E)$ can not be approximated parabolically any longer. The local Poincaré surface of section (right parts in figure 2.2) shows two fixed points which are lying very close to each other. The fixed points in the Poincaré surface of section correspond to the periodic orbits (PO's) as well as to the stationary points in $S_\xi(q;E)$. The phenomenon at which periodic orbits approach each other and finally fall together is called a *bifurcation* and in figure 2.2 this is sketched schematically for the case of a tangent bifurcation. In two-dimensional systems a bifurcation occurs if the stability matrix $\widetilde{M}_\xi$ of a primitive periodic orbit ξ obeys the following condition:

$$\mathrm{Tr}\widetilde{M}_\xi = e^{i2\pi\frac{n}{r}} + e^{-i2\pi\frac{n}{r}} = 2\cos(2\pi n/r) \tag{2.38}$$

with positive integers r and n. The stability matrix of the r-th repetition of this orbit then takes on the value $+2$ so that its contribution to (2.30) diverges.

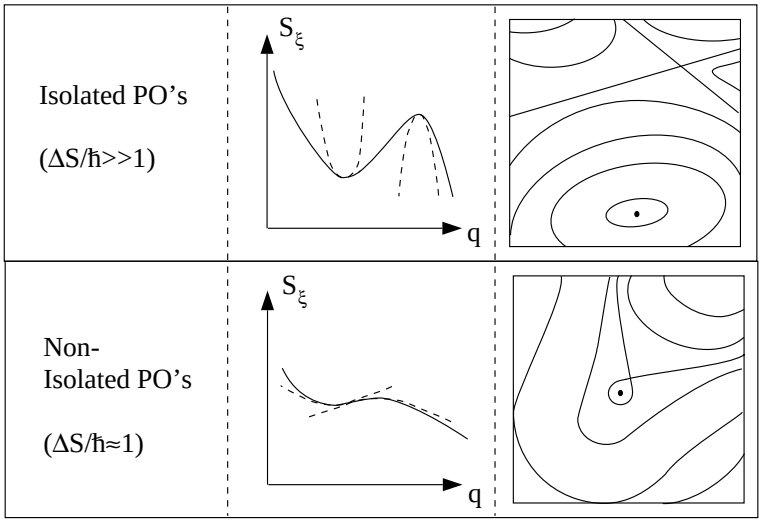

Figure 2.2: *Failure of the stationary-phase approximation for the example of a tangent bifurcation. Top: the function $S_\xi(q;E)$ can well be approximated by parabolas at the stationary points. The corresponding Poincaré surface of section shows an unstable and a stable fixed point far away from each other (right part). Bottom: the function $S_\xi(q;E)$ should be approximated at least by a cubic polynomial. The local Poincaré surface of section shows the fixed points lying very close to each other.*

For integrable systems Gutzwiller's trace formula always fails because in this case a majority of the periodic orbits appears in families which are connected by continuous symmetries. This means that the action S_ξ of the periodic orbits within the family stays constant under these symmetry operations so that the orbits can not be isolated. Consequently the trace of the stability matrix of a periodic orbit of a family always takes on the value $\mathrm{Tr}\widetilde{M}_\xi = +2$, so that the application of Gutzwiller's trace formula is not possible and one has to use the formula of Berry and Tabor (2.17) instead. Due to the energy dependence of the frequencies ω_i it can happen, though, that the system's energy is too small to support all the modes described in (2.15). In this case at a certain value of the system's energy a new family of periodic orbits can be generated out of a single periodic orbit. Exactly at such a bifurcation the contribution of the single periodic orbit to the Gutzwiller formula diverges. Thus the formula of Berry and Tabor should also be improved in order to take into account such scenarios. The methods which can be used to solve these divergence problems will be the topic of the following chapters.

Chapter 3

Normal Forms

The general behaviour of a two-dimensional Hamiltonian dynamical system is examined in the vicinity of periodic-orbit bifurcations. It turns out that near bifurcations the Hamiltonian function can locally be approximated on a Poincaré surface of section by the Birkhoff normal forms, which can be classified by catastrophe theory. From the normal forms of the Hamiltonian a normal form for the generating function of the Poincaré map can be derived. It represents the generalized higher order "action function" which is necessary to extend Gutzwiller's trace formula. Using the normal forms it is then possible to predict the dependence on external parameters for quantities which are related to the bifurcating periodic orbits.

3.1 The Birkhoff normal forms

If the Hamiltonian function of a two-dimensional system is expressed in the local coordinate system (q, s) of section 2.2 (see figure 2.1) as

$$H\left(p_s, p_q, s, q\right) = E \tag{3.1}$$

and if it can be solved for $F \equiv -p_s$ then the motion can always be described in a reduced system in which the coordinate s represents the time variable [Arn 78]:

$$\frac{dq}{ds} = \frac{\partial F}{\partial p_q} \qquad \frac{dp_q}{ds} = -\frac{\partial F}{\partial q} \qquad \frac{dF}{ds} = \frac{\partial F}{\partial s}. \tag{3.2}$$

As a consequence, in the vicinity of a periodic orbit the two-dimensional Hamiltonian system is reduced to a one-dimensional system with periodic s-dependence [Sie 96].

For a further simplification one might be tempted to use a method which goes back to Lindstedt and Poincaré saying that the nonlinear terms of the Hamiltonian flow vector field of a dynamical system can successively be eliminated by polynomial canonical transformations [Ozo 88]. However it is easy to show that this is only possible as long as none of the eigenvalues μ_j of the linearized vector field obeys a resonance condition of the form

$$\mu_j = \sum_{i=1}^{N} m_i \mu_i \tag{3.3}$$

with $m_i \in \mathbb{Z}$ and $i, j \in \{1, ..., N\}$. The order k of the resonance is defined as

$$k \equiv \sum_i m_i. \tag{3.4}$$

Due to the symplectic structure of the phase space of a Hamiltonian system the eigenvalues of the linearized vector field always appear in pairs μ and $-\mu$. One can now recognize with

$$1 \cdot \mu + 2 \cdot (-\mu) = -\mu, \tag{3.5}$$

that in the case of Hamiltonian systems one always finds a third order resonance for every pair of eigenvalues $(\mu, -\mu)$. Therefore, in general, Hamiltonian systems cannot be linearized using polynomial canonical transformations. The same is true for the system (3.2) because it is equivalent to a two-dimensional autonomous Hamiltonian system.

The best one can do is to approximate the Hamiltonian function F up to the first resonant term in q and p_q in a Taylor expansion as well as in a Fourier expansion in the time s in the vicinity of a periodic orbit with orbit period T_s. Instead of performing this expansion in the full coordinate system one uses the periodicity in time and derives the expansion on the Poincaré surface of section with the periodic orbit in the center corresponding to a fixed point of the Poincaré map. The region very close to a stable periodic orbit can then be transformed to the system

$$F\left(q, p_q, s\right) = F_0 + \frac{\omega}{2}\left(q^2 + p_q^2\right) \tag{3.6}$$

by a T_s-periodic linear transformation [Sie 98a]. Here F_0 is a constant and ω is given by $\omega = \alpha/T_s$ with α being the *stability angle* of the central periodic orbit. One can see that the Hamiltonian equations of motion of the system (3.6) describe the linearized motion of the full system stroboscopically after intervals T_s. In the following a parametrization is used for which s goes from 0 to 2π.

Without any loss of generality the calculations can be continued for the case of a stable periodic orbit only [Ozo 88]. The full Taylor-Fourier expansion describing the vicinity of the periodic orbit can be written as

$$F = \frac{\omega}{2}\left(q^2 + p_q^2\right) + \sum_{k+l=3}^{\infty} \sum_{n=-\infty}^{\infty} F_{kln}\, q^k\, p_q^l\, e^{ins} \tag{3.7}$$

with real coefficients F_{kln}. Using complex coordinates

$$z \equiv p_q + iq \qquad z^* \equiv p_q - iq \tag{3.8}$$

it follows

$$q = \frac{1}{2i}\left(z - z^*\right) \quad p_q = \frac{1}{2}\left(z + z^*\right) \tag{3.9}$$

so that the Hamiltonian can be expressed as

$$-2iF\left(p\left(z, z^*\right), q\left(z, z^*\right), t\right) = -i\omega z z^* + \sum_{k+l=3}^{\infty} \sum_{n=-\infty}^{\infty} f_{kln}\, z^k\, z^{*l}\, e^{ins} \tag{3.10}$$

where now the expansion coefficients f_{kln} are real or imaginary.

As mentioned earlier it is not possible to remove all nonlinear terms in (3.10) by polynomial canonical transformations. Nevertheless one can canonically transform it onto coordinates (v, v^*) in which all non-diagonal terms, i.e. all terms where v and v^* appear with different exponents, are eliminated up to the highest possible order. This form will then be called *Birkhoff normal form*. The generating function for the transformation

$$(z, z^*) \to (v, v^*) \tag{3.11}$$

is chosen as

$$S(v, z^*, s) = vz^* + \sum_{k+l=3}^{\infty} \sum_{n=-\infty}^{\infty} S_{kln} v^k z^{*l} \, e^{ins} \tag{3.12}$$

with complex coefficients S_{kln}. The equations which belong to (3.12) are given by (e.g. see [Jel 87])

$$z = \frac{\partial S}{\partial z^*} \qquad v^* = \frac{\partial S}{\partial v} \qquad -2i\tilde{F}(v, v^*, s) = -2iF(z(v, v^*), z^*(v, v^*), s) + \frac{\partial S}{\partial s}. \tag{3.13}$$

With this transformation the Hamiltonian turns into (see the calculations on p. 80 of [Ozo 88])

$$-2i\tilde{F}(v, v^*, s) = -i\omega v v^* + \sum_{k+l=3}^{\infty} \sum_{n=-\infty}^{\infty} \left(f_{kln} + \left[-i\omega(l-k) + in\right] S_{kln}\right) v^k v^{*l} e^{ins}. \tag{3.14}$$

By choosing now the coefficients S_{kln} of the generating function as

$$S_{kln} = \frac{-if_{kln}}{\omega(l-k) - n} \tag{3.15}$$

all terms with (k, l, n) of the Hamiltonian (3.14) can be eliminated except the diagonal ones with

$$l = k \quad \text{and} \quad n = 0. \tag{3.16}$$

The terms that remain yield the Birkhoff normal form

$$-2i\tilde{F} = -i\omega v v^* + f_2 (vv^*)^2 + f_3 (vv^*)^3 + \dots, \tag{3.17}$$

where the definition $f_i \equiv f_{ii0}$ with $i = 2, 3, \dots$ was used. The Hamiltonian has now a simple form depending only on powers of the product vv^*.
This simple Hamiltonian is only possible, though, if ω does not meet the resonance frequency

$$\omega = \frac{n}{m}, \quad m = l - k \tag{3.18}$$

in which a bifurcation occurs. Exactly at the bifurcation the normal form transformation blows up so that one has to use the *resonant normal form*

$$-2i\tilde{F} = -i\omega vv^* + f_2\left(vv^*\right)^2 + f_3\left(vv^*\right)^3 + ... + f_{m0n}v^m e^{ins} + f_{0m,-n}v^{*m}e^{-ins} \tag{3.19}$$

instead. Here the elimination procedure is performed up to the order $m = l - k$ at which the leading order resonant term appears. It corresponds to the most important resonant term near the bifurcation.
Finally applying the time-dependent canonical transformation

$$\xi = v\, e^{i\frac{n}{m}s} \quad \xi^* = v^*\, e^{-i\frac{n}{m}s} \tag{3.20}$$

with the generating function

$$\sigma\left(v, \xi^*, s\right) = v\xi^* \exp\left(ins/m\right) \tag{3.21}$$

transforms the Hamiltonian into a rotating coordinate system (the meaning of this transformation will become clearer below). Using now (3.13) for σ yields the time-independent form

$$-2i\tilde{F} = -i\epsilon\xi\xi^* + f_2\left(\xi\xi^*\right)^2 + f_3\left(\xi\xi^*\right)^3 + ... + 2i\,\Im m\left(f_{m0n}\xi^m\right) \tag{3.22}$$

where it was used that

$$f_{0m,-n} = -f^*_{m0n} \tag{3.23}$$

for $\tilde{F}$ to be real. This can be found by setting the real parts of the resonant terms in (3.19) equal to zero. The distance to the bifurcation appears in front of the first term as

$$\epsilon \equiv \omega\left(E\right) - n/m. \tag{3.24}$$

In order to obtain a real valued normal form one uses real polar coordinates (ϕ, I) on the Poincaré surface of section defined by

$$\xi = \sqrt{2I}e^{i\phi} \qquad \xi^* = \sqrt{2I}e^{-i\phi} \tag{3.25}$$

and obtains the resonant normal form in its most common form:

$$\boxed{\tilde{F}^{(m)}\left(I, \phi\right) = \epsilon I + c_2 I^2 + ... + aI^{m/2}\sin\left(m\phi\right).} \tag{3.26}$$

All coefficients (except ϵ) that appear in (3.26) are real constants depending on the bifurcation which is studied. The controlling parameter E is contained in ϵ by (3.24). Exactly at the bifurcation one has $\epsilon = 0$. The polar coordinates are related to the Cartesian coordinates on the Poincaré surface of section by

$$q = \sqrt{2I}\sin\left(\phi\right) \qquad p_q = \sqrt{2I}\cos\left(\phi\right). \tag{3.27}$$

These are not the same Cartesian coordinates as in (3.7) but they do not differ fundamentally so that the same notation is kept.

For a better understanding of what has been derived so far, figure 3.1 (left part) shows a schematic picture of the vicinity of a stable periodic orbit in phase space. It is always surrounded by thin tori corresponding to invariant circles of the normal form or Poincaré surface of section. If the frequency of one of those invariant circles very close to the central orbit becomes $\dot{\phi} = n/m$ the orbits on this torus are periodic and close after m steps of the Poincaré map.

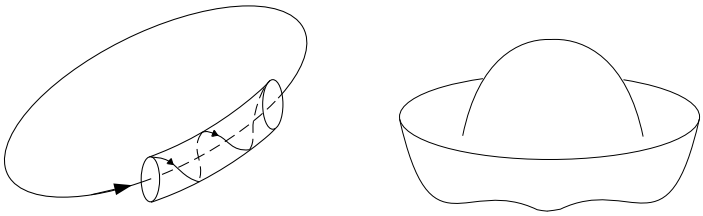

Figure 3.1: *Schematic pictures for the understanding of the normal forms. Left: thin torus surrounding a stable periodic orbit. Right: Mexican hat shape of the 3D plot of the normal forms. The relative extrema which appear at the rim correspond to the stationary points or equivalently to the periodic orbits.*

Exactly at a bifurcation the frequency $\omega(E)$ takes on the value n/m, the normal form transformation blows up and the angle-dependent resonant term has to be included. This results in the destruction of the torus in complete analogy to classical perturbation theory.
Now going back to (3.19), Hamilton's equations in polar coordinates yield

$$\dot{\phi}(I) = \omega + 2c_2 I + ... \tag{3.28}$$

Replacing n/m on the l.h.s and using (3.24) yields the action variable $I_{n/m}$ of the periodic torus as

$$I_{n/m} = -\frac{\epsilon}{2c_2} + O\left(\epsilon^2\right). \tag{3.29}$$

Now the meaning of the transformation (3.20) and (3.21) becomes clear. It took the system to rotating coordinates in which the periodic torus (3.29) corresponds to a circle of fixed points. This can be seen by calculating the derivative with respect to I for the first two terms in (3.26).

At $\epsilon = 0$ the torus and the central orbit coalesce, so that one can imagine the whole scenario as a torus which is destroyed immediately after its creation. The right part of figure 3.1 shows a three-dimensional plot of the normal form. One can see the central relative extremum which corresponds to the central stable periodic orbit as well as the surrounding rim which represents the torus. By the ϕ-dependent term in (3.26) it is broken into several extrema which correspond to the newly created periodic orbits.

For every Hamiltonian $F^{(m)}(I, \phi)$ one has a corresponding generating function for the Poincaré map between the successive Poincaré sections:

$$\hat{S}^{(m)}(I, \phi', E) = S_0(E) + I\phi' - F^{(m)}(I, \phi'), \tag{3.30}$$

where $S_0(E)$ is the action of the central periodic orbit. This can be seen e.g. by iteratively integrating the equations of motion for I and ϕ using $F^{(m)}(I,\phi)$ up to the relevant order in I [Sch 97a]. The coefficients of $F^{(m)}(I,\phi)$ in (3.30) are not the same as the ones in (3.26) but they are simply related. The generating function $\hat{S}^{(m)}(I,\phi',E)$ is now the extension of (2.26). It generates the Poincaré map

$$I' = \frac{\partial \hat{S}}{\partial \phi'} \qquad \phi = \frac{\partial \hat{S}}{\partial I} \qquad T = \frac{\partial \hat{S}}{\partial E} \tag{3.31}$$

from initial coordinates (ϕ, I) to final coordinates (ϕ', I') on the Poincaré surface of section.

The bifurcation scenario which is described by $\hat{S}^{(m)}(I,\phi',E)$ depends on the number of angle-independent terms which are included together with the ϵ-dependent and ϕ-dependent (resonant) term. As will be explained more carefully in the next section, the periodic orbits which are participating in the bifurcation are related to the fixed points of (3.31). Thus the more terms are included in the normal form the more relative extrema exist and the more periodic orbits are described.

The bifurcations which occur at $\epsilon = 0$ independently of other additional bifurcations are called *generic* bifurcations of *codimension* one. They usually occur if only one external, controlling parameter is varied which is then contained in ϵ. In (3.26) this parameter is the energy E. The m-fold symmetric function $\hat{S}^{(m)}(I,\phi',E)$ describes the bifurcation of the central orbit with an orbit of period m. The case $m = 1$ corresponds to an isochronous bifurcation, $m = 2$ describes a period-doubling etc.. All generic bifurcations of codimension one were classified in [Mey 70, Bru 70, Bru]. As an example of a bifurcation of codimension one, figure 3.2 shows the essential equipotential lines (contour plots) of the normal form of a period-doubling bifurcation. The corresponding normal form can be simplified in Cartesian coordinates yielding [Sch 97a]

$$\hat{S}^{(2)}(q',p,E) = S_0(E) + q'p - \frac{\sigma}{2}p^2 - \epsilon q'^2 - aq'^4, \tag{3.32}$$

where σ can take on the values ± 1 depending on the bifurcation which is studied. The fact that one does not have to include higher order terms in p and that the whole scenario occurs on the q-axis is a result of the splitting lemma of catastrophe theory [Pos 78]. The contour plots in figure 3.2 correspond to smooth simplified pictures of the local Poincaré surface of section near a period-doubling bifurcation possessing the same topology and the same qualitative behaviour on the controlling parameter. Furthermore the parameter a as well as the sign factor σ determine the order in which the period-doubling bifurcation occurs in dependence of ϵ (e.g. either the central orbit bifurcates into a new orbit with twice the orbit period or the longer orbit vanishes by coalescing with the central orbit).

All periodic orbits which participate in the bifurcation except the central one are called *satellite* orbits. In the case of (3.32) the satellite orbits are real only on one side of the bifurcation (the "real" side). On the other ("complex") side only the central orbit is real while the satellites correspond to so-called complex *ghost* orbits. They represent the complex continuations of the real satellites to the complex side and can be calculated using the recipes described in appendix B.

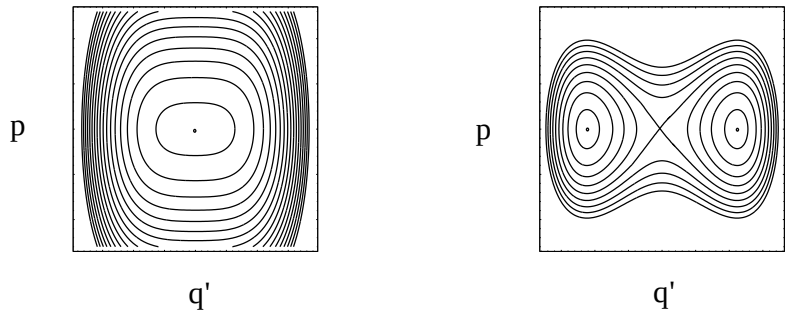

Figure 3.2: *Contour plots of the codimension-one normal form* $\hat{S}^{(2)}(q', p, E)$ *with* $\sigma = -1$. *Left:* $\epsilon < 0$. *Right:* $\epsilon > 0$.

If higher order terms of the expansion are included in the normal forms one obtains so-called "extended normal forms" which describe more than just one generic bifurcation. In fact it turns out that the next stage corresponds to the bifurcations of codimension two. They occur as sequences of two generic bifurcations of codimension one where one of them must be isochronous. It is possible to contract the bifurcations to one bifurcation which occurs for one special choice in a two-dimensional parameter space [Sch 98]. In figure 3.3 the codimension-two bifurcation sequence of an isochronous and a period-tripling bifurcation is shown. The corresponding normal form of this case is given by

$$\hat{S}^{(3)}(I, \phi') = I\phi' + S_0(E) - \epsilon I - bI^2 - aI^{\frac{3}{2}} \cos(3\phi'). \tag{3.33}$$

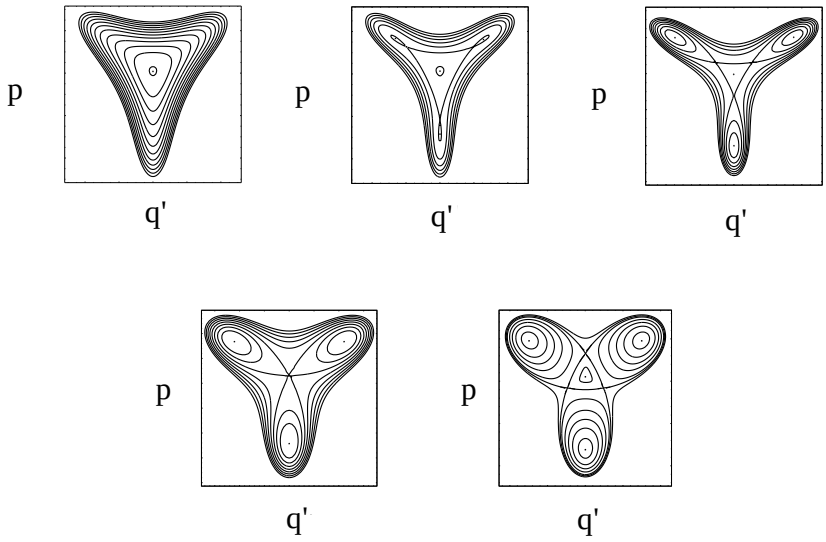

Figure 3.3: *Normal Form* $\hat{S}^{(3)}(I, \phi')$ *of codimension two describing the sequence of an isochronous and a period-tripling bifurcation.*

3.2 Properties of the satellite orbits

With the normal forms it is now possible to predict the classical quantities related to the satellite orbits participating in the bifurcation (or the bifurcation sequences) in dependence of the external parameter (which here is the energy E):
The periodic orbits correspond to the fixed points of the generating function of the Poincaré map (3.31) and are thus determined by the following equations

$$I = \frac{\partial \hat{S}}{\partial \phi'} \qquad \phi' = \frac{\partial \hat{S}}{\partial I} \tag{3.34}$$

while in Cartesian coordinates one obtains

$$p = \frac{\partial \hat{S}}{\partial q'} \qquad q' = \frac{\partial \hat{S}}{\partial p}. \tag{3.35}$$

If the generating function (3.30) is now used in (3.34) or a simplified Cartesian form like (3.32) in (3.35), then one always finds (at least) m fixed points corresponding to a new satellite orbit. Its orbital period is thus m times the period of the central orbit. Only in Cartesian coordinates also the central orbit can be obtained as fixed point.

The generating function $\hat{S}(q', p, E)$ is related to the action integral $S(q', q, E)$ by a Legendre transformation, so that the action of a periodic orbit is given by the value of

$$S(q', q, E) = \hat{S}(q', p, E) - q'p \tag{3.36}$$

or in spherical coordinates of

$$S(q'(I, \phi'), q(I, \phi'), E) = \hat{S}(I, \phi', E) - I\phi', \tag{3.37}$$

for the considered periodic orbit. Thus evaluating (3.36) or (3.37) at the fixed points of (3.35) or (3.34) respectively yields the classical action of the corresponding periodic orbits.

The relation between the period T of a periodic orbit and its classical action is given by

$$T = \frac{\partial S}{\partial E}, \tag{3.38}$$

so that one immediately obtains the orbital periods by evaluating (3.38) at the fixed points.

From the definition of the stability matrix it becomes obvious that it must somehow be related to the second derivatives of the generating function $\hat{S}(q', p, E)$. In fact in Cartesian coordinates one obtains [Sch 97a]

$$\mathrm{Tr}\widetilde{M} = \left(\frac{\partial^2 \hat{S}}{\partial p \partial q'}\right)^{-1} \left(1 + \left(\frac{\partial^2 \hat{S}}{\partial p \partial q'}\right)^2 - \frac{\partial^2 \hat{S}}{\partial p^2}\frac{\partial^2 \hat{S}}{\partial q'^2}\right), \tag{3.39}$$

which again has to be evaluated at the fixed points.

The Maslov indices of the periodic orbits can also be predicted from $\hat{S}(q', p, E)$ as will be explained in section 4.1.

3.3 Remarks on normal forms

- Bifurcation theory is strongly related to catastrophe theory which was introduced by R. Thom [Tho 75, Pos 78]. For example the codimension of a catastrophe gives the dimension of a Lagrangian manifold minus the dimension of the singular sub-manifold of the catastrophe. Thus for a so-called fold catastrophe the codimension is one while for a cusp it is two. The "unfolding" of the fold catastrophe is given by the nontrivial part of the normal form of the isochronous bifurcation. Therefore this bifurcation must be of codimension one. Similar correspondences can be done for other bifurcation types.

- The Birkhoff normal forms can also be used for systems which are not general in the sense that they possess a finite number of discrete symmetries. If this is the case it can happen that on the Poincaré surface of section one finds bifurcation scenarios which look like period-m bifurcations even though they are isochronous. Due to an m-fold symmetry of the system the bifurcation creates a new orbit with an m-fold degeneracy. The equivalence between those non-generic cases and the generic ones was established in [The 99].

- In mixed systems the bifurcation scenarios are often more complicated than the cases given by the Birkhoff normal forms of codimension one or two mentioned above. Increasing the codimension in systems with discrete symmetries can give rise to many highly involved bifurcation scenarios. For example it is possible to encounter sequences of non-generic pitchfork bifurcations which can repeat themselves infinitely often such that they are subsequently created out of a single central periodic orbit and accumulate at one value of the controlling parameter [Bra 01]. For such more delicate situations the current state of the normal form theory is by far not developed enough, meaning that for such cases new types of normal forms have to be constructed.

Chapter 4

Uniform semiclassical approximations

Here the general recipe of how to calculate approximations which uniformly interpolate between the vicinity of periodic orbit bifurcations and the asymptotic Gutzwiller regime is explained. For some of the codimension-one bifurcations there are analytical expressions while for bifurcations of codimension two the necessary integrals must be worked out numerically. Finally it is shown how to derive uniform approximations for symmetry breakings.

4.1 Uniform approximations for bifurcation scenarios of periodic orbits

Instead of evaluating (2.25) using stationary-phase approximations one now replaces the phase function by the normal form of the generating function (3.30):

$$\tilde{S}_\xi\left(s', q', s, p_q, E\right) - q'p \to \hat{S}_\xi\left(s', \phi', s, I, E\right)\big|_{s'=s+l_\xi} - I\phi'. \tag{4.1}$$

Replacing $\hat{S}_\xi$ from (3.30) on the r.h.s one tries to evaluate the integrals exactly. The angle ϕ is only given modulo 2π which must result in a quantization of I. Due to the form $I = \left(p_q^2 + q^2\right)/2$ its spectrum must be the one of the harmonic oscillator $I_n = \hbar\left(n + 1/2\right)$ with $n \in \mathbb{N}_0$.

In [Ber 77] it was shown that in the semiclassical limit one can restrict ϕ to the interval $[0, 2\pi]$ while replacing the integrations over I by

$$\int dI \to \hbar \sum_{I_n} \tag{4.2}$$

where I_n are the quantized values of I. This way one obtains

$$\delta g\left(E\right) \approx \frac{\hbar}{2\pi^2\hbar^2}\,\Re e\int_0^{\frac{l_\xi}{m}} ds \int_0^{2\pi} d\phi' \sum_{n=0}^{\infty} \sqrt{\left|\widehat{D}_\xi\right|}\exp\left\{\frac{i}{\hbar}\hat{S}\left(I_n, \phi', E\right) - \frac{i}{\hbar}I_n\phi' - i\frac{\pi}{2}\nu\right\}. \tag{4.3}$$

The determinant in (4.3) can be reduced to [Lit 90]

$$\widehat{D}_\xi = \det \begin{pmatrix} \frac{\partial^2 \hat{S}_\xi}{\partial s' \partial s} & \frac{\partial^2 \hat{S}_\xi}{\partial s' \partial I} & \frac{\partial^2 \hat{S}_\xi}{\partial s' \partial E} \\ \frac{\partial^2 \hat{S}_\xi}{\partial \phi' \partial s} & \frac{\partial^2 \hat{S}_\xi}{\partial \phi' \partial I} & \frac{\partial^2 \hat{S}_\xi}{\partial \phi' \partial E} \\ \frac{\partial^2 \hat{S}_\xi}{\partial E \partial s} & \frac{\partial^2 \hat{S}_\xi}{\partial E \partial I} & \frac{\partial^2 \hat{S}_\xi}{\partial E^2} \end{pmatrix} = \frac{1}{\dot{s}' \dot{s}} \frac{\partial^2 S}{\partial \phi' \partial I}. \tag{4.4}$$

With $\dot{s} = \dot{s}'$ it follows for a periodic orbit

$$\int_0^{l_\xi/m} ds \, \frac{1}{\sqrt{\dot{s}' \dot{s}}} = \frac{1}{m} \frac{\partial \hat{S}}{\partial E} = \frac{T(\phi', I, E)}{m}, \tag{4.5}$$

where T is the time from s to s' along the orbit. Finally one applies the Poisson summation formula (2.6) to the sum over n which leads to [Sie 96]

$$\boxed{\delta g(E) \approx \frac{1}{2\pi^2 \hbar^2} \, \Re e \sum_{L=-\infty}^{\infty} \int_0^{2\pi} d\phi' \int_0^{\infty} dI \, \Psi(\phi', I) \, e^{\frac{i}{\hbar}\Phi(\phi', I) - \frac{i\pi}{2}\nu - 2\pi i \left(\frac{I}{\hbar} - \frac{1}{2}\right) L}.} \tag{4.6}$$

with

$$\Psi(\phi', I) = \frac{1}{m} \frac{\partial \hat{S}}{\partial E} \left| \frac{\partial^2 S}{\partial I \partial \phi'} \right|^{1/2} \quad \text{and} \quad \Phi(\phi', I) = \frac{i}{\hbar} \hat{S}(I, \phi', E) - \frac{i}{\hbar} I \phi'. \tag{4.7}$$

This is the trace integral in normal form coordinates which represents the semiclassical contribution to the density of states of an arbitrary region on the Poincaré plane described by the phase function $\Phi(\phi', I)$. One can see that in comparison to (2.25) the origin is no stationary point any longer. Its Gutzwiller contribution can be calculated by summing the edge corrections of the I-integration for $I = 0$ over L. The stationary points which correspond to the satellite orbits are included in the term $L = 0$. All other contributions with $L \neq 0$ have no stationary point near the origin and contribute semiclassically only with a boundary contribution.

An approximation of the integral (4.6) which was introduced by Ozorio de Almeida consists in including higher terms only in the phase function $\Phi(\phi', I)$ but setting the Jacobian in the amplitude function $\Psi(\phi', I)$ equal to unity [Ozo 87, Ozo 88]. In the limit $\epsilon \to 0$ the prefactor then tends towards the orbit period T_0 of the central, primitive orbit evaluated at the bifurcation $\epsilon = 0$. In this way one obtains (with $L = 0$)

$$\delta g(E) \approx \frac{T_0}{2\pi^2 \hbar^2} \Re e \int_0^{2\pi} d\phi' \int_0^{\infty} dI \, e^{\frac{i}{\hbar}\Phi(\phi', I) - i\frac{\pi}{2}\nu}. \tag{4.8}$$

This approximation in fact yields finite contributions in the vicinity of a bifurcation. The parameters in $\Phi(\phi', I)$ can be determined uniquely by the numerically determined actions of the periodic orbits together with the relations of their actions in section 3.2 (see eq. (3.36) and (3.37)). The expression (4.8) is very similar to the first order semiclassical perturbation theory by S. Creagh [Cre 96] which says that in first approximation in the trace integration only the action has to be modified due to a perturbation of the system. The similarity between the semiclassical perturbation

theory and the extension of the semiclassical trace formulae using normal forms will show up again in a later section. Approximations of the form (4.8) are called *local approximations*, because they describe $\delta g(E)$ correctly only in the vicinity of a bifurcation. Asymptotically it can not be expected to deliver accurate results, though, because it does not split up into independent periodic orbit contributions.

In order to achieve this one has to extend the normal form expansion to higher terms and treat these terms as perturbation. Using non-canonical coordinate transformations one can then recover the original normal form for the phase while the amplitude function is modified such that it provides enough coefficients to let the integral asymptotically split up into the Gutzwiller contributions [Sch 97c, Sie 98b]. After having derived the amplitude function Ψ, an evaluation of (4.6) in stationary-phase approximation gives the following contributions

$$\delta g^{(SP)}(E) = \frac{1}{\pi\hbar}\frac{\Psi}{\sqrt{|\det\Phi''|}}\,\Re e\,\exp\left(\frac{i}{\hbar}\Phi - i\frac{\pi}{2}\left(\nu - \frac{1}{2}\mathrm{sign}\left(\Phi''\right)\right)\right), \tag{4.9}$$

evaluated at the stationary points. Here the matrix of second derivatives is given by

$$\Phi'' = \begin{pmatrix} \frac{\partial^2\Phi}{\partial q'^2} & \frac{\partial^2\Phi}{\partial q'\partial p} \\ \frac{\partial^2\Phi}{\partial q'\partial p} & \frac{\partial^2\Phi}{\partial p^2} \end{pmatrix} \tag{4.10}$$

and the Maslov index appears as

$$\mu = \nu - \frac{1}{2}\mathrm{sign}\left(\Phi''\right). \tag{4.11}$$

Here $\mathrm{sign}\left(\Phi''\right)$ corresponds to the difference between the number of positive and negative eigenvalues of Φ''. One can see now that also the Maslov indices of the bifurcating periodic orbits as well as their changes can be predicted using normal forms.

For each periodic orbit ξ there exists a contribution of the form (4.9). The idea is now to identify these contributions with the isolated, asymptotic Gutzwiller contributions of (2.30). This immediately leads to the following relations

$$\boxed{\Phi_i = S_\xi, \qquad \frac{\Psi_i}{\sqrt{|\det\Phi_i''|}} = \frac{T_\xi}{\sqrt{\left|\mathrm{Tr}\widetilde{M}_\xi - 2\right|}},} \tag{4.12}$$

where the index i means that the corresponding functions have to be evaluated at the fixed points (the solutions of (3.34) or (3.35)). The parameters of the amplitude function $\Psi(\phi', I)$ are now determined by the Gutzwiller amplitudes. Thus the asymptotic evaluation of (4.6) uniquely fixes its own parameters in the way that it interpolates between the finite local approximation (4.8) and Gutzwiller's trace formula. The resulting expressions are called *uniform approximations*.

For the three types of codimension-one bifurcations with $m \leq 3$ analytical formulae could be derived as final results [Sch 97c]. For the codimension-one bifurcations with $m \geq 4$ only expressions using numerical integrals exist [Sie 98b, Sie 96].

The integrals can be evaluated numerically using series representations or using the method of steepest descent [Sch 97a].
In the case of codimension two the same recipe can be applied. The only difference is that there are more parameters to eliminate due to the larger number of bifurcating orbits. Furthermore the normal forms of the phase and amplitude function are polynomials of higher order for which the integrals (which are often called *diffraction catastrophe integrals*) can not be solved analytically but have to be evaluated numerically.

It has to be emphasized that the uniform approximations are interpolations between the regime near the bifurcation ($\epsilon \to 0$) with a $\hbar^{\alpha}$-dependence ($\alpha > -1$) and the asymptotic limit far away from the bifurcation which corresponds to a $\hbar^{-1}$ dependence. In the transition region one could in principle obtain results which are less accurate. The author has never encountered such a situation and also in this study the transition region could always be approximated so that a comparison to the quantum-mechanical curve could be made.

Furthermore, as is the case in every interpolation between limits, there is some sort of freedom in the way the limits are connected. In the above uniformization this freedom is contained in the choice of the functional form of $\Psi(\phi', I)$. Even though there exist several expressions for the amplitude functions which can be used for the bifurcations [Sie 98b, Sie 96, Sch 98] this does not imply that they are the only choices which yield a good interpolation (reproducing e.g. the leading semiclassical terms). As long as the asymptotic limits are reproduced any reasonable function could in principle be used for $\Psi(\phi', I)$ [Bar 03].

As mentioned in section 3.3 it can occur that one has to introduce new normal forms for the phase function $\Phi(\phi', I)$ itself. For such new forms the above uniformization procedure must then be applicable.

4.2 Uniform approximations for symmetry breakings

The uniformization procedure is slightly modified in cases of a transition from an integrable to a mixed system. It is based on semiclassical perturbation theory which expresses all classical quantities appearing in a trace formula in dependence of the perturbation parameter of the system [Cre 96]. There exist analytical uniform approximations for the $U(1)$-symmetry breaking [Tom 95, Ull 96] and for special cases of the $SU(2)$- and $SO(3)$-symmetry breaking [Bra 99].

Given a Hamiltonian H_0 describing an integrable system whose periodic orbits are degenerate, appearing in orbit families. This system may now be perturbed by a term ϵH_1 with dimensionless $\epsilon \ll 1$ as

$$H = H_0 + \epsilon H_1, \tag{4.13}$$

so that the symmetries of H_0 are broken at least partially. In [Cre 96] it was proven that in first order of ϵ the perturbation of the action of one orbit $\Gamma_g(t)$ of the family Γ is given by

$$\Delta S_{\Gamma}(E) \approx -\epsilon \int_{\Gamma_g(t)} H_1 \, dt. \tag{4.14}$$

The integration over the group measure belonging to the symmetry group of the periodic orbit family yields a so-called *modulation factor*

$$\mathcal{M}_\Gamma\left(\frac{\epsilon}{\hbar}, E\right) = \frac{1}{V_G}\int d\mu\,(g)\;\; e^{i\Delta S_\Gamma(E)/\hbar}, \tag{4.15}$$

where V_G represents the invariant group volume. This factor now multiplies each periodic-orbit term of the trace formula of the unperturbed integrable system. For the calculation of higher-order action shifts one can, in general, no longer neglect the changes of the periodic orbits themselves. The calculation of the modulation factor becomes more tedious but stays straightforward [Cre 96, Kai 00].

For the derivation of a global uniform approximation one has to introduce an amplitude function into the integral of the modulation factor so that asymptotically it splits into the Gutzwiller contributions of the isolated periodic orbits. Furthermore the phase function must be derived up to the order for which the periodic orbit actions emerge from the stationary-phase approximation of the integral. The resulting trace integrals, which often turn out to be very similar to the integrals in the case of bifurcations, have to be worked out exactly. At the end, the parameters appearing in the phase are given by the classical actions of the periodic orbits while the parameters of the amplitude function have to be eliminated using the Gutzwiller amplitudes.

The whole procedure is thus completely analogous to the uniformization procedure in the case of bifurcations with the only difference that the phase function is not a model but exactly derived from semiclassical perturbation theory.

Chapter 5

The system of Hénon and Heiles

In the following chapter the well-known system of Hénon and Heiles is introduced as a model of a continuous classical system with intricate mixed phase-space dynamics. Its periodic orbits are calculated and their bifurcation scenarios which range from single bifurcations of codimension one to infinite bifurcation cascades are studied in detail. After the calculation of the quantum-mechanical spectrum, several types of uniform approximations are used to construct the semiclassical approximation of the density of states. For a situation where the existing formulae fail a new codimension-two uniform approximation is developed.

5.1 Classical mechanics

5.1.1 Classical dynamics

Like the classical three-body problem the system of Hénon and Heiles is known today as a paradigm of a Hamiltonian system with a mixed phase space [Sch 94]. It has been used as a model for various physical systems of different nature [Bra 97, Pom 74, Efs 04]. In fact it belongs to the same class of dynamical systems with two degrees of freedom as the collinear three-body Coulomb problem [Win 92], so that both show similar qualitative features. The Hénon-Heiles system was introduced in 1964 by M. Hénon and C. Heiles in their famous study of the motion of a single star in the potential of a disk-shaped galaxy [Hén 64]. It was argued in the following way:
In the case of an axially symmetric galaxy the gravitational potential can be written in cylindrical coordinates (R, z) as

$$V(R,z) = V_g(R,z) + \frac{L^2}{2R^2}. \tag{5.1}$$

The function $V_g(R,z)$ is arbitrary for the moment and L corresponds to the angular momentum perpendicular to the galactic plane through the center. Due to the axial symmetry, L is a constant of motion. Thus the dynamical system reduces to a two-dimensional one with the Hamiltonian

$$H(p_R, p_z, R, z) = \frac{1}{2}\left(p_R^2 + p_z^2\right) + V(R,z). \tag{5.2}$$

The question which was addressed by Hénon and Heiles was whether (5.2) possesses a further constant of motion besides the conserved total energy E. If this would be the case the system were integrable having two independent constants of motion. The stars would move on regular orbits within the galactic disc. In the opposite case, chaos could exist in the motion of stars.

The model system for (5.2) which was proposed by Hénon and Heiles has a simple polynomial form and can thus be easily studied numerically. At the same time it is completely general which means that non-trivial orbits can exist and that no fundamental differences are created by adding higher order terms. In Cartesian coordinates it has the following form

$$\boxed{H\left(p_x, p_y, x, y\right) = \frac{1}{2}\left(p_x^2 + p_y^2 + x^2 + y^2\right) + x^2 y - y^3/3.} \tag{5.3}$$

System (5.3) corresponds to a two-dimensional, isotropic harmonic oscillator ($m = \omega = 1$) which is perturbed by cubic terms. The symmetry group of the system is $\mathbb{D}_3$ with three reflection axes at the polar angles $\phi = \pi/2$ and $\phi = \pm\pi/6$ as well as rotational symmetries about the angles $2\pi/3$. If a particle has an energy larger than the saddle-point energy $E^* = 1/6$ it can escape over one of the three saddles which are lying on the symmetry axes (in the radial distance one from the origin).

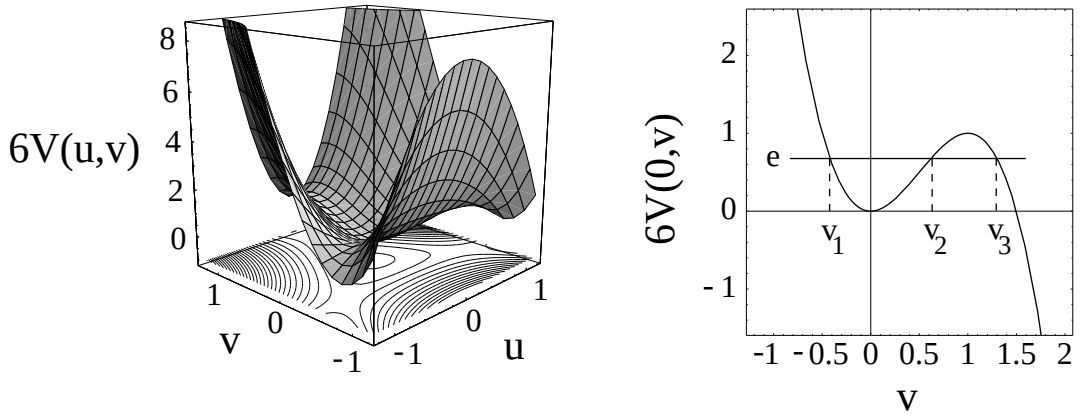

Figure 5.1: The potential of Hénon and Heiles. Left: 3D and contour plot of the potential. Right: cut of the potential along the v-axis.

In order to weight the cubic terms in (5.3) relative to the harmonic oscillator part, one often introduces a perturbation parameter α so that the Hamiltonian becomes

$$H\left(p_x, p_y, x, y\right) = \frac{1}{2}\left(p_x^2 + p_y^2 + x^2 + y^2\right) + \alpha\left(x^2 y - y^3/3\right), \tag{5.4}$$

with the saddle-point energy lying at $E^* = 1/6\alpha^2$. Even though (5.4) now depends on two external parameters E and α, one can transform the Hamiltonian back to the form (5.3) by scaling the coordinates as

$$x \to \frac{u}{\alpha}, \quad y \to \frac{v}{\alpha}. \tag{5.5}$$

The scaled Hamiltonian then reads

$$\widetilde{H}\left(p_u, p_v, u, v\right) = \frac{1}{2}\left(p_u^2 + p_v^2 + u^2 + v^2\right) + u^2 v - v^3/3. \tag{5.6}$$

In the left part of figure 5.1 the potential part of (5.6) is shown while on the right side one can see a cut of the potential along one of the symmetry axes (here along $u = 0$). An additional factor of 6 was introduced in order to fix the saddle-point energy at the value one. Along the v-axis the potential is then given as

$$6V\left(v\right) = 3v^2 - 2v^3, \tag{5.7}$$

with the classical turning points v_1,v_2 and v_3 determined by $6V\left(v_i\right) = e \equiv 6\alpha^2 E$, $i = 1, 2, 3$. The scaled energy $e = 6\alpha^2 E$ remains as the only controlling parameter of the system.

The fact that the phase-space dynamics is mixed possessing regular as well as chaotic regions and that therefore no other constant of motion besides e exists, can be seen from the Poincaré surfaces of section which are shown in figure 5.2 for increasing energy values e. Interestingly, for energies $e > 1$ there still exist small islands of regular motion and within them also periodic motion, as will turn out in the next section.

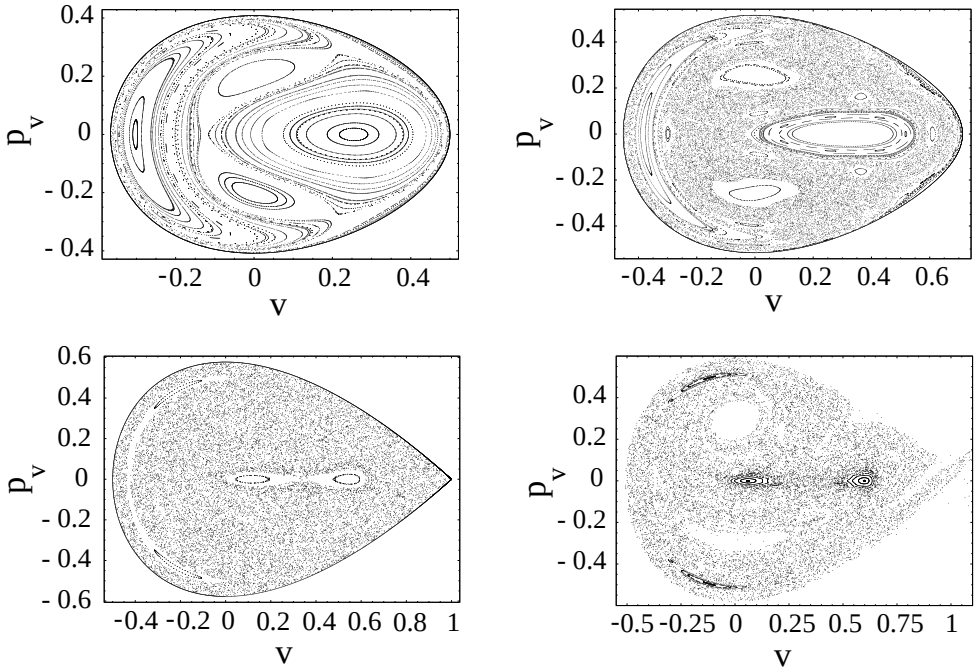

Figure 5.2: *Poincaré sections (with $u = 0$) of (5.6). Top left: $e = 0.5$, top right: $e = 0.8$, bottom left: $e = 1$, bottom right: $e = 1.05$.*

5.1.2 Periodic orbits

The periodic orbits of the system (5.3) were investigated in detail in [Chu 79, Dav 92, Vie 96]. They were calculated in dependence of the energy e using the numerical method described in appendix B. Figure 5.3 gives an overview of all orbit periods up to 5π in an energy range of up to twice the saddle-point energy.

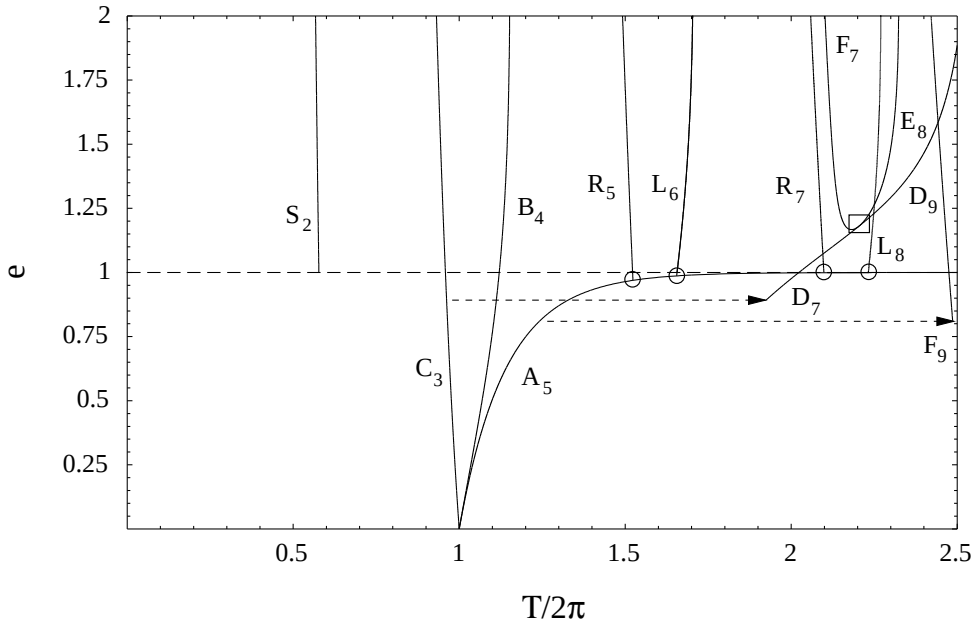

Figure 5.3: *Orbit periods T in dependence of the scaled system energy e. The dashed arrows indicate period-doubling bifurcations while the circles mark isochronous non-generic pitchfork bifurcations. The rectangle at $e \approx 1.179$ and $T \approx 4.4\pi$ frames a codimension-two bifurcation. The indices of the orbits denote the Maslov indices, which are left out in the text.*

Below $e \approx 0.97$ there exist only three types of periodic orbits with periods of the order of 2π. The librations A and B and the rotation C (see figure 5.4). Due to the three-fold symmetry of (5.3), A and B exist in three orientations connected by rotations of $2\pi/3$ and $4\pi/3$. Orbit C is two-fold degenerate because of its two possible opposite senses of rotation.
The action S_A and the period T_A of the orbit A can be calculated analytically due to its one-dimensional motion. One obtains (with v_1, v_2 and v_3 of the preceding section)

$$S_A(e) = 2\int_{v_1}^{v_2} \sqrt{e - 3s^2 + 2s^3}\, ds = \frac{2}{5\alpha^2}\sqrt{6\,(v_3 - v_1)}\,[\mathbf{E}\,(q) + c\mathbf{K}\,(q)] \tag{5.8}$$

and

$$T_A(e) = 2\sqrt{3}\cdot\int_{v_1}^{v_2} \frac{ds}{\sqrt{e - 3s^2 + 2s^3}} = \frac{2\sqrt{6}}{\sqrt{v_3 - v_1}}\mathbf{K}\,(q)\,. \tag{5.9}$$

Here $\mathbf{E}\,(q)$ and $\mathbf{K}\,(q)$ are complete elliptic integrals [Abr 65] with

$$q = \sqrt{\frac{v_2 - v_1}{v_3 - v_1}} \qquad c = -\frac{2}{9}\,(v_3 - v_2)\,(2v_3 - v_2 - v_1)\,. \tag{5.10}$$

The expansion of S_A with respect to the energy e is given by

$$S_A(e) = \frac{\pi e}{3\alpha^2}\left[1 + \frac{5}{12}\left(\frac{e}{6}\right) + \frac{385}{432}\left(\frac{e}{6}\right)^2 + \frac{85085}{31104}\left(\frac{e}{6}\right)^3 + ...\right]. \tag{5.11}$$

Most of the system's other periodic orbits are created at bifurcations of these three orbits A, B and C. In figure 5.3 the bifurcation points at which this occurs are marked with circles as well as dashed arrows. The orbits which are isochronously bifurcating from A are rotations R and librations L. The indices correspond to their Maslov indices. The orbits which participate in period-doubling bifurcations with A are given the letter F. The behaviour at the bifurcation points will be described explicitly in the following sections. The only possibility of creating new periodic orbits out of nothing are tangent bifurcations at which a stable and an unstable orbit are created. Very often they are difficult to find numerically. Except the one at $e = 1.16718$ which belongs to a codimension-two bifurcation at $e = 1.179$ (indicated by the rectangle in figure 5.3) no other tangent bifurcation could be determined numerically or found in the literature up to orbit periods of 5π.

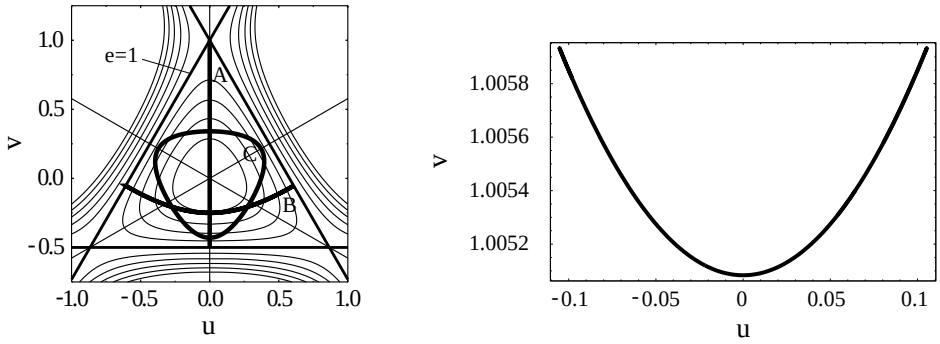

Figure 5.4: *Shortest periodic orbits. Left: contour plot of the potential (including the symmetry axes) together with the periodic orbits A,B and C. Right: one of the librating periodic orbits S at e=1.1.*

At $e = 1$ new librating orbits S appear due to a global bifurcation where the topology of the phase space changes from compact to non-compact. They correspond to oscillations on the three saddles of the potential. In the limit $e \to 1$ their orbital period becomes $2\pi/\sqrt{3}$. The right part of figure 5.4 shows one of the three orbits S evaluated at an energy $e = 1.1$.

5.1.3 A scattering experiment

The fact that the system (5.3) possesses real periodic orbits in the energy range $e > 1$ can be illustrated by the following experiment: Starting at the origin with an arbitrary initial velocity $\mathbf{v}$, a particle will either remain in the potential well for a long time or leave the inner part of the potential by crossing one of the three saddles. If the particle stays in the potential the corresponding position in the two-dimensional space of initial velocities is colored black and otherwise by the color of the corresponding exit channel (see figure 5.5).

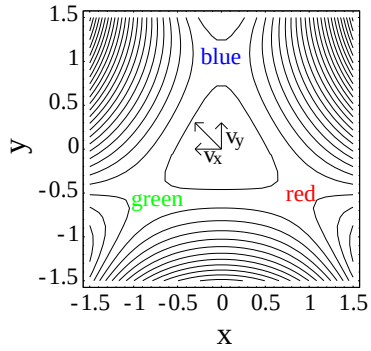

Figure 5.5: *Scattering experiment in the Hénon-Heiles potential (shown here as contour plot). For an energy $e > 1$ the particle starts at the origin with initial velocity $\mathbf{v} = (v_x, v_y)$. If it escapes from the inner part of the potential, the point (v_x, v_y) in velocity space obtains the color of the exit channel. Otherwise it is colored black.*

The result of the experiment uncovers the complexity of the phase-space dynamics of the system. In figure 5.6 the result is shown after having scanned the whole velocity space in small steps in v_x an v_y. One can see that the exit channel over which the particle will escape, strongly depends on the initial velocity. This is characteristic of a chaotic dynamics. The resulting figures have fractal properties reminiscent of the fractal Mandelbrot set with which one could in fact find a conceptual similarity. The right side of figure 5.6 clearly shows that even for energies $e > 1$ trajectories exist which are bound within the potential for a very long time. Their initial velocities correspond to the black points beyond the black disk that corresponds to the bound dynamics for $e \leq 1$. In fact for the periodic orbit D of figure 5.3 the initial velocity lies within this black area (and correspondingly its initial coordinates lie at the origin) for a certain range of $e > 1$. The points on the v_x-axis where this black area becomes thin correspond to bifurcations of higher repetitions of the orbit D [Bra 01b].

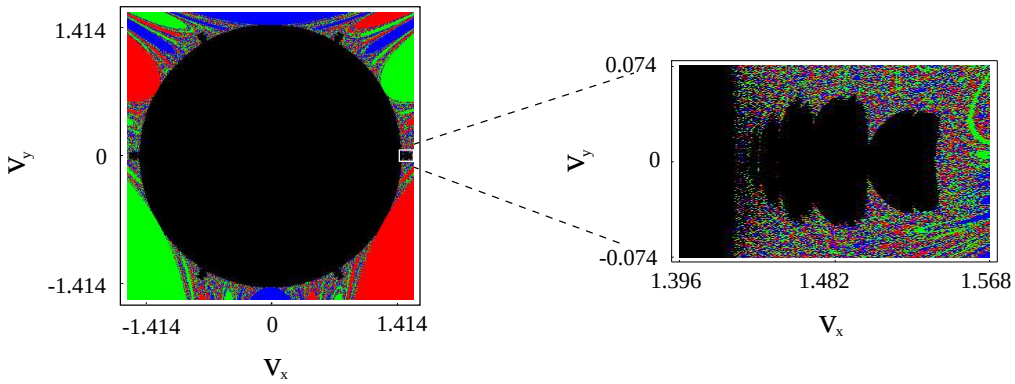

Figure 5.6: *Result of the scattering experiment. Left: scan of the whole velocity space. Right: enlarged fraction of left figure with bound dynamics for $e > 1$.*

5.2 The quantum-mechanical Hénon-Heiles system

5.2.1 Calculation of the quantum spectrum

The quantum-mechanical version of the system of Hénon and Heiles is given by the following Hamiltonian

$$\widehat{H} = -\frac{\hbar^2}{2m}\left(\frac{\partial^2}{\partial x^2} + \frac{\partial^2}{\partial y^2}\right) + \frac{1}{2}m\omega^2\left(x^2+y^2\right) + \alpha\left(x^2 y - \frac{y^3}{3}\right). \tag{5.12}$$

In units with $m = \omega = \hbar = 1$ it reads

$$\widehat{H} = -\frac{1}{2}\left(\frac{\partial^2}{\partial x^2} + \frac{\partial^2}{\partial y^2}\right) + \frac{1}{2}\left(x^2+y^2\right) + \alpha\left(x^2 y - \frac{y^3}{3}\right) \tag{5.13}$$

and in two-dimensional spherical coordinates (r, ϕ) one obtains

$$\widehat{H} = -\frac{1}{2}\left(\frac{\partial^2}{\partial r^2} + \frac{1}{r}\frac{\partial}{\partial r} + \frac{1}{r^2}\frac{\partial^2}{\partial \phi^2}\right) + \frac{r^2}{2} + \alpha\frac{r^3}{3}\sin\left(3\phi\right). \tag{5.14}$$

All states of the system are non-stationary so that according to the complex rotation method of appendix C one may now represent the non-Hermitian operator

$$\widehat{H}\left(\theta\right) = -\frac{1}{2}\left(\frac{\partial^2}{\partial r^2} + \frac{1}{r}\frac{\partial}{\partial r} + \frac{1}{r^2}\frac{\partial^2}{\partial \phi^2}\right)e^{-2i\theta} + \frac{r^2}{2}e^{2i\theta} + \alpha\frac{r^3}{3}\sin\left(3\phi\right)e^{3i\theta} \tag{5.15}$$

in the basis of eigenstates of the two-dimensional harmonic oscillator

$$\psi_{nl}\left(r,\phi\right) = N_{nl}\cdot i^l \cdot r^{|l|}\cdot e^{-il\phi}\cdot L_n^{|l|}\left(\frac{m\omega}{\hbar}r^2\right)\cdot e^{-\frac{m\omega}{2\hbar}r^2}. \tag{5.16}$$

Here the normalization constant is given by

$$N_{nl} = \sqrt{\frac{n!}{\pi\cdot\left(n+|l|\right)!}\cdot\left(\frac{m\omega}{\hbar}\right)^{\left(|l|+1\right)}}. \tag{5.17}$$

The system is not spherically symmetric so that l does not represent a good quantum number. The $\mathbb{D}_3$ symmetry group has three irreducible representations (which means that in principle one could find a special basis in which the Hamiltonian matrix decays into three block matrices). As a consequence only the basis states (5.16) with $\triangle l = \pm 3$ are coupled so that the following symmetry classes of basis states exist

$$\text{I} \;:\; l \in \{\ldots -6,-3,0,3,6,\ldots\} \tag{5.18}$$

$$\text{II} \;:\; l \in \{\ldots -5,-2,1,4,7,\ldots\} \tag{5.19}$$

$$\text{III} \;:\; l \in \{\ldots -4,-1,2,5,8,\ldots\}. \tag{5.20}$$

The Hamiltonian is invariant under time reversal, so that $l \rightarrow -l$. Therefore the classes II and III produce the same spectra. This facilitates the diagonalization, because now it has to be performed only for the basis sets I and II.
Alternatively one can write the scaled Hamiltonian in Cartesian coordinates as

$$\widehat{H}\left(\theta\right) = -\frac{1}{2}\left(\frac{d^2}{dx^2} + \frac{d^2}{dy^2}\right)e^{-2i\theta} + \frac{1}{2}\left(x^2+y^2\right)e^{2i\theta} + \alpha\left(x^2 y - \frac{y^3}{3}\right)e^{3i\theta} \tag{5.21}$$

and represent it in the corresponding harmonic oscillator basis. The matrix elements can then easily be calculated using creation- and annihilation operators (see e.g. [Nol 92]). Even though this does not take into account the symmetries of the system one can nevertheless achieve convergence if one uses the sparse property of the resulting Hamiltonian matrix. This property is given because, besides the diagonal elements, the basis states couple only to other basis states whose quantum numbers differ by a maximum of three units. Therefore it is obviously advantageous to use sparse routines instead of programs which need the whole Hamiltonian matrix. This procedure was performed in all complex cases using the program **matlab**, while for the diagonalizations of the real Hamiltonian it was mainly worked with the basis states (5.16).

Figure 5.7 shows the quantum resonance spectrum for the perturbation parameter $\alpha = 0.1$. It was found to be converged with an accuracy of 6 digits over an interval of about 10 degrees, as is indicated by the example in the inset of figure 5.7. The imaginary parts of the resonant states for $e < 1$ are exponentially small except very near the barrier at $e = 1$. For the states slightly above the barrier a semiclassical prediction of the imaginary parts was given in [Wai 81] which is in good agreement with the numerical results. The non-resonant states were found to behave exactly in the way described in [Yar 78] for a one-dimensional cubic potential. They do not lie on straight lines and some of them even have positive imaginary parts. They can clearly be distinguished from the resonances because they strongly depend on θ. The quasi-regular pattern of the resonance spectrum observed in the region $e > 1$ where some of the resonant states lie on almost parallel "rays" in the complex energy plane, is a reminiscence of the separable system that is obtained if one neglects the coupling term $\alpha x^2 y$. It will be studied in the next chapter.

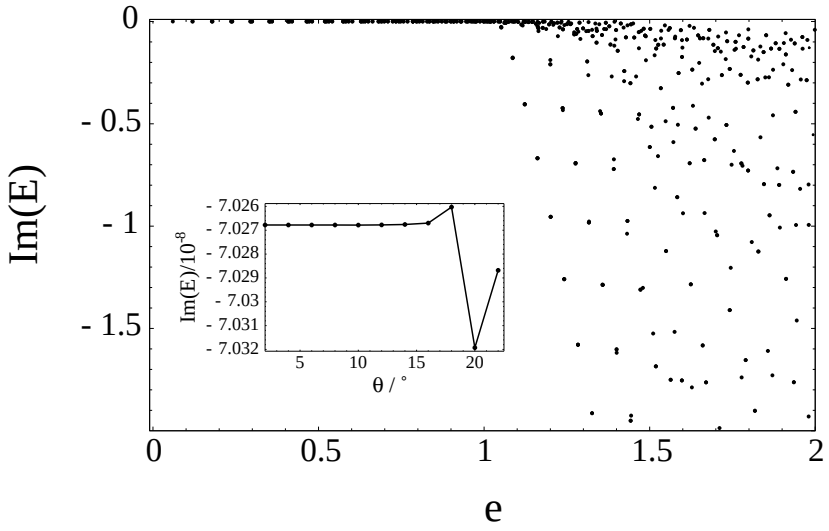

Figure 5.7: *Resonances of the scaled Hénon-Heiles Hamiltonian (5.21) with $\alpha = 0.1$. The inset shows the dependence of the imaginary part of one particular resonance on the rotation angle θ (its real part stays constant at 0.928966 for the whole variation of θ).*

5.2.2 Determination of $\tilde{g}(E)$ and $\delta g(E)$

After having obtained the complex energy spectrum one has to solve the problems of how to derive a density of states and furthermore how to extract its unique smooth average part.

In a given spectrum the resonant states can generally be identified as lines of finite width which are locally given by a Lorentzian-shaped Breit-Wigner distribution. Thus for a discrete spectrum which consists of bound states i and resonant states j the expression

$$g(E) = \sum_i \delta(E - E_i) + \sum_j \frac{1}{\pi} \cdot \frac{\Gamma_j/2}{\left(E - E_j\right)^2 + \frac{\Gamma_j^2}{4}} \tag{5.22}$$

should represent a very good approximation of the spectral density, independent of whether the potential goes to zero asymptotically or not. This can also be seen by considering the difference $\Delta g(E)$ of the total density of states $g_{tot}(E)$ including resonant states and the density of states of the free case $g_{free}(E)$ as [Kai 03b]

$$\begin{aligned} \Delta g(E) &= g_{tot}(E) - g_{free}(E) \\ &= -\frac{1}{\pi} \Im m \sum_m \frac{1}{E - E_m + i\Gamma_m/2} = \frac{1}{\pi} \sum_m \frac{\Gamma_m/2}{\left(E - E_m\right)^2 + \left(\Gamma_m/2\right)^2}. \end{aligned} \tag{5.23}$$

Since the Lorentzians on the r.h.s of (5.23) go over into delta functions for $\Gamma_m \to 0$, the contribution of the bound states is automatically included in (5.23).

As already mentioned in section 2.2 in order to obtain a coarse-grained level density one has to perform a Gaussian convolution of the full density of states. For (5.22) the result can be expressed analytically (using integral 7.4.13 of [Abr 65] for the sum over j) as

$$g_\gamma(E) = \frac{1}{\gamma\sqrt{\pi}} \sum_i e^{-(E-E_i)^2/\gamma^2} + \frac{1}{\gamma\sqrt{\pi}} \sum_j \Re e\left(w(z_j)\right), \tag{5.24}$$

where the function $w(z)$ is the error function with complex argument [Abr 65]

$$w(z) = e^{-z^2} \operatorname{erfc}(-iz) \tag{5.25}$$

and $z_j \equiv \frac{1}{\gamma}\left(E - \left(E_j + i\frac{\Gamma_j}{2}\right)\right)$. The function $w(z)$ is directly given in many mathematical software libraries and algebra programs (e.g. as routine S15DDF of the NAG library). One can see that if the spectrum consists of bound states only, equation (5.24) can be reduced to its first sum because then the Lorentz distributions in (5.22) turn into δ-distributions.

For the determination of the smooth average part $\tilde{g}(E)$ one can apply the Strutinsky averaging method of appendix D. In figure 5.8 the plateau condition which determines the smoothing width $\tilde{\gamma}$ (see appendix D) is tested at $e = 1.5$ for a perturbation parameter $\alpha = 0.1$. Independent of the polynomial orders s, a plateau can be found at $\tilde{\gamma} \approx 2.2$. The quality of the plateau turns out to be dependent on the energy for which it is tested. In figure 5.9 the smoothing value $\tilde{\gamma}_0$, which obeys

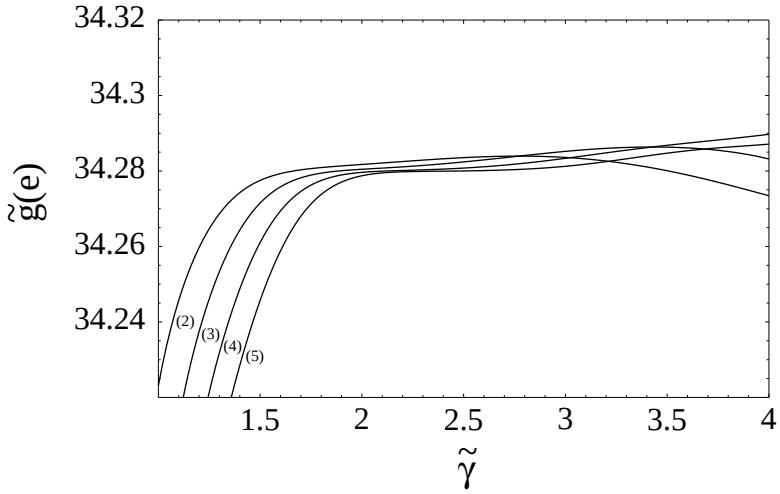

Figure 5.8: *Test of the plateau condition for the Strutinsky average at the energy $e = 1.5$ for $\alpha = 0.1$. The numbers in brackets correspond to the polynomial indices s (see appendix D).*

the plateau condition, is plotted in dependence of e. One can see that in the vicinity of the saddle-point energy $e = 1$ the value of $\tilde{\gamma}_0$ decreases. For energies $e < 0.85$ the plateaux are very pronounced so that choosing a slightly different value than the plotted one does not result in considerable errors. Unfortunately the function $\tilde{g}(E)$ changes very abruptly near the saddle-point energy. The changes are of the order of the variations of the oscillating part so that a clear separation of these two parts is impossible. This becomes evident from figure 5.9 where no plateau can be found near $e = 1$. Even though the obtained data points were fitted by a cubic polynomial there remain considerable discrepancies in this energy range. In the energy region below $e = 1$, it is possible to apply the Strutinsky method only to the real energy spectrum (obtained without the complex scaling method) almost up to the saddle-point energy due to the smallness of the level widths there [Bra 99].

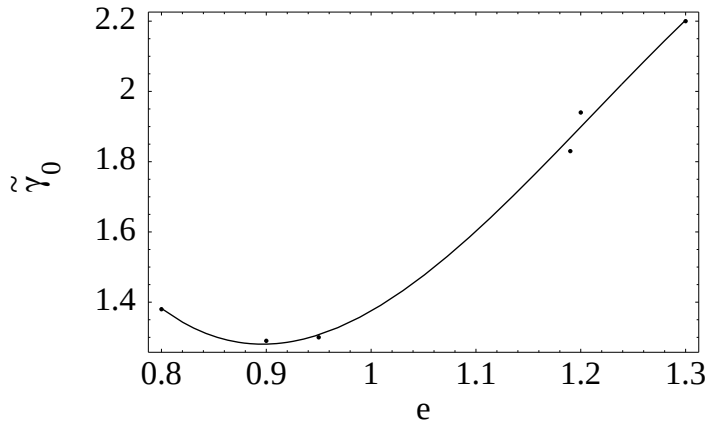

Figure 5.9: *Dependence of $\tilde{\gamma}_0$ on the energy e. The smooth curve corresponds to a cubic polynomial interpolation of the data points.*

Alternatively for energies far below the saddle-point energy, the Thomas-Fermi result of the density of states which in two dimensions [Bra 03] reads

$$\tilde{g}_{TF}(E) = \left(\frac{m}{2\pi\hbar^2}\right) \int d^2r\, \theta\left(E - V\left(\mathbf{r}\right)\right), \tag{5.26}$$

can in the Hénon-Heiles case be simplified to the one-dimensional integral

$$\tilde{g}_{TF}(E) = \left(\frac{m}{\pi\hbar^2}\right) \frac{1}{\alpha} \int_{v_1}^{v_2} \sqrt{\frac{\left(v_1 - v\right)\left(v_2 - v\right)\left(v_3 - v\right)}{v + \frac{1}{2}}}\, dv. \tag{5.27}$$

It can easily be evaluated numerically. Here the v_i with $i = 1, 2, 3$ correspond to the turning points given in section 5.1.1 and $\theta(x)$ is the Heaviside step function. In particular, equation (5.27) can be preferred to the Strutinsky method for small energies because in that regime the latter one does not work accurately due to the energy cut-off at $e = 0$.

5.2.3 Scaled Fourier spectroscopy of $\delta g\left(E\right)$

Gutzwillers's trace formula (2.30) has the form of a Fourier sum over the classical periodic orbits. The Fourier spectrum of the oscillating part $\delta g\left(E\right)$ of the exact quantum-mechanical density of states should therefore be related to the periodic orbits of the corresponding classical system. More precisely, the Fourier spectrum should consist of a discrete set of peaks centered at the classical orbit periods. The number of peaks that appear depends on the value γ used for the coarse-graining of the exact density of states (see section 2.2). For large γ only the shortest orbits contribute and a small number of peaks can be seen. Choosing a small γ increases the resolution of $\delta g\left(E\right)$ and more peaks appear.

As described in 5.1.1 the classical dynamics of the Hénon-Heiles system is governed by the scaled energy $e = \alpha^2 E$, so that this value should be kept fixed while performing the Fourier transform in order to be able to relate the result to a given phase-space structure. This idea of a "constant-scaled-energy-spectroscopy" was first applied successfully to the absorption spectrum of the diamagnetic hydrogen atom for which a complete hierarchy of states could be related to classical closed orbits [Hol 88]. The method has contributed to the renewed interest in semiclassical physics, because it represents an easily obtainable inverse *quantum chaology*. By now it has become one of the standard tools of semiclassical physics and has successfully been applied to various systems [Rao 01, Hüp 95, Ama 01].

In the case of the Hénon-Heiles system one calculates the quantum spectra for a set of perturbation parameters α. The values of fixed scaled energy e correspond to the intersections of the spectrum with a curve given by

$$E = e/\alpha^2. \tag{5.28}$$

Figure 5.10 shows the (real) energy spectrum for the parameters $\alpha \in [0, 0.2]$ as well as the curve corresponding to (5.28) with $e = 0.04$. After having determined the intersection points one can calculate the smooth and oscillating part of their density.

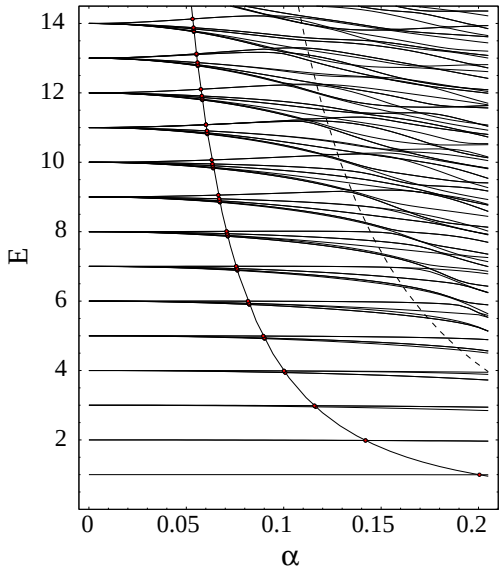

Figure 5.10: *Scaled Fourier spectroscopy of the Hénon-Heiles spectrum. The solid hyperbolic curve is given by (5.28) with* $e = 0.04$*, the dashed curve gives the saddle-point energy* $E^* = 1/6\alpha^2$*.*

The Fourier spectrum then yields information about the periodic orbits which are mainly contributing to $\delta g\,(E)$ for a fixed scaled energy e.
In figure 5.11 one can clearly recognize a pattern of three peaks repeating at multiples of the harmonic oscillator period 2π.

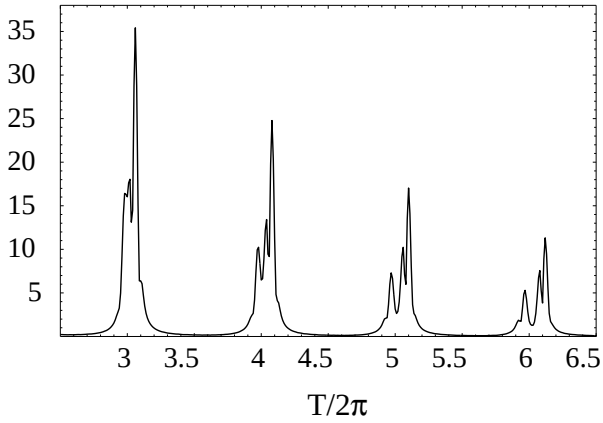

Figure 5.11: *Result of the scaled Fourier transform for* $e = 0.04$*. One can clearly see a structure of three peaks repeating at multiples of* 2π*.*

The averaged peak positions after division of the repetition numbers correspond quite well to the positions determined from the classical numerical integration of the periodic orbits A,B and C for $e = 0.04$, as can be seen from the following table:

PeriodicOrbit	Integration	Fourier
C	0.9877625	0.994332
B	1.0336135	1.010495
A	1.0384698	1.020000

5.3 Semiclassical approximations to the quantum level density

5.3.1 Evaluation of Gutzwiller's trace formula

In section 5.1.2 it was shown that for energies $e < 0.97$ there are three shortest primitive periodic orbits A, B and C. In the low energy range and for a large Gaussian smoothing the coarse-grained density of states should be given by (2.37) evaluated for these three orbits only. Using the corresponding degeneracy factors and Maslov indices $\mu_A = 5$, $\mu_B = 4$, $\mu_C = 3$ in this energy regime it amounts to

$$\begin{aligned}\delta g(E) \approx \frac{1}{\pi\hbar}\cdot\Bigg\{ & \frac{3T_A\cdot e^{\left(-\frac{\gamma T_A}{2}\right)^2}}{\sqrt{\left|\mathrm{Tr}\tilde{\mathrm{M}}_A-2\right|}}\cos\left(\frac{S_A}{\hbar}-\frac{5\pi}{2}\right)+\frac{3T_B\cdot e^{\left(-\frac{\gamma T_B}{2}\right)^2}}{\sqrt{\left|\mathrm{Tr}\tilde{\mathrm{M}}_B-2\right|}}\cos\left(\frac{S_B}{\hbar}-\frac{4\pi}{2}\right)\\ & +\frac{2T_C\cdot e^{\left(-\frac{\gamma T_C}{2}\right)^2}}{\sqrt{\left|\mathrm{Tr}\tilde{\mathrm{M}}_C-2\right|}}\cos\left(\frac{S_C}{\hbar}-\frac{3\pi}{2}\right)\Bigg\}. \end{aligned} \tag{5.29}$$

Figure 5.12 compares the result of evaluating (5.29) including second repetitions with $\mu_{2A} = 10$, $\mu_{2B} = 8$ and $\mu_{2C} = 7$ to the exact quantum result for $\alpha = 0.03$ and $\gamma = 0.4$. One can see a major discrepancy between both curves up to $e \approx 0.35$ as well as at the periodic orbit bifurcations in the region $e \geq 0.89$. The quantum-mechanical curve contains an inaccuracy above $e \approx 0.9925$ because here the imaginary parts of the quantum energies were not taken into account and due to the difficulties with the Strutinsky method near $e = 1$ as was explained in section 5.2.2.

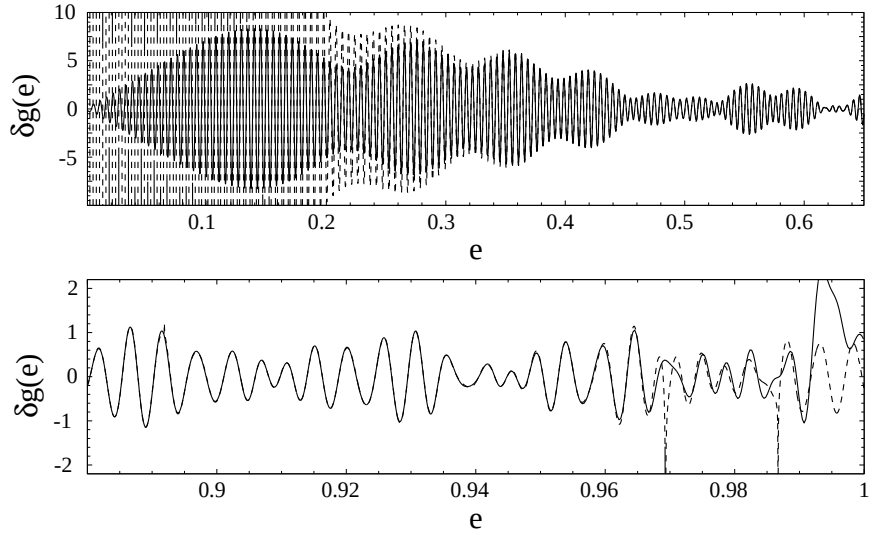

Figure 5.12: *Comparison between standard semiclassical and quantum result for $\alpha = 0.03$ and $\gamma = 0.4$. Dashed: semiclassical (5.29) including second repetitions, solid: exact quantum result.*

In the following several uniform approximations are applied in order to improve the semiclassical curve.

5.3.2 The limit $e \to 0$

In the limit $e \to 0$ the Hénon-Heiles system reaches the two-dimensional isotropic harmonic oscillator potential which possesses the $SU(2)$-symmetry. This must result in a divergence of Gutzwiller's trace formula because all periodic orbits become degenerate under the symmetry operations of the oscillator. On the other hand the oscillating part of the density of states for the two-dimensional harmonic oscillator can easily and exactly be obtained as [Bra 03]

$$\delta g_0(E) = A_0 \sum_{r=1}^{\infty} \cos\left(\frac{r S_0(E)}{\hbar}\right) \qquad A_0(E) = \frac{2E}{(\hbar\omega)^2} \qquad S_0(E) = \frac{2\pi E}{\omega}. \tag{5.30}$$

The uniform approximation procedure for such a symmetry breaking which interpolates between (5.30) and Gutzwiller's trace formula for the periodic orbits A, B and C was outlined in section 4.2 following the prescriptions of [Bra 99].

In the Hénon-Heiles case the actions of the periodic orbits A, B and C split up only in fourth order semiclassical perturbation theory. The action shifts in first and third order vanish while for the second and fourth order one obtains

$$\delta S_2 = \hbar x \left(5 - 7\cos^2\beta\right)/6 \qquad \delta S_4 = -\hbar y \, \sin^3\beta \, \cos(3\gamma), \tag{5.31}$$

with $\hbar x = e \cdot S_0(E)/12$, $y \propto e^3$ and the scaled energy $e = 6\alpha^2 E$. Using these action shifts for the construction of the phase function and choosing an amplitude function so that the asymptotic evaluation gives the Gutzwiller contributions of A, B and C one arrives at a modulation factor

$$\begin{aligned}\mathcal{M} = \frac{1}{2\pi A_0} \int_0^1 du\, e^{(i/\hbar)\Delta S\left(5/7-u^2\right)} \int_0^{2\pi} d\gamma\, e^{-(i/\hbar)\delta S\left(1-u^2\right)^{3/2}\cos(3\gamma)} \\ \times \left\{ \frac{2|\Delta S|}{\hbar} A_C u^2 + \sqrt{\frac{4|\Delta S|}{\hbar\pi}}\left(1-u^2\right)\sqrt{\frac{2\pi|\delta S|}{\hbar}}\left[\bar{A}_{AB} + \Delta A_{AB}\cos(3\gamma)\right]\right\}\end{aligned} \tag{5.32}$$

with the definitions $\delta S \equiv \frac{1}{2}(S_A - S_B)$ and $\Delta S \equiv \frac{1}{2}(S_A + S_B) - S_C$ as well as $\bar{A}_{AB} \equiv (A_A + A_B)/2$ and $\Delta A_{AB} \equiv (A_A - A_B)/2$. Approximating this for the leading terms in $\hbar$ yields the final analytical expression of the uniform approximation

$$\begin{aligned}\delta g(E) \;=\; & A_C \cos\left(\frac{S_C}{\hbar} + \frac{\pi}{2}\right) - \sqrt{\left|\frac{2\delta S}{\Delta S}\right|} \\ & \times \left[\bar{A}_{AB} J_0\left(\frac{\delta S}{\hbar}\right)\cos\left(\frac{S_C}{\hbar} + \frac{\pi}{2}\right) - \Delta A_{AB} J_1\left(\frac{\delta S}{\hbar}\right)\sin\left(\frac{S_C}{\hbar} + \frac{\pi}{2}\right)\right] \\ & + C\left(\sqrt{\frac{2|\Delta S|}{\hbar\pi}}\right)\sqrt{\frac{4\pi|\delta S|}{\hbar}} \\ & \times \left[\bar{A}_{AB} J_0\left(\frac{\delta S}{\hbar}\right)\cos\left(\frac{\bar{S}_{AB}}{\hbar}\right) - \Delta A_{AB} J_1\left(\frac{\delta S}{\hbar}\right)\sin\left(\frac{\bar{S}_{AB}}{\hbar}\right)\right] \\ & + S\left(\sqrt{\frac{2|\Delta S|}{\hbar\pi}}\right)\sqrt{\frac{4\pi|\delta S|}{\hbar}} \\ & \times \left[\bar{A}_{AB} J_0\left(\frac{\delta S}{\hbar}\right)\sin\left(\frac{\bar{S}_{AB}}{\hbar}\right) + \Delta A_{AB} J_1\left(\frac{\delta S}{\hbar}\right)\cos\left(\frac{\bar{S}_{AB}}{\hbar}\right)\right].\end{aligned} \tag{5.33}$$

In figure 5.13 the result of evaluating (5.33) including second repetitions of the periodic orbits is compared to the exact quantum result. The agreement is nearly perfect (so that the curves can hardly be distinguished) and the Gutzwiller result is reached as can be seen when comparing with figure 5.12.

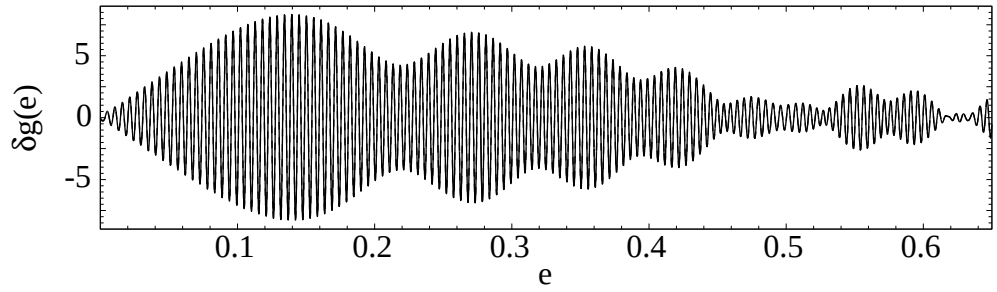

Figure 5.13: *Comparison between semiclassical uniform and exact quantum result for the SU(2) symmetry breaking of the small energy limit of the Hénon-Heiles system with* $\alpha = 0.03$ *and* $\gamma = 0.4$. *Dashed: uniform approximation (5.33) including second repetitions, solid: exact quantum result.*

5.3.3 The bifurcation of codimension one at $e = 0.892$

At the energy $e = 0.892$ the orbit C undergoes a generic period-doubling bifurcation. A new stable orbit D is created which has the shape of a double loop. In figure 5.14 one can see the shape of orbit C at an energy $e = 0.882$ as well as the ones of the orbits C and D at an energy $e = 0.90$ in an equilateral triangle which corresponds to the equipotential line of the Hénon-Heiles potential for $e = 1$. Both orbits are doubly degenerate because they can be traversed in two opposite senses of rotation.

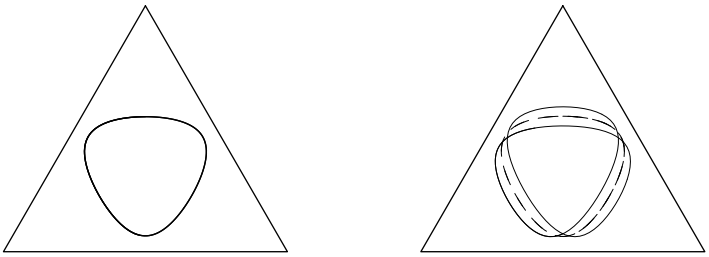

Figure 5.14: *Bifurcation of codimension one at* $e = 0.892$. *Left: orbit C at* $e = 0.882$, *right: orbits C (dashed) and D (solid) at* $e = 0.9$. *Furthermore the equipotential line for* $e = 1$ *is displayed for clarity.*

In figure 5.15 the periodic-orbit data necessary for a uniform approximation is plotted ($2C$ corresponds to the second repetition of C). The data possess the characteristic behavior of a period-doubling bifurcation as is predicted from the corresponding normal form in [Sch 97c]. For example the Gutzwiller amplitudes of the bifurcating orbits coalesce in the vicinity of the bifurcation if a factor $\sqrt{2}$ is included.

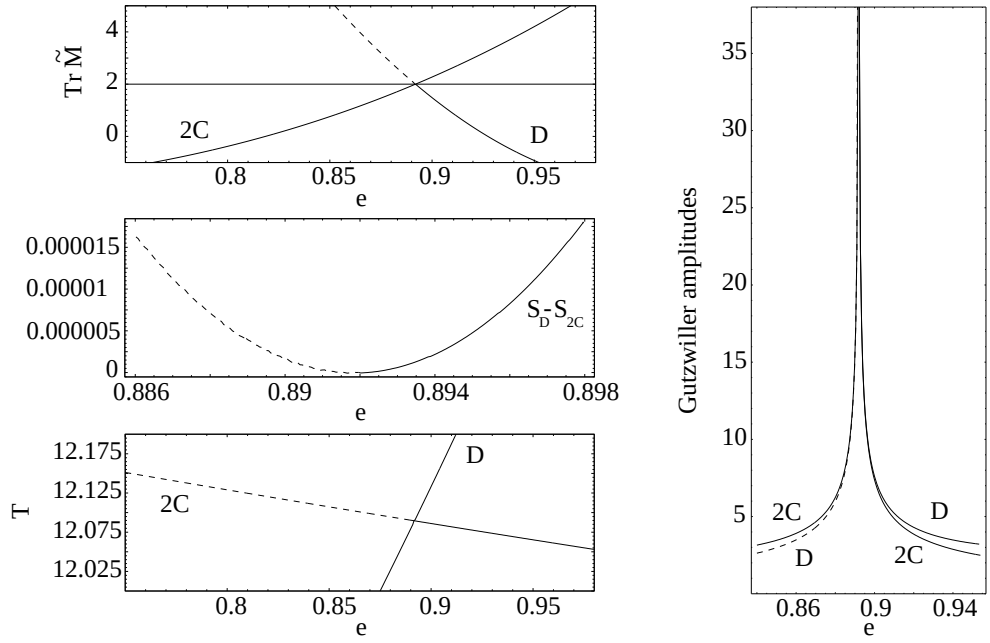

Figure 5.15: *Properties of the periodic orbits 2C and D near the period-doubling bifurcation at $e = 0.89$ plotted versus the scaled energy e. Top left: stability traces; middle left: action difference; bottom left: orbit periods. Right: Gutzwiller amplitudes modified by a factor $\sqrt{2}$ as predicted in [Sch 97c]. The dashed portions of all curves correspond to the complex pre-bifurcation ghost orbits.*

The uniform approximation for a period-doubling bifurcation was given in [Sch 97c] and reads (when expressed by Bessel functions J)

$$\begin{aligned}\delta g(E) = \Re e \Bigg[& \frac{1}{\pi\hbar} \left| \frac{\pi \Delta S}{2\hbar} \right|^{1/2} \exp\left(\frac{i}{\hbar}\bar{S} - \frac{i\pi}{2}\nu - \frac{i\pi}{4}\sigma \right) \\ & \times \Bigg\{ \left(\frac{A_1}{2} + \frac{A_0}{\sqrt{2}} \right) \left(\sigma_2 J_{1/4}\left(\frac{|\Delta S|}{\hbar} \right) e^{i\sigma_1 \pi/8} + J_{-1/4}\left(\frac{|\Delta S|}{\hbar} \right) e^{-i\sigma_1 \pi/8} \right) \\ & + \left(\frac{A_1}{2} - \frac{A_0}{\sqrt{2}} \right) \left(J_{3/4}\left(\frac{|\Delta S|}{\hbar} \right) e^{i\sigma_1 3\pi/8} + \sigma_2 J_{-3/4}\left(\frac{|\Delta S|}{\hbar} \right) e^{-i\sigma_1 3\pi/8} \right) \Bigg\} \Bigg] \end{aligned} \tag{5.34}$$

with the definitions $\Delta S \equiv \frac{1}{2}(S_1 - S_0)$ and $\bar{S} \equiv \frac{1}{2}(S_1 + S_0)$. The index zero corresponds to the central bifurcating orbit (here C) while the index one belongs to the orbit D. The Gutzwiller amplitudes are appearing as A_i (i=1,2). The parameter σ_2 distinguishes between both sides of the bifurcation. It takes on the value $+1$ on the real side, where both orbits are real and -1 on the complex side where the satellite orbit D is complex. The sign of ΔS is indicated by σ_1 and the sign factor σ can be read off Table 2 in [Sch 97c]. Applying (5.34) to the orbits C and D and adding the isolated contributions of the orbits A and B, including second repetitions, leads to the result shown in figure 5.16. The orbit D will participate in a touch-and-go bifurcation at $e = 1.179$. It will be studied as part of a codimension-two bifurcation in section 5.3.6.

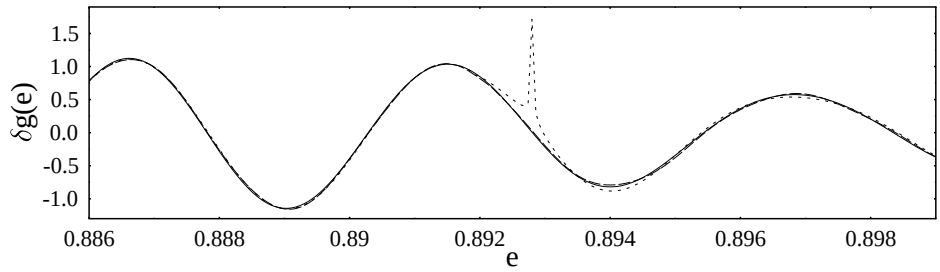

Figure 5.16: *Uniform approximation for the period-doubling bifurcation at* $e = 0.892$ *in the Hénon-Heiles system with* $\alpha = 0.03$ *and* $\gamma = 0.4$*. Solid: exact quantum result, dotted: sum of isolated Gutzwiller contributions, dashed: sum of uniform approximation (5.34) and isolated Gutzwiller contributions of orbits A and B (including second repetitions).*

5.3.4 The bifurcation cascade

The librating orbit A becomes unstable at an energy $e = 0.969309$ creating a stable rotating orbit R_5 in a pitchfork bifurcation. The capital letters may in the following indicate the type of the new born orbits while the subscripts give their Maslov indices. At an energy $e = 0.986709$ orbit A becomes stable again in an inverse pitchfork bifurcation creating the unstable librating orbit L_6. The two pitchfork bifurcations are equivalent to generic period-doubling bifurcations because the orbit A is three-fold degenerate due to the $\mathbb{D}_3$ symmetry of the system while the orbits R_5 and L_6 have an additional degeneracy factor of two due to the two opposite senses of rotation and the reflection symmetry respectively. The new born orbits are displayed in figure 5.17 together with their pre-bifurcation ghost orbits.

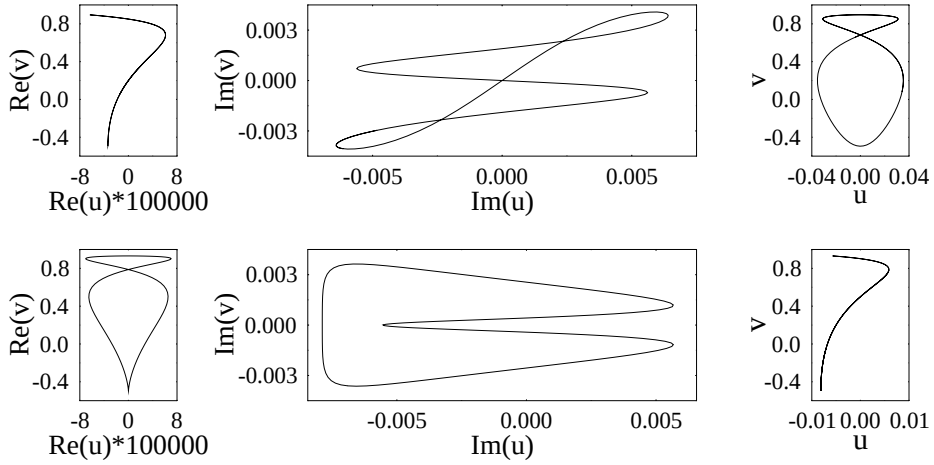

Figure 5.17: *Orbits born in the first pitchfork-bifurcation sequence of the orbit A in the Hénon-Heiles potential. Upper row: real part (left) and imaginary part (middle) of ghost orbit* R_5 *at* $e = 0.9690$*, and real orbit* R_5 *at* $e = 0.9798$ *(right). Lower row: real part (left) and imaginary part (middle) of ghost orbit* L_6 *at* $e = 0.9864$*, and real orbit* L_6 *at* $e = 0.9870$ *(right).*

In [Bra 01] it could be shown that this pattern of two subsequent opposite pitchfork bifurcations of A is repeated infinitely often while the energy e is increased up to the saddle-point energy $e = 1$. In fact the infinite pitchfork-bifurcation cascade is self-similar exhibiting scaling relations reminiscent of the famous Feigenbaum scenario [Fei 78, Bou 81]. In figure 5.18 the stability traces of the orbits involved in the bifurcation cascade of A are plotted against e for the first two pitchfork bifurcation pairs. If n counts the pitchfork bifurcation pairs then in the limit $n \to \infty$ the scaling relation for corresponding bifurcation energies e^* becomes

$$\delta_n \equiv \frac{1 - e_n^*}{1 - e_{n+1}^*} \to e^{2\pi/\sqrt{3}}, \tag{5.35}$$

which is the zooming factor used in figure 5.18. The Maslov index of A increases by one unit at each of the bifurcations.

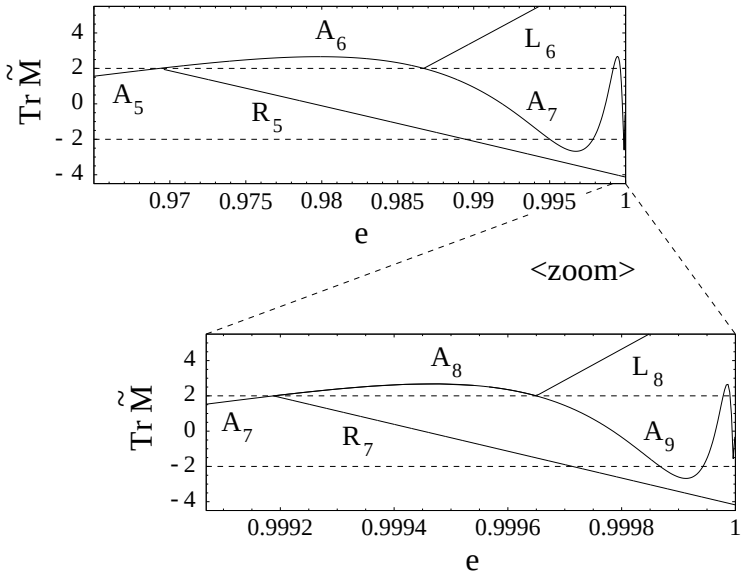

Figure 5.18: *Traces of the stability matrix near the first two pitchfork bifurcations of the orbit A.*

For one of the bifurcation pairs one can introduce the following normal form

$$\begin{aligned} \hat{S}(q', p, E) &= S_0(E) + q'p - \frac{1}{2}\left(\epsilon_1 p^2 + \epsilon_2 q'^2\right) - \frac{a}{4}\left(p^2 + q'^2\right)^2 \\ \hat{S}(I, \phi', E) &= S_0(E) + I\phi' - \left(\epsilon_1 \cos^2\phi' + \epsilon_2 \sin^2\phi'\right) I - aI^2. \end{aligned} \tag{5.36}$$

The fixed point equations (3.34) then read

$$\sin(2\phi) = 0 \qquad \left(\epsilon_1 \cos^2\phi + \epsilon_2 \sin^2\phi\right) + 2aI = 0 \tag{5.37}$$

which have the four solutions

$$\begin{aligned} (\phi_1, I_1) &= \left(0, -\frac{\epsilon_1}{2a}\right) \qquad (\phi_2, I_2) = \left(\frac{\pi}{2}, -\frac{\epsilon_2}{2a}\right) \\ (\phi_3, I_3) &= \left(\pi, -\frac{\epsilon_1}{2a}\right) \qquad (\phi_4, I_4) = \left(\frac{3\pi}{2}, -\frac{\epsilon_2}{2a}\right). \end{aligned} \tag{5.38}$$

The first and third as well as the second and fourth solution have identical radial coordinates and differ only in their angle coordinate by π. In figure 5.19 contour plots of the normal form (5.36) are plotted in dependence of ϵ_1 and ϵ_2. Furthermore the corresponding local Poincaré surface of section for $v = 0$ of the Hénon-Heiles system is shown for three e values near the bifurcation sequence. One can recognize that the normal form plots reproduce the topology of the Poincaré surface of section correctly (up to canonical coordinate transformations).

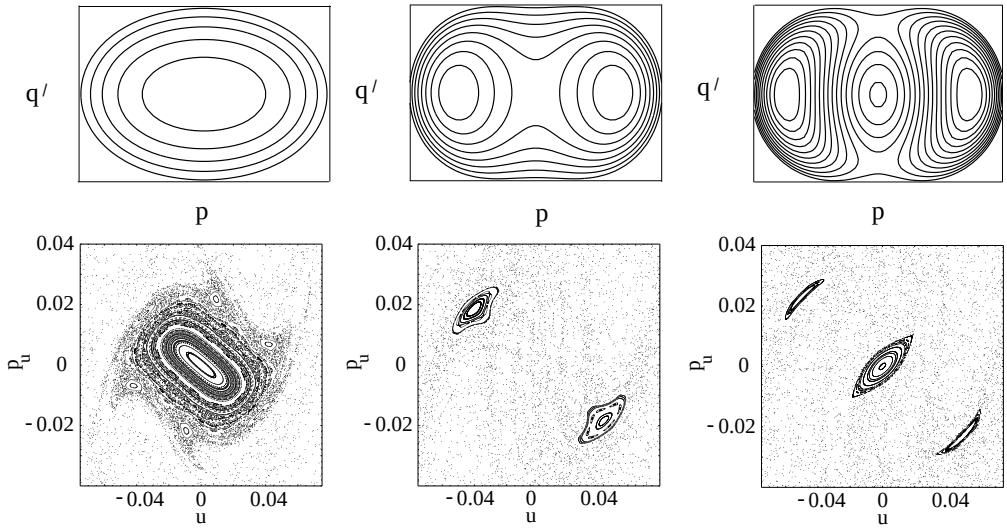

Figure 5.19: *Contour plots of the normal form* (5.36) *in dependence of the parameters* ϵ_i *for the case* $a = -1$. *From left to right:* $\epsilon_2 < \epsilon_1 < 0$, $\epsilon_2 < 0 < \epsilon_1$ *and* $0 < \epsilon_2 < \epsilon_1$. *Furthermore local Poincaré sections* ($v = 0$) *are shown with (from left to right):* $e = 0.969$, $e = 0.982$ *and* $e = 0.989$.

Evaluating the normal form at the four solutions (5.38) leads to the actions of the stationary points (see eq. (3.37))

$$S(\phi_1, I_1) = S(\phi_3, I_3) = S_0(E) - \epsilon_1 I_1 - a I_1^2 = S_0(E) + \frac{\epsilon_1^2}{4a} \tag{5.39}$$

$$S(\phi_2, I_2) = S(\phi_4, I_4) = S_0(E) - \epsilon_2 I_2 - a I_2^2 = S_0(E) + \frac{\epsilon_2^2}{4a}. \tag{5.40}$$

The orbit periods now follow as

$$T_i = T_0(E) + \frac{\epsilon_i}{2a}\frac{\partial \epsilon_i}{\partial E} \qquad i = 1, 2. \tag{5.41}$$

and as stabilities one obtains

$$\mathrm{Tr}\widetilde{M}_0 = 2 - \epsilon_1\epsilon_2, \quad \mathrm{Tr}\widetilde{M}_1 = 2 + 2\epsilon_1\epsilon_2 - 2\epsilon_1^2, \quad \mathrm{Tr}\widetilde{M}_2 = 2 + 2\epsilon_1\epsilon_2 - 2\epsilon_2^2. \tag{5.42}$$

Evaluating the Maslov indices at the stationary points yields

$$\mu_0 = \nu + (\mathrm{sign}(\epsilon_1) + \mathrm{sign}(\epsilon_2))/2 \tag{5.43}$$

$$\mu_1 = \nu + (\mathrm{sign}(\epsilon_2 - \epsilon_1) - \mathrm{sign}(\epsilon_1))/2 \tag{5.44}$$

$$\mu_2 = \nu + (\mathrm{sign}(\epsilon_1 - \epsilon_2) - \mathrm{sign}(\epsilon_2))/2. \tag{5.45}$$

For the amplitude function the following ansatz was found to be sufficient

$$\Psi(\phi, I) = \alpha_0 + \alpha_1 I + \alpha_2 I^2. \tag{5.46}$$

It is only depending on the radial coordinate I but not on the angle ϕ. The full density of states (4.6) can now be written as

$$\begin{aligned}\delta g(E) &= \frac{1}{4\pi^2\hbar^2}\,\Re e\,\exp\left[\frac{i}{\hbar}S_0 - i\frac{\pi}{2}\nu\right]\int_0^{2\pi} d\phi \int_0^{\infty} dI\,\left(\alpha_0 + \alpha_1 I + \alpha_2 I^2\right) \\ &\quad\times \exp\left\{-\frac{i}{\hbar}\left[\left(\epsilon_1\cos^2\phi + \epsilon_2\sin^2\phi\right) I + aI^2\right]\right\}. \end{aligned}\tag{5.47}$$

The parameters in (5.47) can be expressed by the periodic orbit data (see figure 5.20).

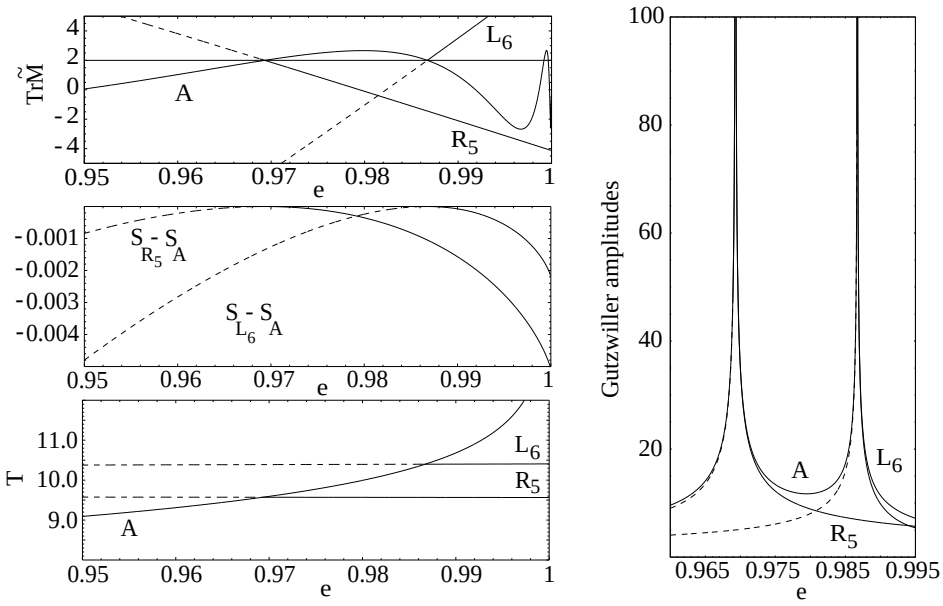

Figure 5.20: *Properties of the periodic orbits A, R_5 and L_6 near their bifurcations in the Hénon-Heiles system (5.6), plotted versus the scaled energy e. Top left: stability traces, middle left: action differences, bottom left: periods. Right: Gutzwiller amplitudes (which coalesce after modification with a factor $\sqrt{2}$). The dashed portions of all curves correspond to the complex pre-bifurcation ghost orbits.*

For example one obtains (with $\sigma_1 = \pm 1$ indicating the side of the bifurcation)

$$\epsilon_i = -2\tilde{\sigma}_i\sigma_1\sqrt{|\Delta S_i|}, \tag{5.48}$$

where it was set

$$a = \tilde{\sigma}_i \equiv \mathrm{sign}\left(\Delta S_i\right). \tag{5.49}$$

The stationary-phase approximation (4.9) gives the following contribution at each of the stationary points (denoted by i)

$$\begin{aligned}\delta g^{(SP)}(E) &= \frac{1}{\pi\hbar}\frac{\left(\alpha_0 + \alpha_1 I_i + \alpha_2 I_i^2\right)}{\sqrt{\left|\det\Phi''(I_i)\right|}} \\ &\quad\times\cos\left\{\frac{1}{\hbar}\left[S_0 - \left(\epsilon_1\cos^2\phi_i + \epsilon_2\sin^2\phi_i\right) I_i - aI_i^2\right]\right\}. \end{aligned}\tag{5.50}$$

With this, one can determine the coefficients α_0,α_1 and α_2 by identifying the Gutzwiller Amplitudes A_i with

$$A_i = \frac{1}{\pi\hbar}\frac{(\alpha_0 + \alpha_1 I_i + \alpha_2 I_i^2)}{\sqrt{|\det\Phi''(I_i)|}}. \tag{5.51}$$

Defining

$$\tilde{\epsilon}(\phi) \equiv \epsilon_1 \cos^2\phi + \epsilon_2 \sin^2\phi, \tag{5.52}$$

the integrals in (5.47) with respect to I can be calculated analytically using

$$F_n \equiv \int_0^\infty dI\ I^n\ e^{-\frac{i}{\hbar}\left[\tilde{\epsilon}(\phi)I + aI^2\right]} = \left(i\hbar\frac{\partial}{\partial\tilde{\epsilon}(\phi)}\right)^n \int_0^\infty dI\ e^{-\frac{i}{\hbar}\left[\tilde{\epsilon}(\phi)I + aI^2\right]}. \tag{5.53}$$

For n=0,1 and 2 they yield:

$$F_0(\phi) = e^{\frac{i}{\hbar}\frac{\tilde{\sigma}_i}{4}\tilde{\epsilon}^2(\phi)}\sqrt{\frac{\pi\hbar}{2}}\left\{\frac{1}{\sqrt{2}}e^{-i\frac{\pi}{4}\tilde{\sigma}_i} + \sigma\left[C\left(\sqrt{\frac{\tilde{\epsilon}^2(\phi)}{2\pi\hbar}}\right) - i\tilde{\sigma}_i S\left(\sqrt{\frac{\tilde{\epsilon}^2(\phi)}{2\pi\hbar}}\right)\right]\right\}, \tag{5.54}$$

$$F_1(\phi) = -\frac{1}{2\tilde{\sigma}_i}\left[i\hbar + \tilde{\epsilon}(\phi)F_0(\phi)\right],\ F_2(\phi) = -\frac{i\hbar}{2\tilde{\sigma}_i}\left[1 - \frac{\tilde{\epsilon}(\phi)}{2\tilde{\sigma}_i} - \frac{\tilde{\epsilon}^2(\phi)}{2i\hbar\tilde{\sigma}_i}F_0(\phi)\right] \tag{5.55}$$

with $\sigma \equiv -\tilde{\sigma}_i \cdot \mathrm{sign}(\tilde{\epsilon}(\phi))$. The remaining ϕ-integral over the interval $[0, 2\pi]$ can easily be calculated numerically. In figure 5.21 the result of the uniformization is compared to the exact quantum-mechanical result for $\alpha = 0.03$ and $\gamma = 0.4$. The semiclassical result has clearly improved in comparison with figure 5.12. The uniform approximation reaches the asymptotic limit below $e = 1$.

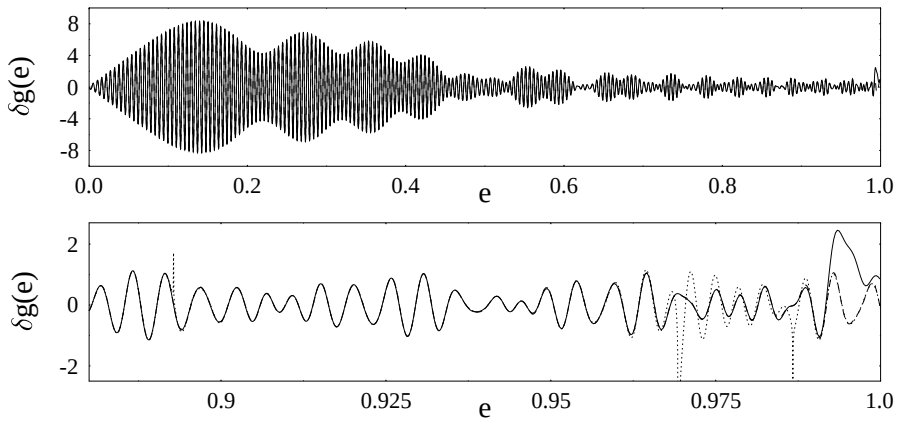

Figure 5.21: *Oscillating part of density of states in the Hénon-Heiles potential. Solid lines: quantum-mechanical results obtained for $\alpha = 0.03$. Dotted lines: sum of Gutzwiller contributions of all periodic orbits of figure 5.3 (except F_9). Dashed lines: codimension-two uniform approximation for the orbits A, R_5 and L_6, including orbits C and D (using the codimension-one uniform approximation of section 5.3.3) as well as the isolated B orbit contribution. Coarse-graining with smoothing width $\gamma = 0.4$.*

5.3.5 The range $e > 1$

The question one can ask now is what meaning Gutzwiller's sum over periodic orbits (2.30) has in the region $e > 1$ or in other words on which periodic orbits the spectral density relies in this energy regime. On the first view one could expect that one has to use complex periodic orbits, as is the case e.g. in semiclassical tunneling. As one can see from figure 5.3 the shortest real periodic orbit in this energy region is the saddle libration S while orbit A does not exist for $e > 1$. The coarse-graining γ determines the number of periodic orbits which have to be included in the Gutzwiller Trace Formula (2.37). In figure 5.22 the orbits B,C,S,$2S$,$3S$,R_5,L_6 were included for a smoothing width of $\gamma = 0.5$ and the result was compared to the exact quantum-mechanical spectral density obtained in the way described in section 5.2.2.

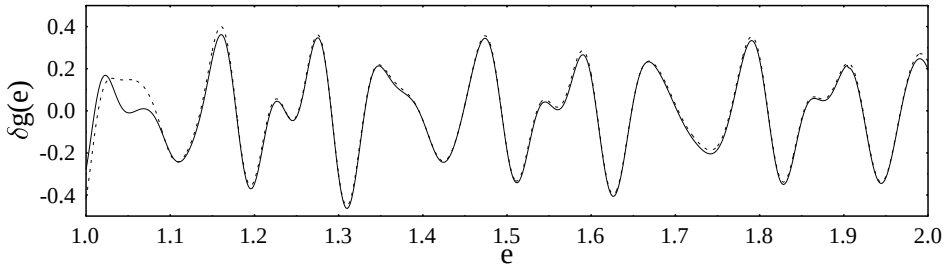

Figure 5.22: *Energy range above the saddle up to twice the saddle-point energy for the Hénon-Heiles system with $\alpha = 0.1$ and $\gamma = 0.5$. Solid: exact quantum-mechanical result, dashed: semiclassical result.*

For a smoothing width $\gamma = 0.25$ one has to include more periodic orbits. The result of summing up the contributions of the orbits B,C,S,$2S$,$3S$,$4S$,R_5,L_6,R_7,L_8,D,E_8 and F_7 can be seen in figure 5.23.

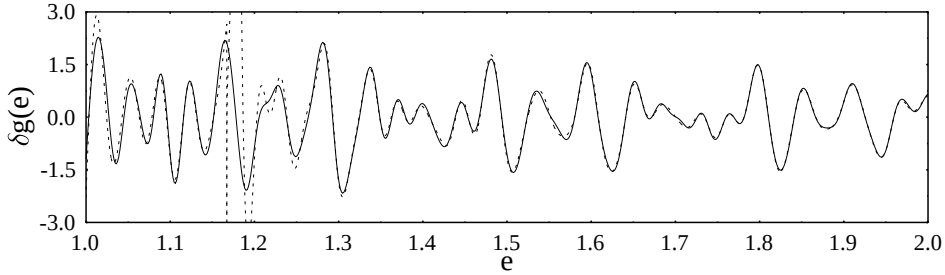

Figure 5.23: *Same as figure 5.22 but now with $\gamma = 0.25$ and using more periodic orbits for the semiclassical curve.*

The semiclassical curves correspond very well to the quantum-mechanical curves. For $\gamma = 0.25$ one can see a large discrepancy between the two curves at $e \approx 1.18$. This is due to a codimension-two bifurcation of the orbit D which will be treated in the next section.

5.3.6 The bifurcation of codimension two at $e = 1.179$

At the energy $e = 1.16718$ an isochronous bifurcation occurs in which an unstable orbit E is created together with the stable orbit F. Both orbits are 6-fold degenerate, because they can be traversed in opposite directions due to the system's time-reversal symmetry and because additionally they map onto new orbits by reflections on the three mirror axes of the potential.

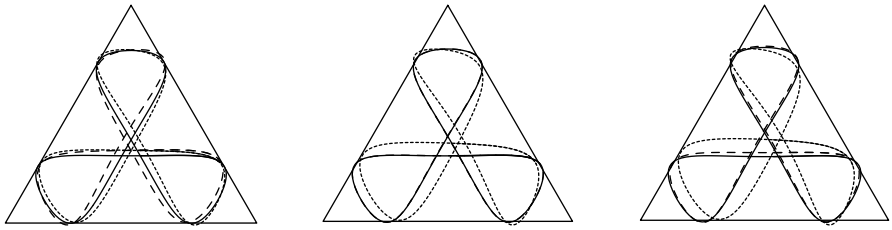

Figure 5.24: *Codimension-two bifurcation ($m = 3$). Periodic orbits D (solid), E (dashed) and F (heavy dashed). Left: $e = 1.16718$, middle: $e = 1.179$, right: $e = 1.194$. Furthermore the equipotential line of the Hénon-Heiles potential for $e = 1$ is displayed for clarity.*

The unstable orbit E subsequently participates in a touch-and-go bifurcation at $e = 1.179$ together with the orbit D. This becomes possible due to the degeneracy 2 of orbit D (see section 5.3.3) resulting in a net degeneracy factor of 3 for the orbit E. Figure 5.24 shows the configurations of the participating orbits for three representative values of e and in figure 5.25 the numerical data for the whole bifurcation sequence is displayed in dependence of e.

For energies $e < 1.16718$ the orbits E and F are complex. In contrast to the ghost orbits of pitchfork bifurcations here also their stability traces, orbit periods, actions and Gutzwiller amplitudes are complex. They can be found using the numerical procedure explained in appendix B. The periodic orbit data at the isochronous bifurcation shows exactly the behaviour predicted in [Sch 97c] (the parts of $\mathrm{Tr}\widetilde{M}$ and T which are symmetric to zero correspond to the imaginary parts, while the real parts are the same for both ghost orbits).

The sequence of a tangent bifurcation and a touch-and-go bifurcation can be interpreted as one bifurcation of codimension two with $m = 3$ [Sch 98]. The normal form of the generating function was already given in section 3.1 (equation (3.33)) together with the contour plots of the normal form.
As amplitude function $\Psi(\phi, I)$ one can use

$$\Psi(\phi, I) = T_0 + \alpha I + \beta I^{\frac{3}{2}} \cos(3\phi) \tag{5.56}$$

so that the density of states (4.6) follows as

$$\delta g(E) = \frac{1}{3\pi^2\hbar^2} \Re e \int_0^\infty dI \int_0^{2\pi} d\phi \left[T_0 + \alpha I + \beta I^{\frac{3}{2}} \cos(3\phi)\right] \times \exp\left\{\frac{i}{\hbar}\left(S_0 - \epsilon I - bI^2 - aI^{\frac{3}{2}} \cos(3\phi)\right) - \frac{i\pi}{2}\nu\right\}. \tag{5.57}$$

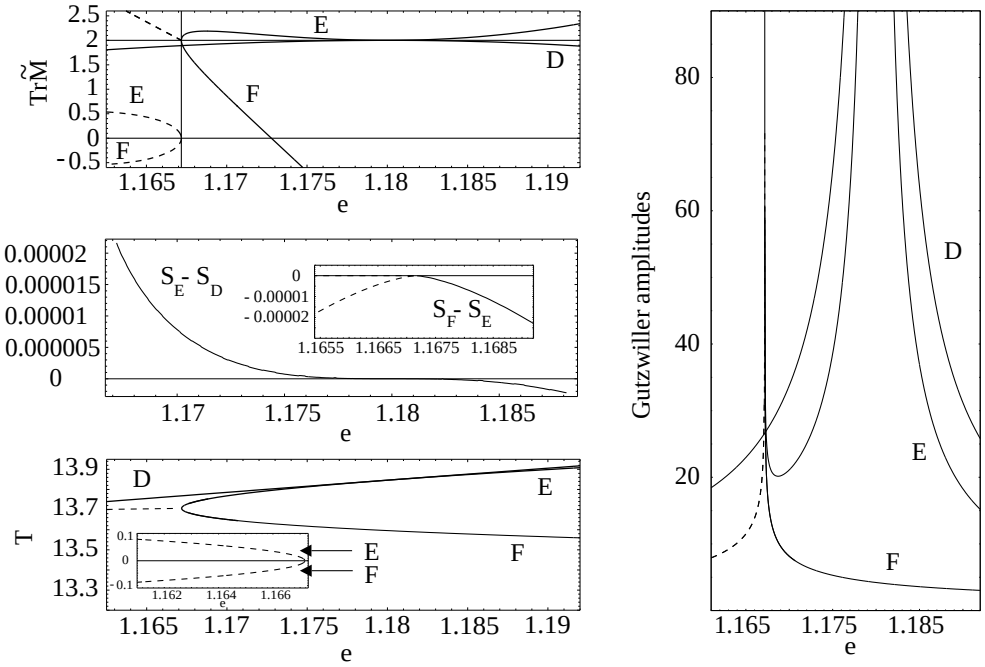

Figure 5.25: *Periodic orbit data for the codimension-two bifurcation. Top left: stability traces, middle left: action differences, bottom left: orbit periods, right: Gutzwiller amplitudes. The dashed portions of all curves correspond to pre-bifurcation ghost orbits.*

The quantities $S_0(E)$ and $T_0(E)$ are the action and period evaluated at the origin which in this case correspond to the action and period of the orbit D (with the degeneracy factor included). Again for a uniformization all parameters appearing in (5.57) have to be expressed by the periodic orbit quantities.
The integration over ϕ can easily be performed using the formula

$$\int_0^{2\pi} d\phi \; \exp\left(iz\cos\left(m\phi\right)\right) = 2\pi J_0\left(z\right), \tag{5.58}$$

where $J_0\left(z\right)$ is the Bessel function with index 0. Even though for the remaining integrals over I there are no simple analytical expressions, series representations exist which are very useful because of their rapid convergence [Sch 97b]. The leading I integral e.g. is of the type

$$\int_0^{\infty} J_0\left(I^{3/2}\right) \exp\left[i\left(\tilde{\epsilon}I + \tilde{b}I^2\right)\right] dI = \frac{\sqrt{\pi}}{2} \sum_{n,m=0}^{\infty} \frac{\left(i\tilde{\epsilon}\right)^n}{n!m!} \left(-i\tilde{b}\right)^{-(n+1)/2} \left(-4i\tilde{b}\right)^{-3m}$$
$$\times \left(\frac{\Gamma\left(\frac{n+1}{2} + 3m\right)}{(2m)!\,\Gamma\left(m + \frac{1}{2}\right)} - \frac{\left(-4i\tilde{b}\right)^{-3/2} \Gamma\left(\frac{n}{2} + 2 + 3m\right)}{(2m+1)!\,\Gamma\left(\frac{3}{2} + m\right)} \right). \tag{5.59}$$

The second integral can easily be derived by using the derivative of (5.59) with respect to $\tilde{\epsilon}$. The equations for the fixed points turn out to be

$$-3aI^{3/2}\sin 3\phi = 0 \qquad -\epsilon - \frac{3a}{2} I^{\frac{1}{2}} - 2bI = 0. \tag{5.60}$$

From the first fixed point equation one can recognize the three-fold symmetry of the normal form. The radial coordinates of the fixed points can be calculated from the second equation and become

$$I_0 = 0 \qquad I_\pm = \frac{p_\pm^2}{2}, \tag{5.61}$$

where $p_\pm$ is given by

$$p_\pm = -\frac{3a}{4\sqrt{2}b} \pm \sqrt{\frac{9a^2}{32b^2} - \frac{\epsilon}{b}}. \tag{5.62}$$

The stationary point I_0 can be identified with the orbit D which lies at the origin. If a and b have the same sign, the orbit E corresponds to the stationary point I_+ while it corresponds to I_- if a and b have opposite signs. This can be seen because at the touch-and-go bifurcation ($\epsilon = 0$) the radial coordinate of the orbit E has to vanish so that orbit D and E coalesce.

The stationary point I_0 at the origin yields for the integral (5.57) in stationary-phase approximation the Gutzwiller contribution of the orbit D

$$\delta g^{(D)}(E) = \frac{1}{\pi\hbar} \cdot \frac{1}{|\epsilon|} \cdot \exp\left[\frac{i}{\hbar} S_0 - i\frac{\pi}{2}(\nu + \text{sign } \epsilon)\right]. \tag{5.63}$$

Now the sign of ϵ and the Morse index ν are uniquely determined by the Maslov index of the central orbit D and using (3.39) one obtains

$$|\epsilon| = \sqrt{2 - \text{Tr } \widetilde{M}_D}. \tag{5.64}$$

The parameter ϵ is now fully determined. Using the other two fixed points I_+ and I_- one now calculates the expressions for $S_\pm = \hat{S} - I\phi'$ with $\hat{S}$ from (3.33). From that it is possible to numerically solve for a and b uniquely because ϵ is already determined. The amplitude coefficients α and β result from the solutions of the linear set of equations

$$A_E = \frac{T_0 + \alpha I_+ + \beta I_+^2}{\sqrt{|\det \Phi''(I_+)|}} \tag{5.65}$$

$$A_F = \frac{T_0 + \alpha I_- + \beta I_-^2}{\sqrt{|\det \Phi''(I_-)|}}. \tag{5.66}$$

because with ϵ, a and b also the values of $I_\pm$ are given. Here the Gutzwiller amplitudes A_E and A_F of the orbits E and F are needed, again including the degeneracies as well as the exponential damping factors of (2.37). The matrix Φ'' is given by (4.10) with $\hat{S}$ from (3.33).

Finally the uniform approximation can be evaluated for the density of states. The result for the bifurcating periodic orbits only (neglecting the isolated contributions of all other periodic orbits) is shown in figure 5.26 together with the corresponding result of applying the Gutzwiller trace formula. The uniform approximation is finite

over the whole energy range and asymptotically reaches the curve corresponding to Gutzwiller's trace formula for $|\epsilon| \to \infty$.

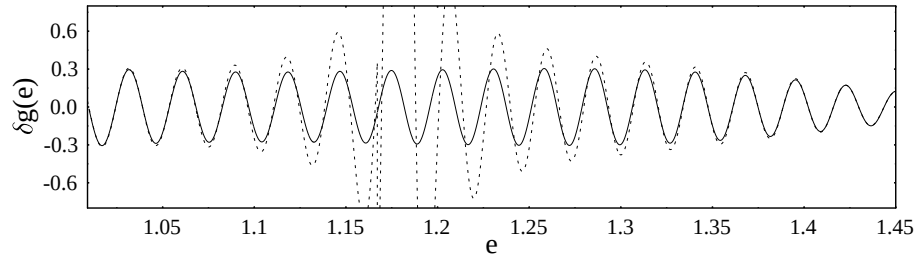

Figure 5.26: *Uniform approximation of the codimension-two bifurcation for the parameters $\alpha = 0.1$ and $\gamma = 0.25$. Dashed: Sum of isolated Gutzwiller contributions for the orbits D, E and F. Solid: uniform approximation (5.57).*

The result after adding the isolated contributions of all other periodic orbits which do not participate in the bifurcations but which were also included in figure 5.23 is shown in figure 5.27. The agreement between the semiclassical curve and the exact quantum curve is very satisfactory.

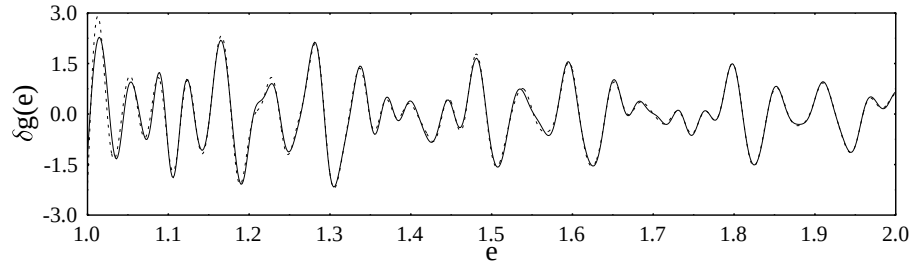

Figure 5.27: *Energy range above the saddle up to twice the saddle-point energy for the Hénon-Heiles system with $\alpha = 0.1$ and $\gamma = 0.25$. Solid: exact quantum-mechanical result, dashed: semiclassical result including the uniform approximation for the codimension-two bifurcation.*

In fact the good agreement is remarkable, because it appears to be sufficient to include only *real* periodic orbits, although the quantum-mechanical result is strongly affected by the imaginary parts (i.e. widths) of the resonance energies. Furthermore the inclusion of the stable orbits is indispensable for reproducing the coarse-grained density of states. A summation only over unstable orbits would not give satisfactory results.

Thus the semiclassical trace formula, evaluated using only the shortest real periodic orbits, obviously represents a very economic tool for the prediction of quantum oscillations also in continuum regions.

Chapter 6

A separable version of the Hénon-Heiles system

The Hénon-Heiles system is slightly modified so that it becomes separable and thus integrable. The classical dynamics as well as the quantum spectrum of the resulting system are studied. Analytical expressions are derived for the uniform approximations of the SU(2)-symmetry breaking at low energies as well as for the bifurcations of a periodic-orbit family from a single periodic orbit.

6.1 Classical mechanics

6.1.1 Classical dynamics

The nonintegrability of the Hénon-Heiles system (5.3) is caused by its non-separable term x^2y. Neglecting this term one arrives at the Hamiltonian function

$$H\left(p_x, p_y, x, y\right) = \frac{1}{2}\left(p_x^2 + p_y^2 + x^2 + y^2\right) - \frac{y^3}{3}, \tag{6.1}$$

which describes an integrable system, because it can be separated into

$$H_x = \frac{1}{2}\left(p_x^2 + x^2\right) = E_x \quad \text{and} \quad H_y = \frac{1}{2}\left(p_y^2 + y^2\right) - \frac{1}{3}y^3 = E_y \tag{6.2}$$

with the constants of motion E_x and E_y obeying

$$E = H\left(p_x, p_y, x, y\right) = H_x + H_y = E_x + E_y. \tag{6.3}$$

Similar to the Hénon-Heiles system the cubic perturbation in (6.1) can be weighted by a perturbation parameter α so that the Hamiltonian function becomes

$$H\left(p_x, p_y, x, y\right) = \frac{1}{2}\left(p_x^2 + p_y^2 + x^2 + y^2\right) - \frac{\alpha}{3}y^3. \tag{6.4}$$

After the scaling

$$x \to \frac{u}{\alpha}, \quad y \to \frac{v}{\alpha} \tag{6.5}$$

the Hamiltonian reads

$$\widetilde{H}\left(p_u, p_v, u, v\right) = \frac{1}{2}\left(p_u^2 + p_v^2 + u^2 + v^2\right) - \frac{v^3}{3}. \tag{6.6}$$

As in the Hénon-Heiles case the dynamics of the system depends on the scaled energy

$$e = \alpha^2 E, \tag{6.7}$$

which can again be multiplied by a factor 6 so that the saddle-point energy becomes $e = 1$. Due to the separability of (6.6) the equations of motion for u and v do not

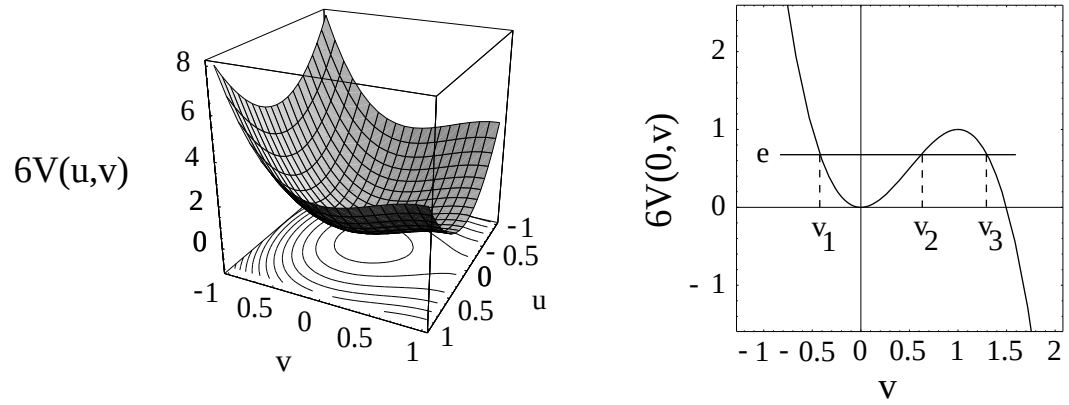

Figure 6.1: *The separable Hénon-Heiles-like potential. Left: 3D and contour plot of the potential part of (6.6) multiplied by a factor 6, right: cut of the potential along the v-axis.*

couple and are given by

$$\dot{u} = \frac{\partial \widetilde{H}_u}{\partial p_u} = p_u, \quad \dot{p_u} = -\frac{\partial \widetilde{H}_u}{\partial u} = -u \tag{6.8}$$

$$\dot{v} = \frac{\partial \widetilde{H}_v}{\partial p_v} = p_v, \quad \dot{p_v} = -\frac{\partial \widetilde{H}_v}{\partial v} = v\left(v-1\right), \tag{6.9}$$

with

$$\widetilde{H}_u = \frac{1}{2}\left(p_u^2 + u^2\right), \quad \text{and} \quad \widetilde{H}_v = \frac{1}{2}\left(p_v^2 + v^2\right) - \frac{v^3}{3}. \tag{6.10}$$

In figure 6.1 one can see that the system has one exit channel in positive v-direction with the saddle point at $v = 1$. Along the v-axis the potential is identical to the corresponding one of the Hénon-Heiles system with the classical turning points given in section 5.1.1.

The system (6.1) is of relevance because its classical dynamics is similar to the one of the elliptic billard which is studied in nuclear physics [Mag 01]. In contrast to the elliptic billiard the separability of the Hamiltonian function (6.1) is immediately given without prior coordinate transformation. Furthermore it is useful due to its relations to the full non-integrable Hénon-Heiles system of chapter five, as will become evident in the following sections.

6.1.2 Periodic orbits

Due to the separability of the system every periodic orbit must be a superposition of two one-dimensional periodic orbits in u- and v-direction. The orbit periods of the primitive periodic orbits are shown in figure 6.2 for a period range of $[0, 6\pi]$ and an energy range of $[0, 2]$.

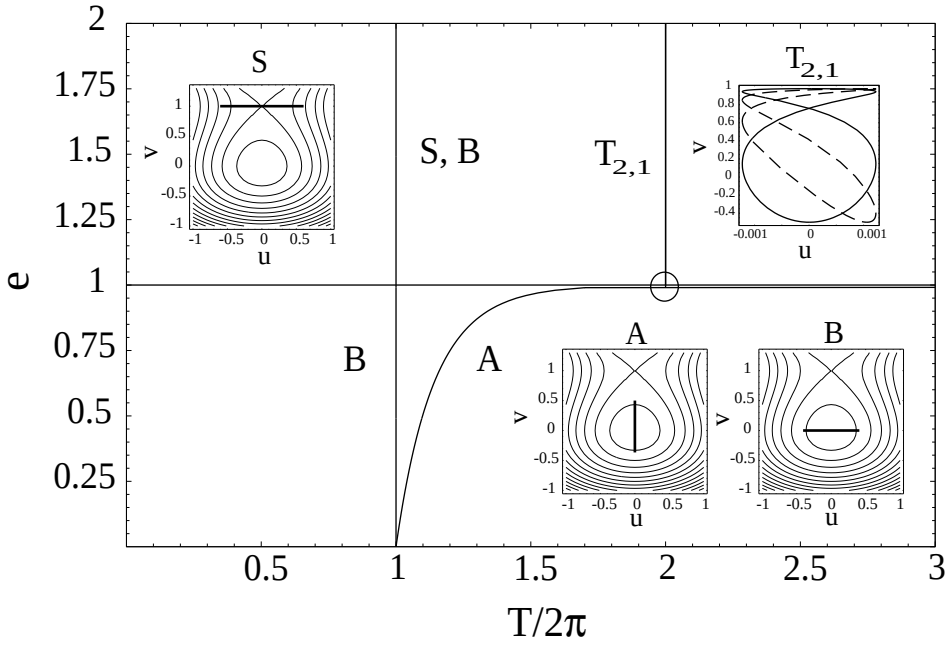

Figure 6.2: Orbit periods of the shortest primitive periodic orbits. The insets show the orbits A and B at $e = 0.5$ and the orbit S at $e = 1.1$ together with the contour lines of the potential as well as two representatives of the orbit family $T_{2,1}$ at $e = 0.9985$.

The one-dimensional libration A along the v-axis corresponds to the orbit A of the Hénon-Heiles system with the same action and period as given in (5.8) and (5.9). The stability trace for a given repetition number r now reads [Bra 01]

$$\mathrm{Tr}\widetilde{M}_A^r(e) = 2 \cdot \cos\left(r \cdot T_A(e)\right). \tag{6.11}$$

The one-dimensional libration B along the u-axis is a solution of the harmonic oscillator (6.8) for which the period T_B, action S_B and stability $\mathrm{Tr}\widetilde{M}_B$ are known:

$$T_B = 2\pi, \quad S_B(e) = 2\pi e \quad \mathrm{Tr}\widetilde{M}_B = +2. \tag{6.12}$$

For energies $e \geq 1$ another one-dimensional orbit S appears in u-direction. It oscillates with a period $T_S = 2\pi$ on the saddle. Therefore its action is $S_S(e) = 2\pi(e-1)$ and its stability reads [Bha 97]

$$\mathrm{Tr}\widetilde{M}_S = 2 \cdot \cosh(2\pi). \tag{6.13}$$

One can recognize that at an orbit period of 4π orbit A participates in a bifurcation creating the family $T_{2,1}$ of two-dimensional periodic orbits. In fact this bifurcation scenario repeats itself every time the orbital period of A becomes a multiple of 2π. Thus A must go through an infinite bifurcation cascade because its orbit period diverges as $e \to 1$. The indices of T will be explained in the next section.

6.1.3 The bifurcation cascade of orbit A

Due to the separability of the system the creation of a family of two-dimensional periodic orbits is only possible if the orbit period in v-direction is identical to the orbit period in u-direction. In u-direction the system is harmonic so that one can conclude that the orbit periods of the periodic orbits on the torus must stay constant at $k_u \cdot 2\pi$. Thus for energies larger or equal to a bifurcation energy $e^*_{k_u,k_v}$ one must have

$$k_v \; T_A\left(e^*_{k_u,k_v}\right) = k_u \; 2\pi, \quad k_u, k_v = 1, 2, 3, \ldots \quad k_u \geq k_v \tag{6.14}$$

where $T_A\left(e\right)$ is the orbit period of the A orbit. Exactly at the bifurcation energies $e^*_{k_u,k_v}$ which obey (6.14), the trace of the stability matrix of orbit A, as given in (6.11), takes on the value $+2$. The trace of the stability matrix of the new tori are constant at $+2$ as is known from periodic-orbit families. The action of the new born tori T_{k_u,k_v} can now easily be given as

$$S_{T_{k_u,k_v}}\left(e\right) = k_v \cdot S_A\left(e^*_{k_u,k_v}\right) + 2\pi k_u \left(e - e^*_{k_u,k_v}\right), \tag{6.15}$$

where $S_A\left(e\right)$ is the action of the orbit A. In [Bra 01] it was shown that the bifurcation cascade of the orbit A obeys a scaling law in which subsequent bifurcation energies for fixed k_v in the limit $e \to 1$ behave like

$$\frac{1 - e^*_{k_u+1,k_v}}{1 - e^*_{k_u,k_v}} = \delta_{k_v} = e^{2\pi/k_v}. \tag{6.16}$$

In figure 6.3 the traces of the stability matrix of the orbit A and of the new born tori are displayed as a function of the scaled energy e near the first three bifurcations with $k_v = 1$. One can see that the bifurcation scenario repeats itself in a self-similar way if one uses $\delta_1 = \exp\left(2\pi\right)$ from (6.16) as zooming factor.

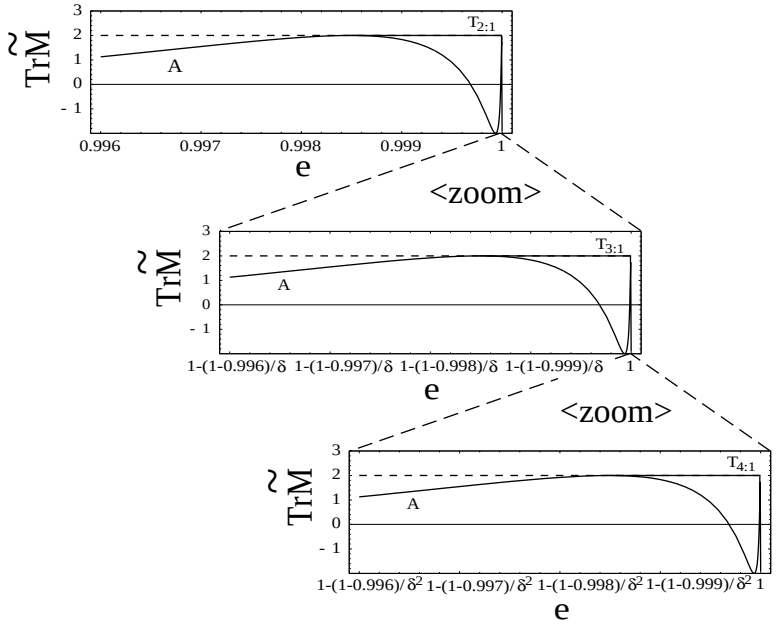

Figure 6.3: *Stabilities of the orbit A and of the first three tori with $k_v = 1$ ($\delta_1 = \exp\left(2\pi\right)$ was used as zooming factor).*

6.2 Quantum mechanics

6.2.1 Determination of the quantum spectrum

The quantum analogue of (6.4) is given by the Hamiltonian ($m = \hbar = 1$)

$$\widehat{H} = -\frac{1}{2}\left(\frac{\partial^2}{\partial x^2} + \frac{\partial^2}{\partial y^2}\right) + \frac{1}{2}\left(x^2 + y^2\right) - \frac{\alpha}{3}\cdot y^3. \tag{6.17}$$

Due to the separability of the system the Schrödinger equation can be divided into two independent one-dimensional equations for x and y

$$\widehat{H}_x\ \psi_n(x) = \left(-\frac{1}{2}\frac{\partial^2}{\partial x^2} + \frac{x^2}{2}\right)\psi_n(x) = E_n\cdot\psi_n(x) \tag{6.18}$$

$$\widehat{H}_y\ \psi_m(y) = \left(-\frac{1}{2}\frac{\partial^2}{\partial y^2} + \frac{y^2}{2} - \frac{\alpha}{3}y^3\right)\psi_m(y) = E_m\cdot\psi_m(y). \tag{6.19}$$

Here n and m are the energy quantum numbers for x and y respectively. The total energy can be written as

$$E_{nm} = E_n + E_m \tag{6.20}$$

and the total wave function reads

$$\psi_{nm}(x,y) = \psi_n(x)\cdot\psi_m(y). \tag{6.21}$$

Equation (6.18) is the Schrödinger equation of the one-dimensional, harmonic oscillator which has the real eigenenergies

$$E_n = n + \frac{1}{2}, \quad n = 0,1,2,\ldots. \tag{6.22}$$

For the y-equation (6.19) the complex scaling method of appendix C can be applied. One determines the complex non-Hermitian matrix

$$\begin{aligned} H_{m'm}(\theta) &= \left\langle m'\left|-e^{-2i\theta}\cdot\frac{1}{2}\frac{\partial^2}{\partial y^2} + e^{2i\theta}\cdot\frac{y^2}{2} - e^{3i\theta}\cdot\frac{\alpha}{3}y^3\right|m\right\rangle \\ &= -\frac{e^{-2i\theta}}{2}\left\langle m'\left|\frac{\partial^2}{\partial y^2}\right|m\right\rangle + \frac{e^{2i\theta}}{2}\left\langle m'\left|y^2\right|m\right\rangle - \frac{\alpha}{3}e^{3i\theta}\left\langle m'\left|y^3\right|m\right\rangle \end{aligned} \tag{6.23}$$

in the real Cartesian basis $\{|m\rangle\}$ of the unperturbed, one-dimensional harmonic oscillator. The matrix elements in (6.23) can easily be worked out using creation- and annihilation operators which can be found in every quantum mechanics text book (see e.g. [Nol 92]).

The complex eigenvalues of $H_{m'm}(\theta)$ which are stationary in θ are the resonance energies E_m. With (6.20) also the total energies become complex so that similar to the Hénon-Heiles case one does not find any stationary states but only resonances. Figure 6.4 shows an example of the behaviour of the imaginary and real part of one resonant eigenvalue E_m in dependence of the rotation angle θ for a parameter choice

of $\alpha = 0.1$. For this parameter the saddle-point energy (which corresponds to $e = 1$) is $E = 1/6\alpha^2 \approx 16.666$. The angle θ was chosen real from the interval $[0, 25°]$. One can see a clear stationarity in the same θ-interval for the imaginary and real part. Using a larger basis set, the position of this stationarity is not altered. As in the Hénon-Heiles case the continuum threshold lies at $E = -\infty$, so that every positive angle θ can uncover the resonance states [Yar 78]. Also the non-resonant states show a similar behaviour as in the full Hénon-Heiles system (see section 5.2.1).

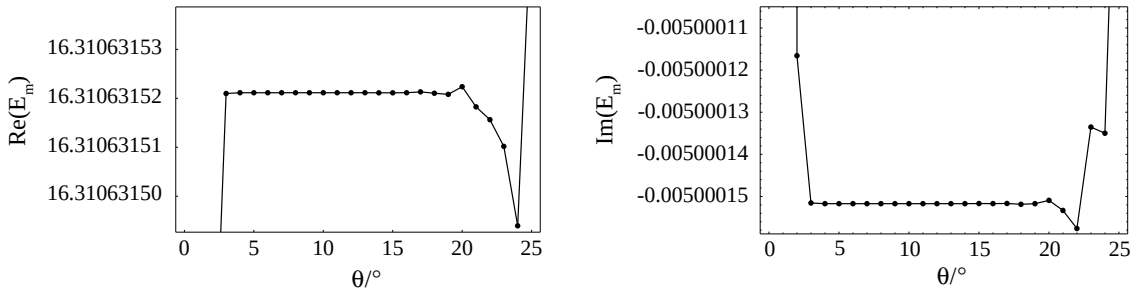

Figure 6.4: *Example of the behaviour of the real and imaginary part of one resonant eigenvalue E_m as a function of the rotation angle θ for $\alpha = 0.1$.*

Figure 6.5 shows the resonance spectra for the one-dimensional cubic potential of (6.23) as well as for the full system (6.17) in the case of the parameter $\alpha = 0.1$.

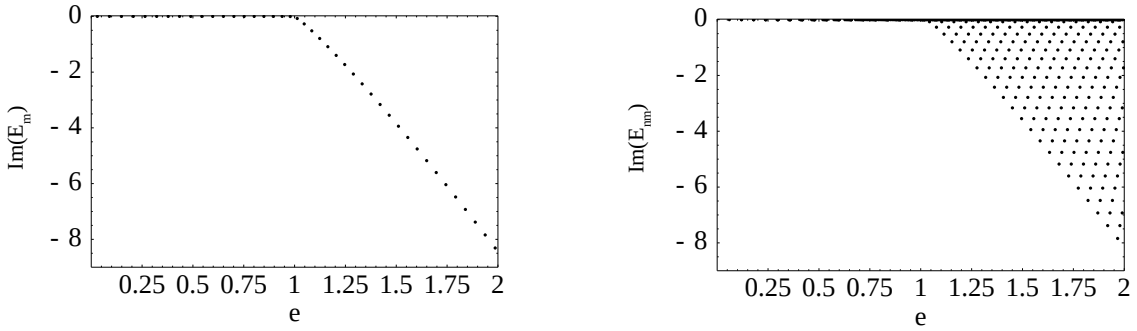

Figure 6.5: *Resonance spectra for $\alpha = 0.1$. Left: resonant eigenvalues E_m for the one-dimensional potential of (6.23), right: resonant eigenvalues E_{nm} of the full system (6.17).*

For the resonances below as well as slightly above the saddle-point energy, the difference of their real parts compared to the real energy eigenvalues obtained from a diagonalization procedure without complex rotation is tiny. In the following sections it will turn out that therefore, in contrast to the full Hénon-Heiles system, quite good results can be achieved for the density of states slightly above $e = 1$, by using only this real eigenenergy spectrum. The inclusion of the complex resonances can then improve the results for even higher energies.

6.2.2 Determination of $\tilde{g}(E)$ and $\delta g(E)$

With the resonance spectrum of the integrable Hénon-Heiles potential from section 6.2.1 it is now possible to examine the spectral distribution. This can be done in the same way as for the full non-integrable Hénon-Heiles system using the Strutinsky method of appendix D (modified for the complex resonance energy spectrum). Figure 6.6 shows the average part of the density of states $\tilde{g}(e)$ evaluated at $e = 1.5$ as a function of $\tilde{\gamma}$ for the parameter $\alpha = 0.1$. One can clearly see that the plateau condition is obeyed in the vicinity of the value $\tilde{\gamma} \approx 2.0$ independent of the polynomial order s.

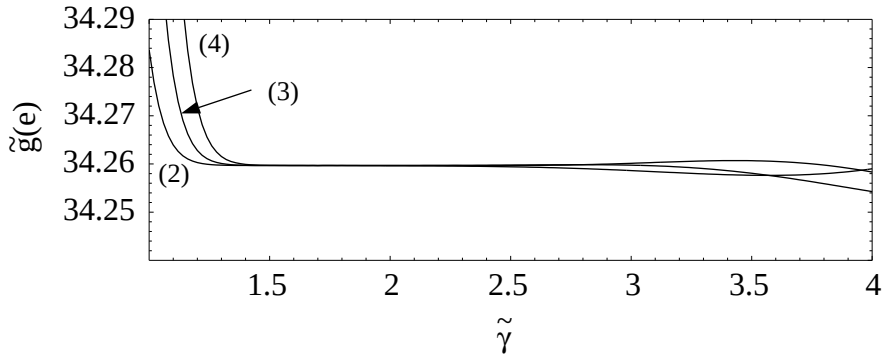

Figure 6.6: *Test of the plateau condition for the Strutinsky averaging at* $e = 1.5$ *in the case of* $\alpha = 0.1$. *The numbers in brackets denote the polynomial indices s (see appendix D).*

For the integrable version of the Hénon-Heiles potential one can also apply the Strutinsky method using the real spectrum obtained by a real diagonalization of the Hamiltonian matrix (as was already mentioned in the previous section). Below $e = 1$ and also for energies slightly above the saddle-point energy it is possible to obtain reasonable plateaux for the average part of the level density $\tilde{g}(e)$. In figure 6.7 this is shown for the case $\alpha = 0.06$ in which the plateau condition can be obeyed for $e = 1.188$.

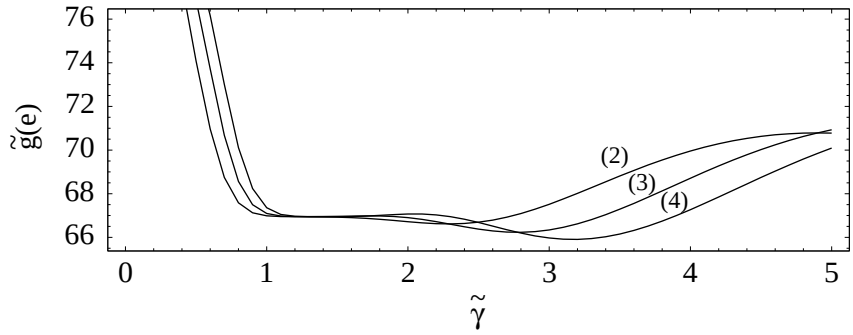

Figure 6.7: *Same as figure 6.6 but now using a real spectrum for* $\alpha = 0.06$ *and evaluating* $\tilde{g}(e)$ *at* $e = 1.188$.

6.3 Semiclassical approximations of $\delta g(E)$

6.3.1 EBK quantization and the convolution integral

Due to the separability of the system (6.17) the exact density of states corresponds to a convolution of two one-dimensional densities

$$g(E) = \int_0^E g_x(E - E')\, g_y(E')\, dE' \tag{6.24}$$

with

$$g_x(E) = \sum_n \delta(E - E_n), \quad g_y(E) = \sum_m \delta(E - E_m). \tag{6.25}$$

This is of course only a reasonable assumption for the energy region far below the saddle-point energy, where the imaginary parts of the energies E_m are very small. For the inclusion of states near $e = 1$ or above, the expression (5.22) has to be used instead of the second equation in (6.25).
The system is integrable so that one can perform the EBK quantization of section 2.1 with

$$H_i = H(I_i), \quad I_i = \frac{1}{2\pi} S_i = \frac{1}{2\pi} \oint p_i dq_i = \hbar(n_i + 1/2) \tag{6.26}$$

where $i = \{x, y\}$, $n_x = n$ and $n_y = m$. It yields the one-dimensional semiclassical trace formulae [Bra 03]

$$g_i(E) = \frac{T_i(E)}{2\pi\hbar} \sum_{k_i=-\infty}^{\infty} (-1)^{k_i} \cos\left(\frac{k_i}{\hbar} S_i(E)\right). \tag{6.27}$$

Using (6.24) it follows

$$g(E) = \frac{1}{(2\pi\hbar)^2} \sum_{k_x,k_y=-\infty}^{\infty} (-1)^{k_x+k_y} \int_0^E T_x(E - E')\, T_y(E') \times \cos\left(\frac{k_x}{\hbar} S_x(E - E')\right) \cos\left(\frac{k_y}{\hbar} S_y(E')\right) dE'. \tag{6.28}$$

Equation (6.28) corresponds to a trace formula which gives the full EBK spectrum if evaluated exactly. In particular the term $k_x = k_y = 0$ gives the smooth Thomas-Fermi part of the density of states as a convolution integral over the primitive classical periods T_x and T_y of the orbits B and A of section 6.1.2 in x- and y-direction respectively:

$$\tilde{g}(E) \approx g_{TF}(E) = \frac{1}{(2\pi\hbar)^2} \int_0^E T_x(E - E')\, T_y(E')\, dE. \tag{6.29}$$

6.3.2 The topological sum

Alternatively using the EBK spectrum (6.26) the Poisson summation of section 2.1 can be performed. One obtains the topological sum

$$\begin{aligned} g^{(2)}(E) &= \frac{1}{\hbar^2}\sum_{k_x,k_y=-\infty}^{\infty}\int_0^{I_{x_{max}}} dI_x \int_0^{I_{y_{max}}(I_x)} \delta\left(E - H_x(I_x) - H_y(I_y)\right) \\ &\quad \times \exp\left(\frac{i}{\hbar} 2\pi\left(k_x I_x + k_y I_y\right) - i\pi\left(k_x + k_y\right)\right) dI_y \qquad (6.30) \\ &= \frac{1}{2\pi\hbar^2}\sum_{k_x,k_y=-\infty}^{\infty}(-1)^{k_x+k_y}\int_0^{I_{x_{max}}} T_y\left(E - E_x(I_x)\right) \\ &\quad \times \exp\left(\frac{ik_y}{\hbar} S_y\left(E - E_x(I_x)\right) + \frac{i}{\hbar} 2\pi k_x I_x\right) dI_x. \qquad (6.31) \end{aligned}$$

From the first to the second equation it was used that [Bra 03]

$$\delta\left(E - E_y\right) = \delta\left(I_y - F(E_y)\right)\left|F'(E_y)\right| \quad \text{with} \quad F(E_y) = S_y(E_y)/2\pi. \qquad (6.32)$$

Instead of having replaced the upper integration limits by ∞ as in (2.7) here energy conservation was (explicitly) obeyed resulting in finite upper limits $I_{x_{max}}$ and $I_{y_{max}}$. Furthermore, instead of replacing the lower limit by $\hbar/2$ it was set to zero for reasons which will become clear later. Using

$$dI_i = \frac{1}{2\pi} dS_i = \frac{1}{2\pi} T_i(E_i)\, dE_i, \qquad i = x, y \qquad (6.33)$$

it follows

$$\begin{aligned} g^{(2)}(E) = \frac{1}{(2\pi\hbar)^2}\sum_{k_x,k_y=-\infty}^{\infty}(-1)^{k_x+k_y}\int_0^{E} T_y\left(E - E_x\right) T_x(E_x) \\ \times \exp\left(\frac{ik_y}{\hbar} S_y\left(E - E_x\right) + \frac{ik_x}{\hbar} S_x(E_x)\right) dE_x. \qquad (6.34) \end{aligned}$$

The terms containing the sin-function cancel pairwise in the sum from $-k_x$ up to $+k_x$ and from $-k_y$ up to $+k_y$. With the substitution $E' = E - E_x$ one obtains

$$\begin{aligned} g^{(2)}(E) = \frac{1}{(2\pi\hbar)^2}\sum_{k_x,k_y=-\infty}^{\infty}(-1)^{k_x+k_y}\int_0^{E} T_x\left(E - E'\right) T_y(E') \\ \times \cos\left(\frac{k_x}{\hbar} S_x\left(E - E'\right)\right)\cos\left(\frac{k_y}{\hbar} S_y(E')\right) dE', \qquad (6.35) \end{aligned}$$

which is identical to the full semiclassical result (6.28). As a consequence the mistake one has done due to the shift of the lower boundaries of the integral (6.31) must cancel the remaining single-sum terms of the Poisson summation.
Using the classical actions and orbit periods of the orbits A and B one obtains as full semiclassical formula

$$\boxed{g(E) = \frac{1}{2\pi\hbar^2}\sum_{k_x,k_y=-\infty}^{\infty}(-)^{k_x+k_y}\int_0^{E} T_A\left(E_y\right) e^{i\left[k_y S_A\left(E_y\right) + 2\pi k_x\left(E - E_y\right)\right]/\hbar} dE_y,} \qquad (6.36)$$

which will now serve as starting point for the derivation of the asymptotic semiclassical contributions of the periodic orbits and periodic-orbit families of the system.

6.3.3 Calculation of the asymptotic semiclassical contributions

Using the analytical expression (6.11) of $\mathrm{Tr}\widetilde{M}_A(E)$, the semiclassical contribution of the k_y-th repetition of the orbit A according to (2.30) is given by

$$\delta g_{k_y}^{(A)}(E) = \frac{T_A(E)}{2\pi\hbar\left|\sin\left[k_y T_A(E)/2\right]\right|}\cos\left[\frac{k_y}{\hbar}S_A(E) - \frac{\pi}{2}\sigma_{k_y}\right]. \tag{6.37}$$

The Maslov index here equals $\sigma_{k_y} = 1 + 4k_y$ for small energies for which no bifurcation has occurred. At each bifurcation of the k_y-th repetition of the A orbit it increases by two units. Alternatively one can derive the contribution (6.37) from the upper endpoint of (6.36) at $E_y = E$ summed over all k_x [Kai 03].

The contributions of the tori are calculated by the asymptotic evaluation of the integral (6.36) in stationary-phase approximation. Here the stationarity condition of the phase is identical to (6.14). Furthermore since $T_A\left(E_y\right) \geq T_B$ one has $k_x \geq k_y$. The case $k_x = k_y$ happens only at the harmonic-oscillator limit $E = 0$. The result for the torus T_{k_x,k_y} reads

$$\delta g^{\left(T_{k_x,k_y}\right)}(E) = \frac{2}{\hbar^{3/2}}\frac{k_x}{k_y}\sqrt{\frac{2\pi}{k_y T_A'\left(E^*_{k_x,k_y}\right)}}\cos\left[\frac{1}{\hbar}S_{T_{k_x,k_y}}(E) - \frac{\pi}{2}\left(2k_x + 2k_y\right) + \frac{\pi}{4}\right], \tag{6.38}$$

with $S_{T_{k_x,k_y}}(e)$ (and thus $S_{T_{k_x,k_y}}(E)$) given in (6.15).

The same way as the A orbit contribution corresponds to an edge correction of (6.36) for $E_y = E$, the B orbit contribution corresponds to an edge correction with $E_x = E$. For $k_x = k_y = k$ the stationary point is given by $E^*_{k_x,k_y} = 0$ yielding the contribution

$$\delta g^{\left(B,k_x=k_y\right)}(E) = \frac{1}{\hbar^{3/2}}\sqrt{\frac{2\pi}{T_A'(0)}}\sum_{k=1}^{\infty}\frac{1}{\sqrt{k}}\cos\left(\frac{k}{\hbar}2\pi E + \frac{\pi}{4}\right). \tag{6.39}$$

One can see that even though this contribution is attributed to a single orbit, its $\hbar$-dependence is of the order $O\left(\hbar^{-3/2}\right)$ which is characteristic of a torus. The orbit B must therefore be considered as a *quasi-torus*. For $k_x \neq k_y$ the end-point contributions amount to

$$\delta g^{\left(B,k_x\neq k_y\right)}(E) = \frac{2}{\pi\hbar}\sum_{k_x=1}^{\infty}\cos\left[\frac{k_x}{\hbar}2\pi E - \frac{\pi}{2}\left(2k_x+1\right)\right]\sum_{k_y\neq k_x>1}(-1)^{k_y}\frac{k_x}{\left(k_x^2 - k_y^2\right)}. \tag{6.40}$$

Since this contribution is of order $\sqrt{\hbar}$ relative to the diagonal quasi-torus term (6.39), it is of minor importance as will become evident from the numerical results.

6.3.4 The limit $e \to 0$

In the limit $e \to 0$ Gutzwiller's trace formula diverges because the system reaches the two-dimensional harmonic oscillator with SU(2)-symmetry whose periodic orbits occur in orbit families and are not isolated. One has to find a uniform approximation which interpolates between the harmonic oscillator result and the sum of the isolated semiclassical contributions of the orbit A and the quasi-torus B. To achieve this one can use two different but - as will turn out - equivalent approaches.

The first approach is the semiclassical perturbation theory from section 4.2 which yields a trace formula of the form

$$\delta g_{pert}(E) = \frac{2E}{\hbar^2} \Re e \left\{ \sum_{k=1}^{k_{max}} \mathcal{M}(\xi_k) \cdot e^{\frac{i}{\hbar} 2\pi k E} \right\}. \tag{6.41}$$

The modulation factor $\mathcal{M}(\xi_k)$ must tend to unity in the limit $e \to 0$ in order to reproduce the harmonic oscillator result. It is given by a Fresnel integral in which the second order action shift $\delta_2 S_A$ appears

$$\mathcal{M}(\xi_k) = \int_0^1 e^{\frac{i}{\hbar} k \cdot \delta_2 S_A \cdot y^2} dy. \tag{6.42}$$

The action shift turns out as $\delta_2 S_A = \frac{T'_A(0)}{2} E_y^2$ so that the modulation factor becomes

$$\mathcal{M}(\xi_k) = \frac{1}{E} \cdot \int_0^E e^{\frac{i}{\hbar} \cdot \frac{k}{2} T'_A(0) E_y^2} \, dE_y. \tag{6.43}$$

The second possibility consists in an expansion of the action $S_A(E_y)$ around $E_y = 0$ up to second order in E_y

$$S_A(E_y) \approx 2\pi E_y + \frac{5\pi}{6} \alpha^2 E_y^2 = \frac{1}{2} T'_A(0) E_y^2, \tag{6.44}$$

where the prime indicates the derivative with respect to energy. For small energies E_y the period $T_A(E_y)$ is identical to the orbital period 2π of the one-dimensional harmonic oscillator. The bifurcation condition (6.14) yields the condition $T_A(0) = 2\pi$ only if $k_x = k_y$. In the summation of (6.36) the imaginary parts cancel so that only the real parts contribute. With $k \equiv |k_x| = |k_y|$ one obtains as result

$$\delta g(E) \approx \frac{2}{\hbar^2} \Re e \left\{ \sum_{k=1}^{k_{max}} e^{\frac{i}{\hbar} 2\pi k E} \int_0^E e^{\frac{i}{\hbar} \cdot \frac{k}{2} T'_A(0) E_y^2} \, dE_y \right\}. \tag{6.45}$$

The expression (6.45) is only a good approximation for small energies E. Therefore one needs a uniform approximation which uniformly interpolates between (6.45) and the sum of the isolated semiclassical contribution of A and of the quasi-torus B, valid for larger energies. One starts from the integral

$$\delta g_{uni}(E) = \Re e \sum_{k=1}^{k_{max}} \int_0^E (\alpha_0 + \alpha_1 E_y) \; e^{\frac{i}{\hbar} a E_y^2} \, dE_y. \tag{6.46}$$

where α_0, α_1 and a are real constants. The construction of the uniform approximation is completely analogous to the uniformization procedure for the torus bifurcation described in the following section with the quasi-torus B replacing the tori. The uniform approximation of the symmetry breaking reads

$$\delta g_{uni}(E) = \sum_{k=1}^{k_{max}} \left(A_A(E) - \sqrt{\frac{\hbar}{\pi \Delta S_A(E)}} A_B(E) \right) \cos\left(\frac{k \cdot S_A(E)}{\hbar} - \frac{\pi}{2} \right) + \sqrt{2} A_B \, \Re e \left[C\left(\sqrt{\frac{2\Delta S_A}{\pi\hbar}} \right) + iS\left(\sqrt{\frac{2\Delta S_A}{\pi\hbar}} \right) \right] e^{\frac{i}{\hbar} 2\pi k E}. \quad (6.47)$$

with A_A and A_B the Gutzwiller- and Berry-Tabor amplitudes of the orbit A and the torus B respectively. The difference of the action of orbit A and the torus B is denoted by ΔS_A.

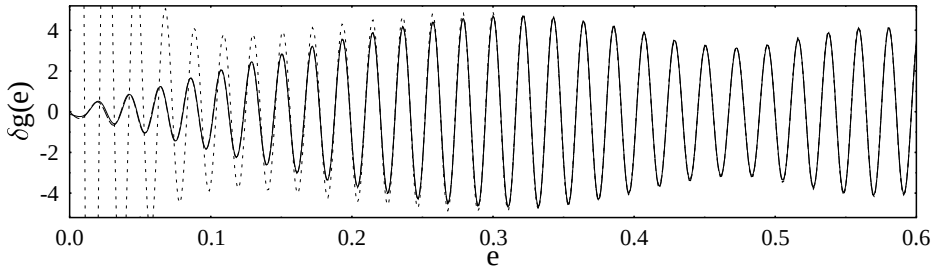

Figure 6.8: *Uniform approximation of the limit $e \to 0$ for the parameters $\alpha = 0.06$ and $\gamma = 0.4$. Solid: quantum-mechanical result, dashed: uniform approximation (6.47), heavy dashed: sum of the contributions of the orbits A and B. The difference between the uniform approximation and the quantum result can only be seen for small energies due to small discrepancies of the quantum result (see section 5.2.2).*

6.3.5 The bifurcations of the periodic orbit A

At the bifurcations of the periodic orbit A, new tori are created as was shown in section 6.1.2 and 6.1.3. For one bifurcation of a torus from a single orbit the normal form of the generating function is given by [Ozo 88]

$$\hat{S}(\phi', I) = S_0 - \epsilon I - aI^2 + I\phi', \quad (6.48)$$

in the radial normal form coordinates of (3.27). Application of (3.34) yields one stationary point with the radial coordinate

$$I_1 = -\frac{\epsilon}{2a}, \quad (6.49)$$

which corresponds to the torus. If $I_1 > 0$ the periodic orbits on the torus are real. If $I_1 < 0$ the phase-space coordinates of the periodic orbits on the torus are imaginary, which can easily be understood from the relation

$$I = \frac{p^2 + q'^2}{2}. \quad (6.50)$$

In figure 6.9 the behaviour near the bifurcation is shown by (schematic) contour plots of the normal form (6.48). To determine between the real side of the bifurcation, where the torus is real and the side where it is complex one defines

$$\sigma \equiv \text{sign}(I_1) = \begin{cases} +1 & I_1 > 0 \\ -1 & I_1 < 0 \end{cases} . \tag{6.51}$$

Evaluating (6.48) at I_1 gives the action S_1 of the torus

$$S_1 = S_0 + \frac{\epsilon^2}{4a}. \tag{6.52}$$

The difference ΔS between the torus action and the action of the central periodic orbit is then given by

$$\Delta S \equiv S_1 - S_0 = \frac{\epsilon^2}{4a}. \tag{6.53}$$

The sign of the action difference is defined as

$$\sigma_a \equiv \text{sign}(\Delta S) = \text{sign}(a) . \tag{6.54}$$

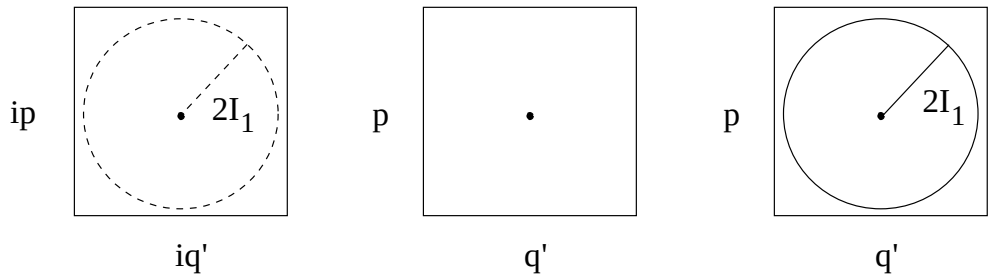

Figure 6.9: *Contour plots of the normal form (6.48). Left: $I_1 < 0$, the torus is complex, middle: $I_1 = \epsilon = 0$, the torus and the central orbit coalesce, right: $I_1 > 0$ the torus is real.*

The phase function appearing in (4.6) becomes

$$\Phi(\phi', I) = S_0 - \epsilon I - aI^2. \tag{6.55}$$

As amplitude function it is possible to choose the following form

$$\Psi(\phi', I) = \alpha + \beta I, \tag{6.56}$$

with α and β expressed by α_0, α_1 and α_2 of (5.46) as

$$\alpha = \alpha_0 , \qquad \beta = \left(\alpha_1 - \frac{\epsilon}{2a}\alpha_2\right) . \tag{6.57}$$

This can be seen by the following partial integration

$$\begin{aligned} -\frac{\epsilon}{2a}\int_0^\infty dI\ I \exp\left(\frac{i}{\hbar}\Phi\right) &= \frac{1}{2a}\int_0^\infty dI\ I \exp\left(\frac{i}{\hbar}\Phi\right)(-\epsilon - 2aI + 2aI) \\ &= \frac{1}{2a}\int_0^\infty dI\ I \exp\left(\frac{i}{\hbar}\Phi\right)\left(\frac{\partial\Phi}{\partial I} + 2aI\right) \\ &= \int_0^\infty dI\ I^2 \exp\left(\frac{i}{\hbar}\Phi\right) + O(\hbar). \end{aligned} \tag{6.58}$$

The second part is of the order $\hbar$ smaller than the first one, so that (6.56) can be used in leading order of $\hbar$.
After having performed the ϕ'-integration the density of states (4.6) becomes

$$\delta g(E) = \frac{1}{\pi\hbar^2}\,\Re e\left\{e^{\frac{i}{\hbar}S_0 - i\frac{\pi}{2}\nu}\int_0^\infty (\alpha+\beta I)\,e^{-\frac{i}{\hbar}\left(\epsilon I + aI^2\right)}dI\right\}. \tag{6.59}$$

In (6.59) there appear two integrals which can be expressed by Fresnel functions $S(x)$ and $C(x)$:

$$\begin{aligned} F_1 &\equiv \int_0^\infty e^{-\frac{i}{\hbar}\left(\epsilon I + aI^2\right)}\,dI \\ &= e^{\frac{i}{\hbar}\frac{\epsilon^2}{4a}}\cdot\sqrt{\frac{\pi\hbar}{2\,|a|}}\cdot\left\{\frac{e^{-\frac{i\pi}{4}\sigma_a}}{\sqrt{2}} + \sigma\left[C\left(\sqrt{\frac{\epsilon^2}{2\pi\hbar\,|a|}}\right) - i\sigma_a S\left(\sqrt{\frac{\epsilon^2}{2\pi\hbar\,|a|}}\right)\right]\right\} \end{aligned} \tag{6.60}$$

as well as

$$\begin{aligned} F_2 \;&\equiv\; \int_0^\infty I\cdot e^{-\frac{i}{\hbar}\left(\epsilon I + aI^2\right)}\,dI = i\hbar\cdot\frac{\partial}{\partial\epsilon}\int_0^\infty e^{-\frac{i}{\hbar}\left(\epsilon I + aI^2\right)}dI \\ &=\; e^{\frac{i}{\hbar}\frac{\epsilon^2}{4a}}\cdot\sqrt{\frac{\pi\hbar}{2\,|a|}}\cdot\left(-\frac{\epsilon}{2a}\right)\cdot\left\{\frac{e^{-\frac{i\pi}{4}\sigma_a}}{\sqrt{2}} + \sigma\left[C\left(\sqrt{\frac{\epsilon^2}{2\pi\hbar\,|a|}}\right) - i\sigma_a S\left(\sqrt{\frac{\epsilon^2}{2\pi\hbar\,|a|}}\right)\right]\right\} \\ &\quad -\frac{i\hbar}{2a}. \end{aligned} \tag{6.61}$$

For the density of states (6.59) one obtains

$$\begin{aligned} \delta g(E) &= \frac{1}{\pi\hbar^{3/2}}\cdot\sqrt{\frac{\pi}{2\,|a|}}\cdot\left(\alpha - \frac{\beta\epsilon}{2a}\right) \\ &\quad\times\Re e\left\{e^{\frac{i}{\hbar}\left(S_0+\frac{\epsilon^2}{4a}\right)-i\frac{\pi}{2}\nu}\left(\frac{e^{-\frac{i\pi}{4}\sigma_a}}{\sqrt{2}} + \sigma\left[C\left(\sqrt{\frac{\epsilon^2}{2\pi\hbar\,|a|}}\right) - i\sigma_a S\left(\sqrt{\frac{\epsilon^2}{2\pi\hbar\,|a|}}\right)\right]\right)\right\} \\ &\quad+\frac{1}{\pi\hbar}\cdot\frac{\beta}{2a}\cdot\cos\left(\frac{S_0}{\hbar} - \frac{\pi}{2}(\nu+1)\right). \end{aligned} \tag{6.62}$$

The asymptotic evaluation of (6.62) corresponds to the approximation of the Fresnel functions for large arguments $x \gg 1$ [Abr 65]

$$C(x) \;\sim\; \frac{1}{2} + \frac{1}{\pi x}\sin\left(\pi x^2/2\right) \tag{6.63}$$

$$S(x) \;\sim\; \frac{1}{2} - \frac{1}{\pi x}\cos\left(\pi x^2/2\right). \tag{6.64}$$

This yields

$$\begin{aligned} \delta g(E) \;&\sim\; \frac{1}{\pi\hbar^{3/2}}\cdot\sqrt{\frac{\pi}{|a|}}\cdot\frac{1+\sigma}{2}\cdot\left(\alpha - \frac{\beta\epsilon}{2a}\right)\cdot\cos\left(\frac{S_0 + \frac{\epsilon^2}{4a}}{\hbar} - \frac{\pi}{2}\left(\nu + \frac{\sigma_a}{2}\right)\right) \\ &\quad+\frac{1}{\pi\hbar}\cdot\frac{\alpha}{|\epsilon|}\cdot\cos\left(\frac{S_0}{\hbar} - \frac{\pi}{2}(\nu + \mathrm{sign}(\epsilon))\right). \end{aligned} \tag{6.65}$$

In (6.65) the contribution of the order $\hbar^{-3/2}$ asymptotically vanishes on the complex side if $\sigma = -1$. This phenomenon of switching off a semiclassical contribution even though the isolated contributions are finite is known as *Stokes transition* [Ber 89, Boa 95, Sch 97a].
It is now possible to identify the semiclassical amplitudes as well as the Morse index as

$$A_0 = \frac{1}{\pi\hbar} \cdot \frac{\alpha}{|\epsilon|} \tag{6.66}$$

$$A_1 = \frac{1}{\pi\hbar^{3/2}} \cdot \sqrt{\frac{\pi}{|a|}} \cdot \left(\alpha - \frac{\beta\epsilon}{2a}\right) \tag{6.67}$$

$$\nu = \mu_0 - \mathrm{sign}(\epsilon). \tag{6.68}$$

The contribution of the central orbit is of the order $\hbar$ while that of the torus is proportional to $\hbar^{-3/2}$. Together with (6.51), (6.52) and (6.54) equation (6.62) becomes

$$\delta g(E) = \sigma\sigma_a \left(\sqrt{\frac{\hbar}{4\pi\,|\Delta S|}} A_1 - A_0\right) \cdot \cos\left(\frac{S_0}{\hbar} - \frac{\pi}{2}(\nu+1)\right)$$
$$+ \frac{A_1}{\sqrt{2}} \cdot \Re e\left\{ e^{\frac{i}{\hbar}S_1 - i\frac{\pi}{2}\nu} \left[\frac{e^{-\frac{i\pi}{4}\sigma_a}}{\sqrt{2}} + \sigma \cdot \left(C\left[\sqrt{\frac{2\,|\Delta S|}{\pi\hbar}}\right] - i\sigma_a S\left[\sqrt{\frac{2\,|\Delta S|}{\pi\hbar}}\right]\right)\right]\right\}. \tag{6.69}$$

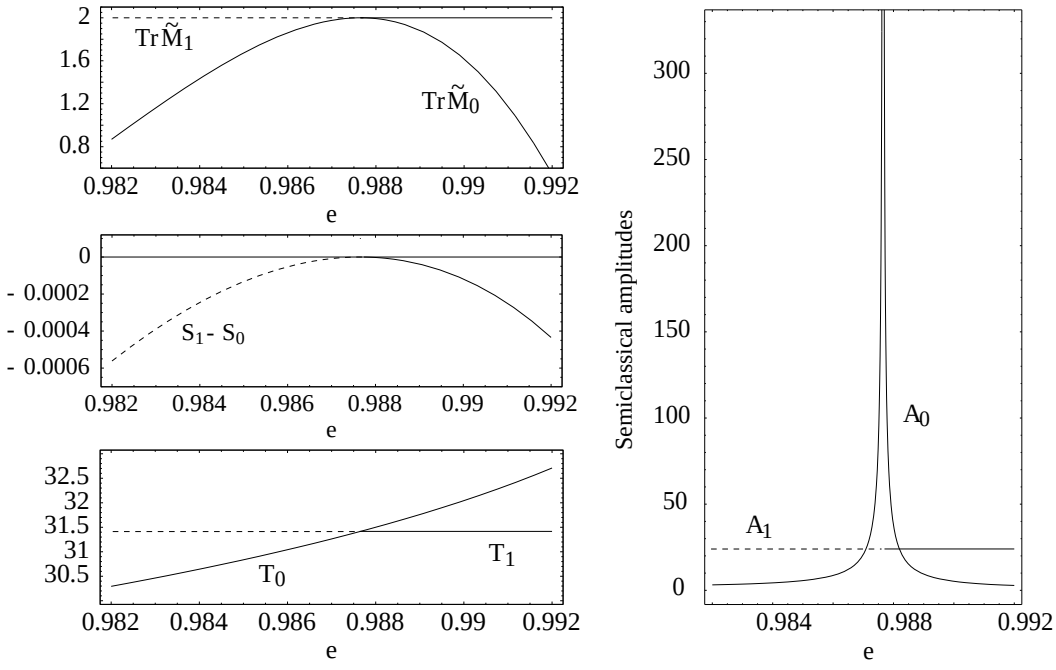

Figure 6.10: *Properties of the periodic orbit A and the torus which is created at the bifurcation of the $k_u : k_v = 5 : 3$ resonance at $e = 0.987655$. The central A orbit is labeled by "0", the bifurcated 5:3 torus by "1".*

Figure 6.11 compares the result of the uniformization with an exact quantum calculation for the bifurcation with $k_x : k_y = 5 : 3$ at $e = 0.987655$ for a smoothing $\gamma = 0.1$ (the orbital data for this bifurcation is displayed in figure 6.10 in dependence of e). The dashed curve consists of the sum of the uniform approximation (6.69) and the isolated contributions of all other tori (with $k_x, k_y \leq 8$), which are not bifurcating, as well as the contribution of the quasi-torus B. Furthermore the result of the application of Gutzwiller's trace formula to the orbit A, and summing up the isolated torus contributions is shown (dotted curve). One can recognize that the result using the uniform approximation (6.69) accurately reproduces the quantum-mechanical curve over the whole energy range.

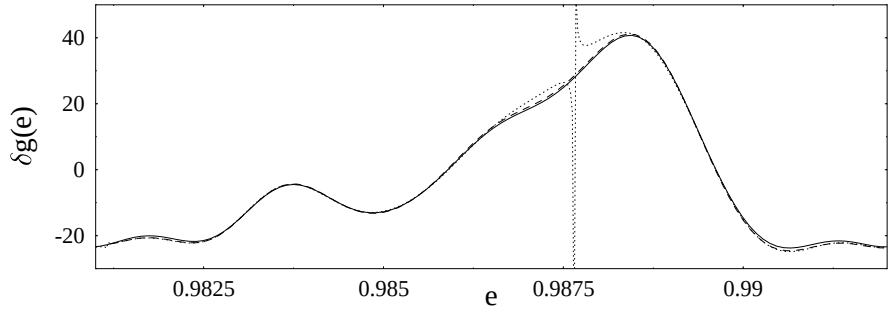

Figure 6.11: *Uniformization applied to the 5:3 resonance at* $e = 0.987655$ *for* $\alpha = 0.06$ *and* $\gamma = 0.1$. *Solid: exact quantum-mechanical, dotted: application of Gutzwiller's trace formula for A plus the isolated contributions of the tori with* $k_u, k_v \leq 8$, *dashed: uniform approximation for the 5:3 torus plus isolated contributions of tori.*

In [Kai 03] it was shown that the uniform approximation (6.69) can be summed over many bifurcations of the separable Hénon-Heiles system as long as these bifurcations are not lying too close. The result can then reproduce the fine structure of the density of states very accurately. Only the energy range very near to the saddle-point energy can not be reproduced because there infinitely many bifurcations accumulate. Furthermore the uniform approximation of the symmetry breaking at $e = 0$ can be included so that one obtains a "grand uniform approximation". In figure 6.12 comparisons are shown between the exact quantum result and three kinds of semiclassical approximations. First only the contributions (6.38) of the tori are taken into account. Even though this already gives a satisfactory result it can still be improved by including the isolated contribution of the orbit A. Removing the divergences using the uniform approximation (6.69) leads to an almost perfect agreement between the semiclassical and the quantum-mechanical curves.

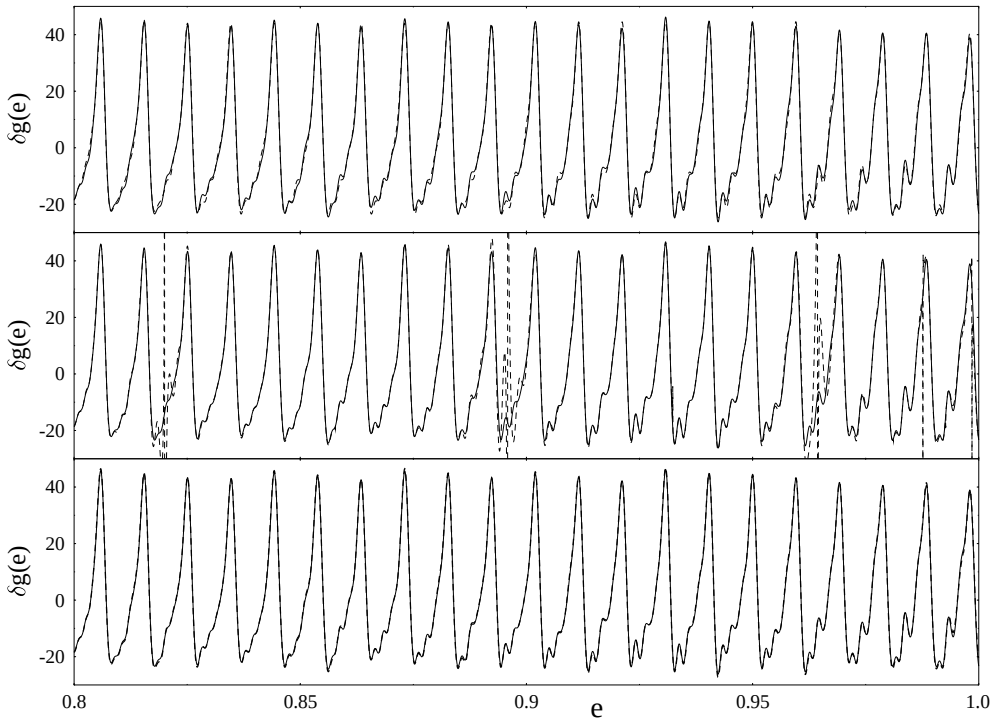

Figure 6.12: *Oscillating part of level density coarse-grained with* $\gamma = 0.1$ *for* $\alpha = 0.06$*. Solid lines: quantum-mechanical result. Dashed lines: semiclassical results with* $k_u, k_v \leq 8$*. Top: contributions (6.38) of the tori only. Center: sum of the tori contributions plus Gutzwiller result for the isolated A orbit. Bottom: uniform approximation (6.69) plus sum of contributions of other tori.*

6.3.6 The range $e > 1$

Above the saddle-point energy, formula (6.36) can not be used because the orbit A does not exist there so that $T_A(E)$ is not defined in that regime. No additional bifurcations occur in this energy range so that the coarse-grained density of states should be given by the sum of the asymptotic contributions of the tori (6.38) and of the quasi-torus B (6.39). Furthermore one obtains a contribution coming from the new saddle orbit S of section 6.1.2 reading [Bha 97]

$$\delta g^{(S)}(e) = \frac{1}{\hbar} \sum_{k=1}^{\infty} \frac{(-1)^k}{\sinh(k\pi)} \cos\left(\frac{k}{\hbar} 2\pi (e-1)\right), \quad e \geq 1. \tag{6.70}$$

This orbit has the same orbit period as the orbit B but a larger Lyapunov exponent so that its amplitude can be expected to be smaller. Furthermore, in the case of a strong coarse-graining the contributions of the tori and the higher repetitions of the B orbit ($k \geq 2$) can be neglected due to the exponentially small damping factor. In figure 6.13 the quasi-torus contribution (6.39) is calculated for $\alpha = 0.06$ and compared to the corresponding exact quantum-mechanical result obtained from a diagonalization (without complex scaling) for a Gaussian smoothing of $\gamma = 0.4$. One can see that the agreement is very good up to an energy of about $e = 1.2$. This means that the contribution of the quasi-torus B (with $k = 1$) almost completely reproduces the

quantum coarse-grained level density above the saddle-point energy. For the fine-structure with small dampings $\gamma \leq 0.15$ the contributions of the tori, the higher repetitions of B as well as (6.70) become important.

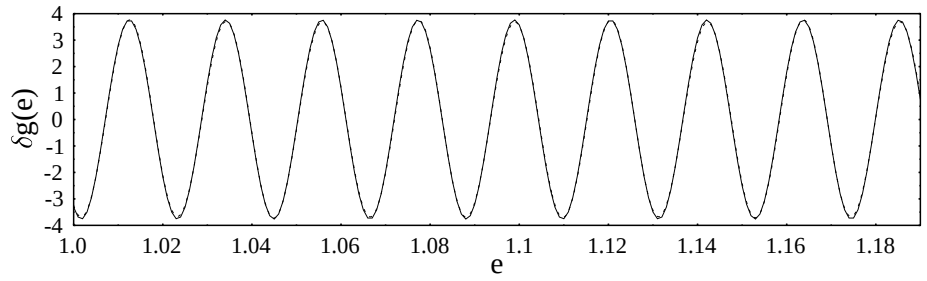

Figure 6.13: *Coarse-grained density of states above the saddle-point energy for* $\alpha = 0.06$ *and* $\gamma = 0.4$*. Solid: quantum-mechanical result, dashed: B orbit contribution (6.39) with* $k = 1$*.*

The analogous procedure was performed for a complex quantum-mechanical spectrum obtained using the complex scaling method of appendix C. For a parameter $\alpha = 0.1$ and a smoothing value $\gamma = 0.25$ figure 6.14 shows the comparison of the exact quantum-mechanical and the semiclassical result, obtained from summing the B orbit contribution (with $k = 1$) and the contributions of the tori (with $k_u, k_v \leq 8$). The agreement is very good even though the inclusion of more tori and higher repetitions of B can be expected to improve the correspondence at the maxima of the curve. This can be inferred because for a larger value $\gamma \geq 0.25$ the quality of the agreement is comparable to the one of figure 6.13 for $e \in [0, 2]$.

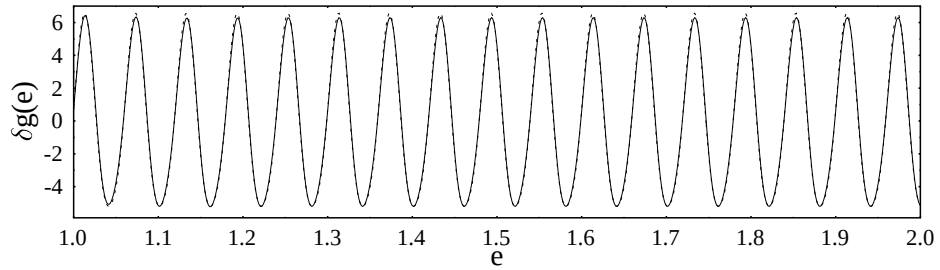

Figure 6.14: *Coarse-grained density of states above the saddle-point energy for* $\alpha = 0.1$ *and* $\gamma = 0.25$*. Solid: quantum-mechanical result, dashed: B orbit contribution (6.39) (with* $k = 1$*) plus contributions of tori (6.38) with* $k_u, k_v \leq 8$*.*

Chapter 7

A two-dimensional double-well potential

In the following a two-dimensional double-well system with mixed phase-space dynamics is studied. The behaviour of the shortest periodic orbits is examined. Using the uniform approximation developed for the Hénon-Heiles system, the quantum-mechanical density of states is approximated semiclassically.

7.1 Classical mechanics and periodic orbits

The Hamiltonian

$$H = \frac{1}{2}\left(p_x^2 + p_y^2\right) + \frac{1}{2}\left(x^2 - y^2\right) + \alpha\left(y^4 - \frac{1}{2}x^2y^2\right) + \frac{1}{16\alpha} \tag{7.1}$$

describes a two-dimensional non-integrable double-well system. The potential part of it has two minima at $x = 0$ and $y = \pm 1/2\sqrt{\alpha}$ with energy $E = 0$, separated by a saddle at $x = y = 0$ with energy $E^* = 1/16\alpha$. Using scaled variables $u = \sqrt{\alpha}x$ and $v = \sqrt{\alpha}y$ the classical dynamics only depends on one parameter, namely the scaled energy $e \equiv E/E^* = 16\alpha E$ with the central saddle at the height $e = 1$. The scaled Hamiltonian reads

$$\widetilde{H} = \frac{1}{2}\left(p_u^2 + p_v^2\right) + \frac{1}{2}\left(u^2 + v^2\right) + \left(v^4 - \frac{1}{2}u^2v^2\right) + 1/16. \tag{7.2}$$

At the scaled energy $e = 9$ the system possesses four other saddles at $v = \pm 1$ and $u = \pm\sqrt{3}$ over which a particle can escape. At all energies $e > 0$ there exists a straight-line orbit A that librates along the v-axis. It undergoes two bifurcation cascades, one approaching the saddle at $e = 1$ from below in one of the wells and one approaching $e = 1$ from above, extending itself over both wells. We consider the system only for energies $e \leq 1$ for which all periodic orbits appear twice due to the two potential wells along the v-axis. Figure 7.1 shows a contour plot of the potential with the two shortest periodic orbits A and B as well as a one-dimensional cut of the potential along the v-axis.

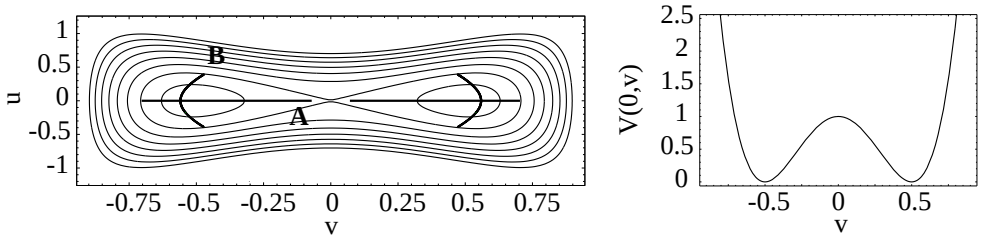

Figure 7.1: *Scaled double-well potential. Left: contour plot together with the two shortest periodic orbits A and B evaluated at $e = 0.96$. Right: cut of the potential along the v-axis.*

The action as well as the orbit period of the orbit A can be given analytically in terms of its two turning points in the well with $v > 0$

$$v_1 = \frac{1}{2}\sqrt{1-\sqrt{e}}, \quad v_2 = \frac{1}{2}\sqrt{1+\sqrt{e}}. \tag{7.3}$$

The orbit period is given by

$$T_A(e) = \frac{\sqrt{2}}{v_2}\mathbf{K}(q), \tag{7.4}$$

with the modulus q of the complete elliptic integral $\mathbf{K}(q)$ reading

$$q = \frac{1}{v_2}\sqrt{v_2^2 - v_1^2}. \tag{7.5}$$

Using a further complete elliptic integral $\mathbf{E}(q)$ the action can be expressed as

$$S_A(e) = \frac{2\sqrt{2}}{3\alpha}v_2\left[\frac{1}{2}\mathbf{E}(q) - 2v_1^2\mathbf{K}(q)\right]. \tag{7.6}$$

7.2 Bifurcations of the periodic orbits

While orbit B is stable for energies $e < 1$, the orbit A becomes unstable at the energy $e = 0.91232$ creating the rotational orbit R which has the Maslov index 5. At the energy $e = 0.94272$ orbit A becomes stable again creating the unstable libration L with the Maslov index 6. Similar to the pitchfork bifurcations of the straight-line orbit in the Hénon-Heiles system, the newly created rotation and libration are two-fold degenerate due to time-reversal and mirror symmetry of the double-well system respectively. The Maslov index of A which is $\mu_A = 3$ for $e \leq 0.91232$ increases by one unit at every pitchfork bifurcation. In figure 7.2 the periodic orbits R and L are shown together with their complex predecessors which correspond to librations in the real and imaginary parts respectively. In figure 7.3 the orbit data necessary to evaluate the semiclassical trace formulae are plotted in dependence of the scaled energy e. The Gutzwiller amplitudes of the orbits R and L in figure 7.3 were divided by $\sqrt{2}$ so that at the pitchfork bifurcations they show the same divergences

as the ones of the orbit A. This behaviour is known from period-doubling bifurcations [Sch 97c]. The two pitchfork bifurcations correspond to the first pair of an infinite pitchfork-bifurcation cascade. The first pitchfork bifurcation of the second pair occurs at a fairly large energy very near to the saddle at $e \approx 0.99984$.

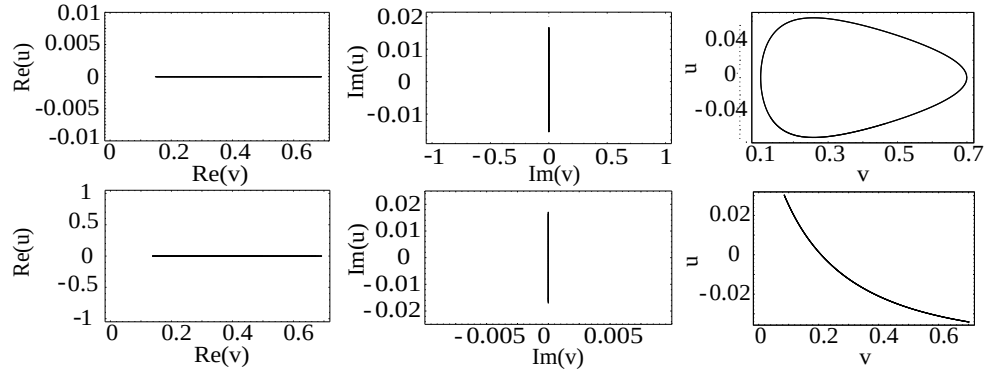

Figure 7.2: *Orbits born in the first two pitchfork bifurcations of the orbit A. Upper row: real part (left) and imaginary part (middle) of ghost orbit R at $e = 0.98064$, and real orbit R at $e = 0.95$ (right). Lower row: real part (left) and imaginary part (middle) of ghost orbit L at $e = 0.94$, and real orbit L at $e = 0.95$ (right).*

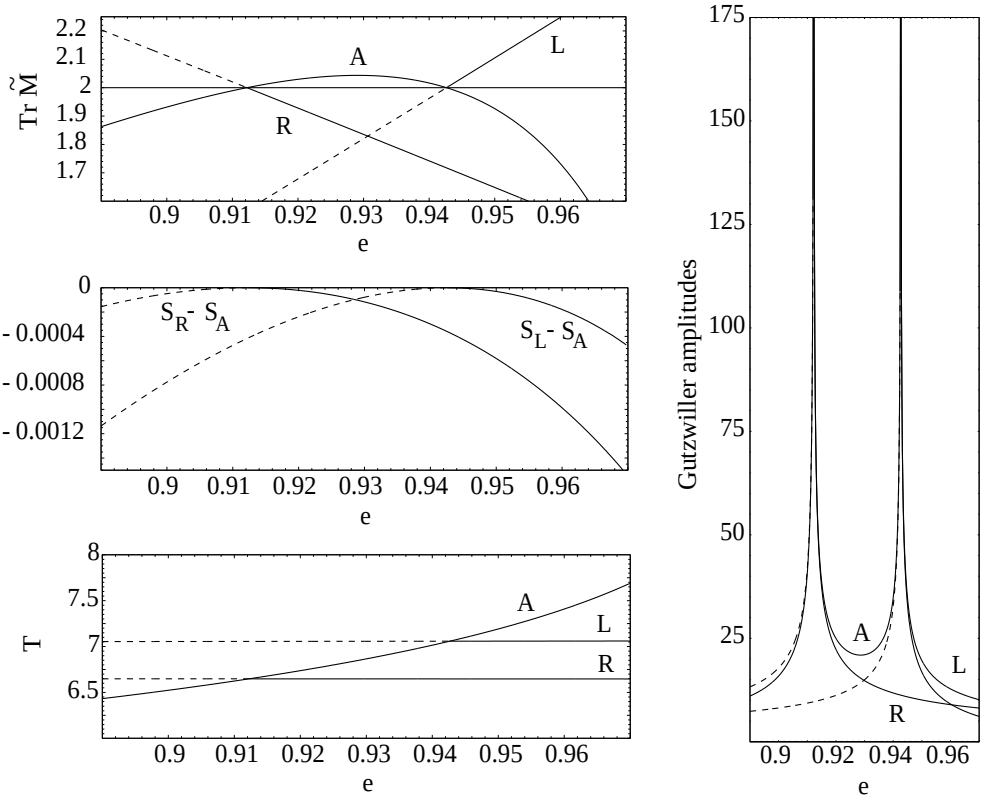

Figure 7.3: *Orbit data of the periodic orbits participating in the first two pitchfork bifurcations in dependence of the scaled energy e. Top: stability traces. Middle: action differences between the new born orbits and orbit A. Bottom: orbit periods. Right: Gutzwiller amplitudes. The amplitudes of R and L were divided by $\sqrt{2}$ as explained in the text. All dashed parts of the curves correspond to ghost orbits.*

7.3 Quantum mechanics

The quantum spectrum of the system (7.1) can easily be calculated in the Cartesian basis of the two-dimensional harmonic oscillator using creation and annihilation operators. In very good approximation the system is closed for $e < 1$, so that the eigenenergy spectrum can be considered as real and discrete. Using the Strutinsky averaging method of appendix D for the determination of the smooth part of the level density usually yields inaccuracies at small energies due to the edge of the energy window at $e = 0$. Therefore it is more accurate to use the Thomas-Fermi approximation to the average level density in the low energy regime. Including a factor 2 which accounts for the two wells this is given by the integral

$$\tilde{g}_{TF}(E) = \frac{2\sqrt{2}}{\pi\hbar^2\sqrt{\alpha}} \int_{v_1}^{v_2} \frac{\sqrt{(v_2^2 - v^2)(v^2 - v_1^2)}}{\sqrt{1 - v^2}}\, dv \tag{7.7}$$

which can easily be evaluated numerically. For larger energies ($e \geq 0.1$) the Thomas-Fermi result is (practically) identical to the result of the Strutinsky method.

7.4 Evaluation of Gutzwiller's trace formula

For the semiclassical approximation of the oscillating part of the coarse-grained density of states one can evaluate Gutzwiller's trace formula using only the orbits A,B,R and L including their degeneracy factors:

$$\delta g_{scl}(E) = \frac{1}{\pi\hbar} \left\{ \frac{2T_A \cdot e^{-\left(\frac{\gamma T_A}{2}\right)^2}}{\sqrt{\left|\mathrm{Tr}\widetilde{\mathrm{M}}_\mathrm{A} - 2\right|}} \cos\left(\frac{S_A}{\hbar} - \frac{3\pi}{2}\right) + \frac{2T_B \cdot e^{-\left(\frac{\gamma T_B}{2}\right)^2}}{\sqrt{\left|\mathrm{Tr}\widetilde{\mathrm{M}}_\mathrm{B} - 2\right|}} \cos\left(\frac{S_B}{\hbar} - \frac{5\pi}{2}\right) \right.$$
$$\left. + \frac{6T_R \cdot e^{-\left(\frac{\gamma T_R}{2}\right)^2}}{\sqrt{\left|\mathrm{Tr}\widetilde{\mathrm{M}}_\mathrm{R} - 2\right|}} \cos\left(\frac{S_R}{\hbar} - \frac{5\pi}{2}\right) + \frac{6T_L \cdot e^{-\left(\frac{\gamma T_L}{2}\right)^2}}{\sqrt{\left|\mathrm{Tr}\widetilde{\mathrm{M}}_\mathrm{L} - 2\right|}} \cos\left(\frac{S_L}{\hbar} - \frac{6\pi}{2}\right) \right\}. \tag{7.8}$$

In figure 7.4 the result is compared to the curve obtained from the exact quantum calculation for the case $\alpha = 0.0008$ and $\gamma = 0.5$. The agreement is perfect up to an energy of about $e = 0.86$ (for the range $e \leq 0.825$ see upper part of figure 7.5).

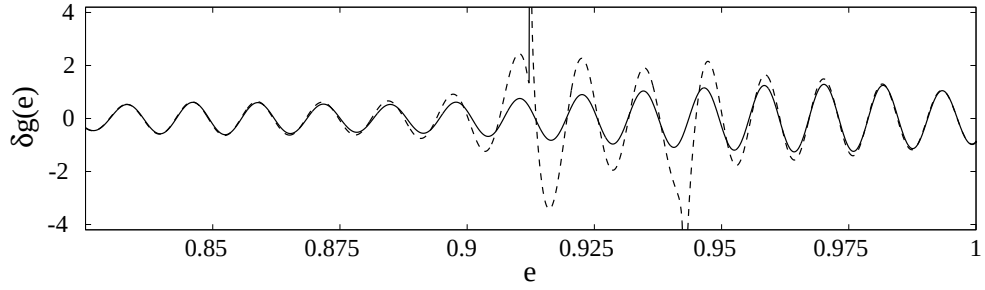

Figure 7.4: *Comparison between the result using Gutzwiller's trace formula (dashed) and the exact quantum result (solid) for* $\alpha = 0.0008$ *and* $\gamma = 0.5$.

For energies above that value the pitchfork bifurcations of the orbit A cause divergences of the semiclassical curve so that a uniform semiclassical approximation becomes necessary. Precisely, the two divergences follow each other so rapidly that between both of them the semiclassical curve does nowhere agree with the quantum curve. This indicates that both divergences cannot be treated separately using the existing uniform approximations for codimension-one bifurcations, but that a uniform approximation of codimension two for the full pitchfork bifurcation pair must be found instead.

7.5 Uniform approximation for a pair of pitchfork bifurcations

For the inclusion of the first two pitchfork bifurcations it is now possible to use the uniform approximation which was developed for the Hénon-Heiles system in section 5.3.4. A nice property of the double-well system is that it shows an infinite pitchfork-bifurcation cascade due to the barrier between both wells and at the same time has a real discrete quantum spectrum. In figure 7.5 the result of the uniform approximation including the isolated contribution of orbit B is compared to the exact quantum curve as well as to the result of summing the Gutzwiller contributions of the orbits A,B,R and L. One can see that the uniform approximation yields a finite result near the bifurcations and that it reaches the asymptotic limit far away from the bifurcations. It gives a semiclassical result which is in very good agreement with the quantum-mechanical result for a situation where Gutzwiller's trace formula as well as the uniform approximations for codimension one cannot be applied.

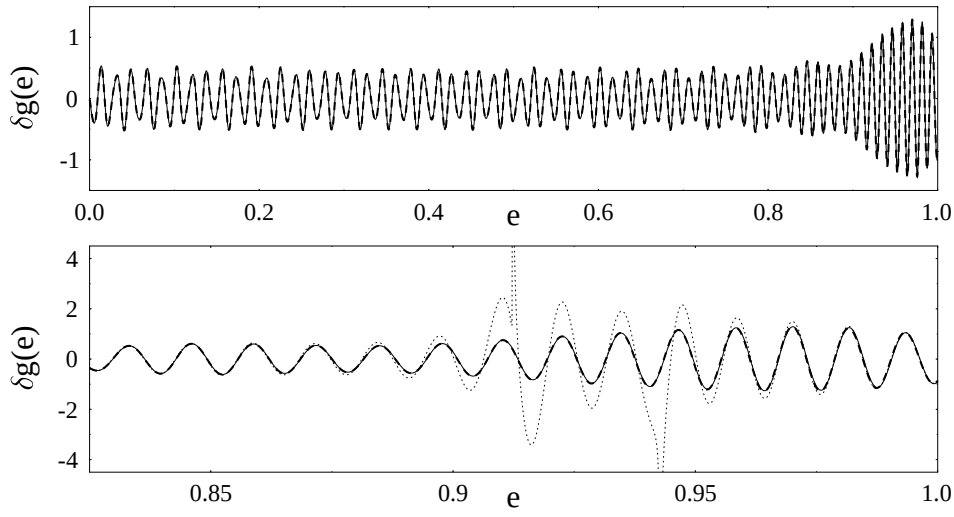

Figure 7.5: *Oscillating part of density of states in the double-well system (7.1). Solid line: exact quantum result obtained with* $\alpha = 0.0008$. *Dashed line: uniform approximation including isolated contribution of orbit B. Dotted line: sum of Gutzwiller contributions of orbits A,B,R and L, diverging at the two lowest bifurcations of the A orbit. (The other bifurcations, lying at* $e > 0.9998$, *cannot be seen at this resolution.) Coarse-graining by Gaussian convolution with energy width* $\gamma = 0.5$.

Chapter 8

Summary and outlook

In this thesis the spectral properties of quantum systems whose classical counterparts have mixed phase spaces were attempted to analyze in the semiclassical limit. The most important tool for a semiclassical description of a quantum-mechanical spectrum is the Gutzwiller trace formula for the density of states. Unfortunately it can not be applied to mixed systems directly, because of periodic-orbit bifurcations at which it becomes divergent. Similarly, the formula of Berry and Tabor for integrable systems fails in the case of torus bifurcations. Therefore it was tried to apply and develop extensions of the standard semiclassical approaches with an emphasis on mixed systems.

After having introduced the standard semiclassical trace formulae it was shown that they rely on stationary-phase approximations and that this is the reason why they fail at bifurcations of periodic orbits. More accurate higher expansions in the vicinity of periodic orbits in phase space, so-called normal forms, were introduced. Using these normal forms it became possible to improve the trace integration. Furthermore the idea behind uniform approximations was explained. They represent interpolations between the vicinity of a bifurcation and the region far away from it, where the standard approximations can be applied.

As a model of a non-trivial system of mixed type the two-dimensional Hénon-Heiles system was studied. Its classical dynamics was characterized in detail with an emphasis on the periodic orbits and their bifurcation scenarios. Afterwards the quantum-mechanical spectrum consisting of a discrete set of complex resonance energies was calculated. It was shown that the main contributions to the density of states come from the periodic orbits A, B and C. It was tried to semiclassically reproduce the quantum-mechanical coarse-grained level density using several uniform approximations. For the infinite bifurcation cascade of the librating orbit A, a new normal form could be introduced for the sequence of two pitchfork bifurcations. This led to a new uniform approximation which could improve the semiclassical result remarkably almost up to the saddle-point energy. For the evaluation of the uniform approximations it was necessary to calculate complex continuations of the periodic orbits, so-called ghost orbits. Finally the oscillating part of the density of states could also be introduced above the saddle-point energy where the classical phase space is non-compact. It was possible to nicely approximate it semiclassically using the shortest real periodic orbits only.

The Hénon-Heiles system was modified so that it looses its chaoticity by neglecting the non-separable term in the Hamiltonian. The classical dynamics of the resulting integrable system was studied and it was shown that it possesses an infinite cascade of bifurcations as well. Different to the non-integrable Hénon-Heiles case, whole new orbit families are created out of a single periodic orbit. For the occurring bifurcations a new analytical uniform approximation could be constructed which is in good agreement with the result of exact quantum calculations. Also the region above the saddle-point energy was studied quantum-mechanically as well as semiclassically. The agreement of the results again turned out to be very satisfying.

The new uniform approximation for a pair of pitchfork bifurcations was furthermore applied to a two-dimensional double-well potential with real discrete quantum spectrum and mixed classical phase space. Also in this case the agreement turned out to be very good.

Even though the extensions which were used in this study were shown to be successful, the problem of the semiclassical treatment of mixed systems is still far from being solved completely. First of all, today uniform approximations exist only for single generic bifurcations of codimension one as well as for sequences of two bifurcations corresponding to unfoldings of codimension-two bifurcations and now also, as was established in this thesis, for sequences of pitchfork bifurcations. The approximations work well only if no further bifurcation lies close by. Again the approximations should be valid if the actions of the periodic orbits involved in a further bifurcation differ by a large multiple of $\hbar$ from the actions of the periodic orbits participating in the bifurcations which are uniformized. If they get too close though, again new normal forms and uniform approximations have to be found. The corresponding trace integrals will become more complicated. This problem becomes especially apparent in the case of infinite cascades of bifurcations where the bifurcations lie infinitely close to each other accumulating at one parameter value. Even though the results of treating the cascades could be improved in this thesis, a full uniform treatment is still lacking.

An alternative approach to the problem is called the "method of replacement manifolds" which was developed by J. Vanicek and E. Heller [Van 01]. The method was applied to semiclassical wavefunctions whose phase functions are also related to the classical action functions. The idea is to replace the complicated phase functions which occur in mixed systems, at homoclinic tangles or infinite bifurcation cascades, by simpler smooth ones. However, as far as to the author's understanding, up to now the method could not be used to treat a full homoclinic tangle or an infinite bifurcation cascade uniformly. In fact the method appears similar to the normal form theory and it seems that one does not loose any degree of difficulty by preferring this method for the above scenarios.

A further approach was given by A. G. Magner et al. (see for example [Mag 01]). Instead of the full trace integral which led to the Gutzwiller trace formula, in this approach finite boundaries are used. The boundaries are derived from energy conservation. By performing the integration over a finite integral the divergence of the stationary-phase approximation, the actual reason for the bifurcation problem, can be avoided. The method is therefore called "improved stationary phase method" (ISPM). It works successfully for several integrable systems but could not be ap-

plied to mixed systems yet. Due to several similarities in the formalism as well as in the results between this approach and uniform approximations which are based on normal forms, a comparison between both approaches is in progress.

Finally it has to be mentioned that the results for the Hénon-Heiles cases in the energy range above the saddle-point energy indicate that the semiclassical formalism can accurately reproduce the quantum oscillations also in a general continuum region. This is of high importance because in this regime, phenomena of direct transmission, like conductance fluctuations, weak localization etc. can be studied. In this respect, the thesis can serve as a starting point to include now a transverse magnetic field and to examine the properties of a "Hénon-Heiles quantum dot".

Chapter 9

Appendix

9.1 Appendix A: On the calculation of the Maslov index

The only classical quantity appearing in Gutzwiller's trace formula (2.30) whose meaning is not commonly known is the Maslov index ν_ξ. It corresponds to a phase correction which is essential because it determines how the periodic-orbit contributions interfere.

It differs from the Morse index $\hat{\nu}_\xi$ which appears in the semiclassical Green function (2.20) due to the trace integration over the Green function which has to be calculated in order to obtain the density of states. The stationary-phase approximation of this integral leads to an additional contribution $\hat{\mu}_\xi$ so that

$$\nu_\xi = \hat{\nu}_\xi + \hat{\mu}_\xi. \tag{9.1}$$

While $\hat{\nu}_\xi$ and $\hat{\mu}_\xi$ for unstable periodic orbits may depend on the starting condition, ν_ξ is always a topological invariant [Cre 90].

Using methods described in the work cited above the Maslov index of a periodic orbit with $\mathrm{Tr}\widetilde{M} \neq 2$ in a two-dimensional system of the form Hamiltonian=kinetic energy+potential energy can be calculated as follows:
The Hamiltonian flow vector $\mathbf{v}(\gamma_0) = \dot{\gamma}_0 = (\dot{x}, \dot{y}, \dot{p}_x, \dot{p}_y)$ as well as the vector

$$\mathbf{e_0} = \begin{cases} (0,0,1,-\dot{x}/\dot{y}) & \text{if} \quad \dot{y}(0) \neq 0 \\ (0,0,-\dot{y}/\dot{x},1) & \text{if} \quad \dot{x}(0) \neq 0 \end{cases} \tag{9.2}$$

are propagated along one full periodic orbit according to

$$\mathbf{e}(t) = X(t)\,\mathbf{e}_0 \qquad \mathbf{v}(t) = X(t)\,\mathbf{v}, \tag{9.3}$$

using the matrizant $X(t)$ of (2.32). The Morse index $\hat{\nu}_\xi$ is then given as the number of zeros of $\det U(t)$ with

$$U(t) \equiv \begin{pmatrix} e_1(t) & v_1(t) \\ e_2(t) & v_2(t) \end{pmatrix}, \tag{9.4}$$

not counting the zero at the starting point. The matrix elements $e_i(t)$ and $v_i(t)$ are the i-th components of the vectors $\mathbf{e}(t)$ and $\mathbf{v}(t)$ respectively.
The index $\hat{\mu}_\xi$ is determined by the sign of the quantity

$$w = \frac{\mathrm{Tr}\widetilde{M}_\xi - 2}{b} \tag{9.5}$$

where b is given as upper right element of the stability matrix

$$\widetilde{M}_\xi = \begin{pmatrix} a & b \\ c & d \end{pmatrix}. \tag{9.6}$$

The rule is then

$$\hat{\mu}_\xi = \begin{cases} 0 & \text{if} \quad w > 0 \\ 1 & \text{if} \quad w < 0 \end{cases}. \tag{9.7}$$

The matrix element b is given by

$$b = \frac{\partial r_\perp \left(t = T\right)}{\partial p_\perp \left(t = 0\right)} \tag{9.8}$$

so that its sign can be found by numerically determining $\delta r_\perp \left(t = T\right)$ and $\delta p_\perp \left(t = 0\right)$ for a trajectory which is slightly differing from the original periodic orbit ξ in the initial velocity. For higher iterates of a periodic orbit the Maslov index is multiplied by the repetition number only in the case of an unstable orbit, but not for a stable orbit. The recipe above can also be generalized to higher dimensional systems [Cre 90].

Due to the fact that ν_ξ is a topological invariant related to the stability matrix of the periodic orbit, it can only change when the topology of its vicinity in phase space changes. This happens at periodic-orbit bifurcations. Consequently it should be possible to predict the changes of the Maslov indices from the higher order phase-space approximations of the trace integral at periodic-orbit bifurcations. This can in fact be done as was described in section 4.1 (see eq. (4.11)).

Furthermore in [Sug 00] it could be proven that in two-dimensional Hamiltonian systems with smooth potentials the Maslov index of an unstable periodic orbit is always even while for periodic orbits with $\mathrm{Tr}\widetilde{M}_\xi < 2$ it is always odd. A generalization of the calculation of the Maslov index to momentum-dependent potentials based on the path-integral formalism was recently given in [Plet 03].

9.2 Appendix B: How to calculate periodic orbits and their ghosts

As explained in section 3.2 the periodic orbits correspond to fixed points of the Poincaré map f of a Poincaré plane onto itself. In general a Poincaré map is not stroboscopic, i.e. if one step of the map takes the trajectory starting from γ_0 on the Poincaré plane the time T_0, another trajectory starting from $\gamma_1 \neq \gamma_0$ on the Poincaré plane will need the time T_1 with $T_1 \neq T_0$.
If γ_1 and γ_0 differ only by a small amount one can write in linear approximation

$$f(\gamma_1) = f(\gamma_0) + M(\gamma_1 - \gamma_0), \tag{9.9}$$

where M is the monodromy matrix of section 2.2 evaluated at the time T_0. Using (9.9) a first approximation of the wanted fixed point $\gamma_1 = f(\gamma_1)$ can now immediately be found as

$$\gamma_1 = \gamma_0 + (M - I)^{-1}(\gamma_0 - f(\gamma_0)). \tag{9.10}$$

This equation has to be modified so that the fixed point γ_1 again falls on the Poincaré plane. A system of equations which ensures that, keeping γ_1 on the energy shell, was given in [Cvi] and has the following form

$$\begin{pmatrix} I - M & \mathbf{v}(\gamma_0) & H'(\gamma_0) \\ \mathbf{a}^\dagger & 0 & 0 \\ (H'(\gamma_0))^\dagger & 0 & 0 \end{pmatrix} \begin{pmatrix} \gamma_1 - \gamma_0 \\ \delta t \\ \delta E \end{pmatrix} = \begin{pmatrix} f(\gamma_0) - \gamma_0 \\ 0 \\ 0 \end{pmatrix}. \tag{9.11}$$

Here $H' = \partial H / \partial \gamma$ indicates the derivative of the classical Hamiltonian function and $\mathbf{v}(\gamma_0) = \dot{\gamma}_0$ is the flow of the Hamiltonian equations of motion. The vector $\mathbf{a}$ is an arbitrary vector normal to the Poincaré plane. Even though (9.11) represents only a linear approximation, the recursive iteration of this $(2D+2)$-dimensional system of equations delivers rapid convergence against a real γ_1.

For the calculation of complex periodic ghost orbits, a complex continuation of the system (9.11) becomes necessary. The first step consists in complexifying the phase space only, while performing the integration along real time. One obtains equations of motion for real and imaginary parts and the system (9.11) becomes a $2\cdot(2D+2)$-dimensional one. It is then necessary to choose complex starting conditions which can be found easily in the vicinity of bifurcations, because they do not differ very much from the real starting values of the other periodic orbits involved in the bifurcation or the real periodic orbits whose complex continuation they represent. This procedure is enough to find ghost orbits which are created at pitchfork bifurcations, because in this case their stabilities, actions and orbit periods are always real. The pitchfork bifurcation represents an exception, though, so that in general the ghosts which are created at other types of bifurcations are characterized by complex classical quantities e.g. by complex orbit periods. Therefore it is necessary to not only generalize (9.11) to complex phase-space coordinates but also to complex times.

To the author's knowledge a practical recipe of how to accomplish that has not

been written down yet, so that here is now the possibility to introduce one possible method. First one chooses complex integration time steps as

$$\Delta t = dt \cdot e^{i\phi} \tag{9.12}$$

with real dt and ϕ and changes the equations of motion for the real and imaginary parts accordingly. After that one propagates the trajectory until the sign of $\Re e\,(x)$ changes at the complex time t_0. For that point $x_0 \equiv x\,(t_0)$ one has in general

$$\Re e\,(x_0) = 0 \qquad \Im m\,(x_0) \neq 0. \tag{9.13}$$

Every other complex time t_1 is then given by $t_1 = t_0 + \tau e^{i\theta}$ with real τ and θ. If t_0 and t_1 differ by only a small amount one gets in first approximation

$$x_1 \equiv x\left(t_0 + \tau e^{i\theta}\right) \approx x_0 + \left.\frac{dx}{dt}\right|_{t_0} \tau e^{i\theta} = x_0 + p_0 \tau e^{i\theta}, \tag{9.14}$$

with the definition $p_0 \equiv \dot{x}\,(t_0)$. One is looking now for that x_1 which lies on the

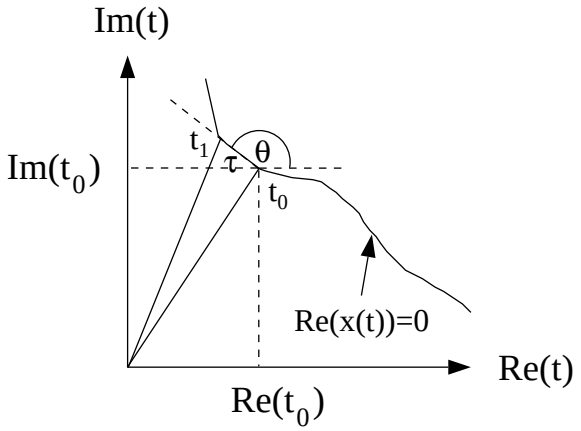

Figure 9.1: *Calculation of the complex time after which the Poincaré-plane is cut.*

Poincaré plane and therefore obeys the following two equations

$$\Re e\,(x_1) = \Re e\,(x_0) + \tau \cdot \Re e\left(p_0 e^{i\theta}\right) = 0 \tag{9.15}$$

$$\Im m\,(x_1) = \Im m\,(x_0) + \tau \cdot \Im m\left(p_0 e^{i\theta}\right) = 0. \tag{9.16}$$

From equations (9.15) it follows that

$$\theta = \arctan\left(\frac{\Re e\,(p_0)}{\Im m\,(p_0)}\right). \tag{9.17}$$

Equation (9.16) then determines τ as

$$\tau = -\frac{\Im m\,(x_0)}{\Im m\left(p_0 e^{i\theta}\right)}. \tag{9.18}$$

One has now obtained a better approximation to t_1 so that one recursively iterates this procedure until convergence in τ and θ is reached and a good approximation of γ_1 on the Poincaré plane is found. After that the next iteration of (9.11) can be performed. To sum up, the whole method of finding ghost orbits consists of two generalized Newton-algorithms which are running in parallel.

9.3 Appendix C: The complex rotation method

A resonant state is defined as a long-living state of a system which has enough energy to decay into two or more subsystems [Moi 98]. In the density of states they appear as Lorentzians of finite width Γ centered at the resonant energies E_R. Together these two quantities define the complex energy

$$E \equiv E_R - i\frac{\Gamma}{2}. \tag{9.19}$$

The width Γ of a Lorentzian is related to the lifetime τ of the resonant state by

$$\tau = \hbar/\Gamma. \tag{9.20}$$

For a potential which asymptotically vanishes ($V(r \to \infty) = 0$) the solution to the time-independent Schrödinger equation reads

$$\phi\left(r \to \infty\right) = A\left(k\right) e^{-ikr} + B\left(k\right) e^{+ikr}, \quad E = \frac{\left(\hbar k\right)^2}{2m} \tag{9.21}$$

corresponding to an incoming plane wave with amplitude $A(k)$ and an outgoing plane wave with amplitude $B(k)$. The scattering matrix is determined as $S\left(k\right) = B(k)/A(k)$ which actually amounts only to a scattering function if no angular momentum quantum numbers play a role. The resonances are known to correspond to the complex poles k_n of $S(k)$ in the fourth quarter of the complex plane ($\Re e(k_n) > 0, \Im m(k_n) < 0$) with the energies $E_n = \epsilon_n - i\Gamma_n/2$, where n counts the number of the resonance [Moi 98].
For these resonances one can write the Schrödinger equation as

$$\widehat{H}\phi_n^{res}\left(r\right) = \left(\epsilon_n - \frac{i}{2}\Gamma_n\right)\phi_n^{res}\left(r\right). \tag{9.22}$$

With $k_n \equiv \left|k_n\right| e^{i\phi_n}$ the resonant wavefunction asymptotically becomes

$$\begin{aligned} \phi_n^{res}\left(r \to \infty\right) &= A\left(k_n\right) e^{-i\left|k_n\right|e^{-i\phi_n}} + B\left(k_n\right) e^{+i\left|k_n\right|e^{-i\phi_n}} \\ &= A\left(k_n\right) e^{-ia_n r} e^{-b_n r} + B\left(k_n\right) e^{ia_n r} e^{b_n r} \end{aligned} \tag{9.23}$$

where the coefficients are given by

$$a_n = \frac{\sqrt{2m}}{\hbar}\left(\epsilon_n^2 + \left(\frac{\Gamma_n}{2}\right)^2\right)^{1/4} \cos\left(\phi_n\right) > 0 \tag{9.24}$$

$$b_n = a_n \cdot \tan\left(\phi_n\right) > 0 \tag{9.25}$$

$$\phi_n = \arctan\left(\frac{\Im m\left(k_n\right)}{\Re e\left(k_n\right)}\right) = \arctan\left(\sqrt{\frac{\sqrt{\epsilon_n^2 + \frac{\Gamma_n^2}{4}} - \epsilon_n}{\sqrt{\epsilon_n^2 + \frac{\Gamma_n^2}{4}} + \epsilon_n}}\right). \tag{9.26}$$

Asymptotically the first term in (9.23) vanishes while the second one diverges causing the whole resonance wavefunction to become divergent. Therefore one can say that the Hamiltonian $\widehat{H}$ in (9.22) is not Hermitian because $\phi_n^{res}(r)$ is not bounded, let alone square-integrable. Thus one can in fact obtain complex eigenvalues.
According to the *complex rotation method* [Moi 98, Bal 71, Sim 73, Rei 82] one should now apply the following similarity transformation:

$$\mathbf{r} \to \mathbf{r}e^{i\theta} \tag{9.27}$$

where the rotation angle θ can be chosen as real. Now the scaled resonance wavefunction asymptotically becomes

$$\hat{S}\phi^{res}(r \to \infty) = B(k_n)\, e^{+i|k_n|\exp(i(\theta-\phi_n))r} = B(k_n)\, e^{i\alpha_n r} e^{-\beta_n r} \tag{9.28}$$

with the coefficients

$$\begin{aligned} \alpha_n &= a_n(\cos\theta - \tan\phi_n \cdot \sin\theta) \\ \beta_n &= a_n(\sin\theta - \tan\phi_n \cdot \cos\theta) \\ \phi_n &= \arctan\left(\sqrt{\frac{\sqrt{\epsilon_n^2 + \frac{\Gamma_n^2}{4}} - \epsilon_n}{\sqrt{\epsilon_n^2 + \frac{\Gamma_n^2}{4}} + \epsilon_n}}\right). \end{aligned} \tag{9.29}$$

One can now see that (9.28) asymptotically goes to zero if θ becomes larger than the critical value

$$\theta_{crit} = \arctan\left(\sqrt{\frac{\sqrt{\epsilon_n^2 + \frac{\Gamma_n^2}{4}} - \epsilon_n}{\sqrt{\epsilon_n^2 + \frac{\Gamma_n^2}{4}} + \epsilon_n}}\right). \tag{9.30}$$

Thus $\hat{S}\phi_n^{res}(r)$ becomes a normalizable function which can be expanded in Hilbert space. The scaled Schrödinger equation reads

$$\left(\hat{S}\widehat{H}\hat{S}^{-1}\right)\left(\hat{S}\phi_n^{res}(r)\right) = \left(\epsilon_n - \frac{i}{2}\Gamma_n\right)\left(\hat{S}\phi_n^{res}(r)\right), \tag{9.31}$$

from which it becomes obvious that among the eigenvalues of the non-Hermitian operator $\left(\hat{S}\widehat{H}\hat{S}^{-1}\right)$ there are the exact scattering resonances $\left(\epsilon_n - \frac{i}{2}\Gamma_n\right)$.
Using the relation

$$\arctan\left(\frac{2z}{1-z^2}\right) = 2\arctan(z) \qquad |z| < 1 \tag{9.32}$$

one can show that $2\theta_{crit} = \arctan\left(\Gamma_n/2\epsilon_n\right)$.
About the spectrum of $\widehat{H}(\theta) \equiv \left(\hat{S}\widehat{H}\hat{S}^{-1}\right)$ it is generally known that [Rei 82] ...

- ... the bound-state eigenvalues of $\widehat{H}(0)$ are also eigenvalues of $\widehat{H}(\theta)$ for arbitrary θ,
- ... the continuum eigenvalues which are not corresponding to resonances are rotated into the lower half of the complex E-plane by an angle of -2θ (see Fig. 9.2),
- ... if θ becomes so large that one of the rotated continuum branches passes the position of a resonance pole, a new eigenvalue of $\widehat{H}(\theta)$ appears at the position of the pole,
- ... once a resonance eigenvalue is uncovered it stays at its position independent of a further variation of the rotation angle until θ becomes so large that another branch passes the pole. In this case the eigenvalue vanishes.

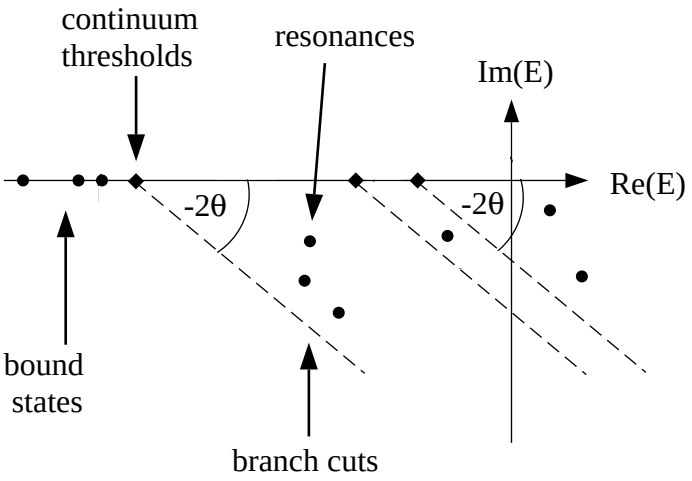

Figure 9.2: *Schematic view of the eigenvalue spectrum of a complex scaled Hamiltonian $\widehat{H}(\theta)$. The n-th resonance is uncovered for $2\theta \geq 2\phi_n = \arctan(\Gamma_n/2\epsilon_n)$.*

The transformed Hamiltonian can be expressed as

$$\widehat{H}(\theta) = \widehat{T}(\theta) + V(\theta). \tag{9.33}$$

Here $\widehat{T}(\theta = 0)$ and $V(\theta = 0)$ correspond to the operators of the kinetic energy and the potential part of the unscaled system respectively. To calculate the resonances one represents $\widehat{H}(\theta)$ in a suitably chosen finite basis set which yields the matrix $H(\theta)$ and the finite-dimensional eigenvalue problem

$$\{H(\theta) - E_n(\theta) I\} \phi_n(\theta) = 0. \tag{9.34}$$

If one chooses the basis set independent of θ, the eigenvalue problem (9.34) is solved by diagonalizing the non-Hermitian matrix

$$H(\theta) = T(0) \cdot e^{-2i\theta} + V(\theta), \tag{9.35}$$

where e.g. for polynomial potentials the dependence on θ appears in $V(\theta)$ as complex exponential factors of the unscaled terms of the potential. The matrix representations of these terms are real and independent of θ so that they have to be calculated only once.

The use of a finite basis set instead of an infinite one makes the resonance positions depend slightly on the angle θ. Nevertheless it is still possible to identify them because the $E(\theta)$-trajectories in the complex plane have stationary points exactly at the positions of the resonances. This has been proven as a consequence of the complex virial theorem [Yar 78, Yar 78b]. Practically one repeats the diagonalization for different values of θ to find that value of θ for which $E(\theta)$ is stationary in its real and imaginary part.

The complex rotation method was proven to work for dilatation analytical potentials i.e. for potentials which go to zero at infinity [Bal 71, Sim 73] including the many-body Coulomb and Yukawa potentials. However, the method could also successfully be applied to systems which are not vanishing at infinity like the potential of the Stark effect [Chu 77]. Even though to the author's knowledge there exists no proof of the validity of the method for arbitrary potentials, it could still be heuristically shown that for simple model systems which are not dilatational analytical the resulting resonance eigenvalues are isolated on the non-physical energy-sheets obeying a complex virial theorem [Yar 78].

9.4 Appendix D: The Strutinsky averaging procedure

In order to determine the average level density $\tilde{g}(E)$ of a quantum-mechanical discrete bound state energy spectrum $\{E_i\}$ in cases in which it cannot be approximated analytically using the Thomas-Fermi model, one can apply a numerical averaging procedure which was introduced by V. M. Strutinsky [Str 66]. The idea is to perform a Gaussian convolution of the density of states (2.4) which replaces each of its δ-functions by a Gaussian of width $\tilde{\gamma}$, where $\tilde{\gamma}$ should be at least of the order of the average level spacing. The value of $\tilde{\gamma}$ is thus much larger than the γ which is used for the coarse-graining of the density of states as described in section 5.2.2. Even though a Gaussian convolution reproduces the normalization of the δ-functions it does not yield its second and higher moments. This can be ensured though by multiplying each Gaussian by a Laguerre polynomial of integer order s so that the resulting function reproduces all moments of the δ-function up to order $(2s+1)$ [Bra 73]. The average part of the density of states for a discrete spectrum of bound states i is then approximated by

$$\tilde{g}(E) \approx \frac{1}{\tilde{\gamma}\sqrt{\pi}} \sum_i e^{-(E_i-E)^2/\tilde{\gamma}^2} L_s^{\frac{1}{2}} \left[\left(\frac{E_i - E}{\tilde{\gamma}} \right)^2 \right]. \tag{9.36}$$

The exact function $\tilde{g}(E)$ is unique so that there should exist one parameter $\tilde{\gamma}$ for (9.36) yielding the best approximation. This value can be found e.g. by plotting $\tilde{g}(E)$ of (9.36) in dependence of $\tilde{\gamma}$ with fixed E corresponding to the energy for which the density of states is supposed to be given. At the best $\tilde{\gamma}$-value the curves obey a plateau condition independent of the polynomial order s.

As was shown in [Ros 72] the Strutinsky averaged level density $\tilde{g}(E)$ is modified if the spectrum is not consisting of bound states only but if it contains also resonant states. The fluctuations in the resonant part of the spectrum are then related to the derivative of the scattering phase shift of the j-th partial wave with respect to the energy. The formula for the average density of states for such cases is given by

$$\begin{aligned} \tilde{g}(E) = & \frac{1}{\tilde{\gamma}\sqrt{\pi}} \sum_i e^{-(E-E_i)^2/\tilde{\gamma}^2} L_s^{\frac{1}{2}} \left[\left(\frac{E - E_i}{\tilde{\gamma}} \right)^2 \right] \\ & + \frac{1}{\tilde{\gamma}\sqrt{\pi}} \frac{1}{\pi} \sum_j (2j+1) \sum_{l=j-\frac{1}{2}}^{l=j+\frac{1}{2}} \int_{-\infty}^{\infty} \frac{d\delta_{l,j}(E')}{dE'} L_s^{\frac{1}{2}} \left[\left(\frac{E - E'}{\tilde{\gamma}} \right)^2 \right] e^{-\left(\frac{E-E'}{\tilde{\gamma}}\right)^2} dE'. \end{aligned} \tag{9.37}$$

Knowing the energy ϵ as well as the width Γ of a resonance one can write its phase shift δ as [Fey 64, Moi 98]

$$\delta = \arctan\left(\frac{\Gamma/2}{E - \epsilon} \right) + ... \tag{9.38}$$

The derivative of (9.38) with respect to the energy yields again a Lorentzian curve but without its normalization constant $1/\pi$. As final expression of the average part

of the density of states one arrives at

$$\begin{aligned}\tilde{g}(E) &= \frac{1}{\tilde{\gamma}\sqrt{\pi}}\sum_i e^{-(E-E_i)^2/\tilde{\gamma}^2} L_s^{\frac{1}{2}}\left[\left(\frac{E-E_i}{\tilde{\gamma}}\right)^2\right] \\ &\quad + \frac{1}{\tilde{\gamma}\sqrt{\pi}}\sum_j \int_{-\infty}^{\infty}\frac{1}{\pi}\frac{\Gamma_j/2}{\left(E'-E_j\right)^2+\frac{\Gamma_j^2}{4}} L_s^{\frac{1}{2}}\left[\left(\frac{E-E'}{\tilde{\gamma}}\right)^2\right] e^{-\left(\frac{E-E'}{\tilde{\gamma}}\right)^2} dE' \end{aligned} \quad (9.39)$$

which again must obey a plateau condition in $\tilde{\gamma}$. Here j indicates the number of the resonance. One obtains the same expression as for the bound-state case except that for the resonant states the δ-distributions are replaced by Lorentz distributions in the convolution integral. This is in agreement with (5.23) so that the introduction of (9.38) is justified.

For every Laguerre polynomial $L_s^{\frac{1}{2}}$, the integrals in (9.39) can be worked out analytically using

$$\int_{-\infty}^{\infty} dE' \frac{\left(\frac{E'-E}{\tilde{\gamma}}\right)^n e^{-\left(\frac{E'-E}{\tilde{\gamma}}\right)^2}}{\left(\frac{\Gamma_j}{2}\right)^2+\left(E_j-E'\right)^2} = \frac{2\pi(-)^n}{\Gamma_j}\Re e\left\{\frac{d^{\frac{n}{2}}}{d\lambda^{\frac{n}{2}}} w\left(\frac{\sqrt{\lambda}}{\tilde{\gamma}}\left(E_j+i\frac{\Gamma_j}{2}-E\right)\right)\right\}_{\lambda=1}, \quad (9.40)$$

with $n \in \mathbb{N}_0$. The case $s = 0$ corresponds to (5.24). The final expressions for $\tilde{g}_{\tilde{\gamma}}(E)$ up to the Laguerre polynomial of 10th order read:

s	$\left(\tilde{\gamma}\sqrt{\pi}\right)\cdot\tilde{g}_{\tilde{\gamma}}(E)$
0	$\sum_j \Re e\, w(z_j)$
1	$\sum_j \Re e\left[L_1^{\frac{1}{2}}\left(z_j^2\right)\cdot w(z_j)+\frac{iz_j}{\sqrt{\pi}}\right]$
2	$\sum_j \Re e\left[L_2^{\frac{1}{2}}\left(z_j^2\right)\cdot w(z_j)-\frac{iz_j}{4\sqrt{\pi}}\left(2z_j^2-9\right)\right]$
3	$\sum_j \Re e\left[L_3^{\frac{1}{2}}\left(z_j^2\right)\cdot w(z_j)+\frac{iz_j}{24\sqrt{\pi}}\left(4z_j^4-40z_j^2+87\right)\right]$
4	$\sum_j \Re e\left[L_4^{\frac{1}{2}}\left(z_j^2\right)\cdot w(z_j)-\frac{iz_j}{192\sqrt{\pi}}\left(8z_j^6-140z_j^4+690z_j^2-975\right)\right]$
5	$\sum_j \Re e\left[L_5^{\frac{1}{2}}\left(z_j^2\right)\cdot w(z_j)+\frac{iz_j}{1920\sqrt{\pi}}\left(16z_j^8-432z_j^6+3752z_j^4-12180z_j^2+12645\right)\right]$

with $w(z)$ given by (5.25) and $z_j \equiv \frac{1}{\tilde{\gamma}}\left(E-\left(E_j+i\frac{\Gamma_j}{2}\right)\right)$. Again the expressions have to be evaluated at a fixed energy in dependence of $\tilde{\gamma}$ in order to find a plateau which is independent of s.

Bibliography

[Abr 65] M. Abramowitz and I. A. Stegun, *Handbook of Mathematical Functions*, (Dover, New York, 1965).

[Ama 01] C. Amann, Ph.D. thesis, University of Regensburg, 2001.

[Arn 78] V. I. Arnold, *Mathematical Methods of Classical Mechanics*, (Springer, New York, 1978).

[Bal 71] E. Balslev and J. C. Combes, *Commun. Math. Phys.* **22** (1971) 280.

[Bar 03] T. Bartsch, private communication, Novosibirsk 2003.

[Ber 72] M. V. Berry and K. E. Mount, *Rep. Prog. Phys.* **35** (1972) 315.

[Ber 77] M. V. Berry, *Phil. Trans. R. Soc.* **287** (1977) 237.

[Ber 89] M. V. Berry, *Proc. R. Soc. Lond. A* **422** (1989) 7.

[Bha 97] R. K. Bhaduri, Avinash Khare, S. M. Reimann and E. L. Tomusiak, *Ann. Phys.* **254** (1997) 25.

[Boa 95] P. A. Boasman and J. P. Keating, *Proc. R. Soc. Lond. A* **449** (1995) 629.

[Bou 81] T. C. Bountis, *Physica* **3D** (1981) 577.

[Bra 73] M. Brack, Ph.D. thesis, University of Basel, 1973.

[Bra 97] M. Brack, J. Blaschke, S. C. Creagh, A. G. Magner, P. Meier and S. M. Reimann, *Z. Phys.* **D 40**, 276 (1997); L. Christensson, H. Linke, P. Omling, P. E. Lindelof, I. V. Zozoulenko and K.-F. Berggren, *Phys. Rev. B* **57** (1998) 19.

[Bra 98] M. Brack, S. C. Creagh and J. Law, *Phys. Rev. A* **57** (1998) 788.

[Bra 99] M. Brack, P. Meier and K. Tanaka, *J. Phys. A: Math. Gen.* **32** (1999) 331.

[Bra 01] M. Brack, *Foundations of Physics* **31** (2001) 209.

[Bra 01b] M. Brack, Private communication, Regensburg 2001.

[Bra 03] M. Brack and R. K. Bhaduri, *Semiclassical Physics* (Westview Press, Boulder, 2003).

[Bri 26] L. Brillouin, *J. Phys. Radium* **7** (1926) 353.

[Bru] A. D. Bruno, *Research on the restricted three body problem. I: Periodic solutions of a Hamiltonian system*, preprint 18 (Moscow: Inst. Prikl. Mat. Akad. Nauk SSSR.) (1972) (in Russian).

[Bru 70] A. D. Bruno *Math. USSR Sbornik* **12** (1970) 271.

[Chu 77] S-I. Chu and W.P. Reinhardt, *Phys. Rev. Lett.* **39** (1977) 1195.

[Chu 79] R. C. Churchill, G. Pecelli and D. L. Rod in *Stochastic Behavior in Classical and Quantum Hamiltonian Systems*, (Springer, New York, 1979).

[Cre 90] S. C. Creagh, J. M. Robbins and R. G. Littlejohn, *Phys. Rev. A* **42** (1990) 1907.

[Cre 96] S. C. Creagh, *Ann. Phys.* **248** (1996) 60.

[Cvi] P. Cvitanovich et al. http://www.nbi.dk/ChaosBook.

[Dav 92] K. T. R. Davies, T. E. Huston and M. Baranger, *Chaos* **2** (1992) 215.

[Efs 04] K. Efstathiou and D. A. Sadovskií, *Nonlinearity* 17 (2004) 415.

[Ein 17] A. Einstein, *Verh. Dtsch. Phys. Ges.* **19** (1917) 82.

[Eke 90] I. Ekeland, *Convexity Methods in Hamiltonian Mechanics, Ergebnisse der Mathematik und ihrer Grenzgebiete 3. Folge Bd. 19* (Springer, 1990).

[Fei 78] M. J. Feigenbaum, *J. Stat. Phys.* **19** (1978) 25; M. J. Feigenbaum, *Physica* **7 D** (1983) 16.

[Fey 64] R. Feynman, *The Feynman Lectures on Physics vol. II*, (Addison-Wesley, 1964).

[Gut 71] M. C. Gutzwiller, *J. Math. Phys.* **12** (1971) 343.

[Gut 90] M. C. Gutzwiller, *Chaos in Classical and Quantum Mechanics* (Springer, New York, 1990).

[Hén 64] M. Hénon and C. Heiles, *Astr. J* **69** (1964) 73.

[Hol 88] A. Holle, J. Main, G. Wiebusch, H. Rottke and K. H. Welge, *Phys. Rev. Lett.* **61** (1988) 161.

[Hüp 95] B. Hüppner, J. Main and G. Wunner, *Phys. Rev. Lett.* **74** (1995) 2650.

[Jel 87] R. J. Jellito, *Theoretische Physik Band 2*, (AULA, Wiesbaden, 1987).

[Kai 00] J. Kaidel, Diploma thesis, University of Regensburg, 2000.

[Kai 03] J. Kaidel and M. Brack, nlin.CD/0308026.

[Kai 03b] J. Kaidel, P. Winkler and M. Brack, nlin.CD/0312022.

[Kel 58] J. B. Keller, *Ann. Phys.* (N.Y.) **4**, (1958) 180.

[Lit 90] R. G. Littlejohn, *J. Math. Phys.* **31** (1990) 2952.

[Mag 01] A. G. Magner, S. N. Fedotkin, K. Arita, K. Matsuyanagi and M. Brack, *Phys. Rev. E* **63** (2001) 065201(R).

[Meh 91] M. L. Mehta, *Random Matrices and the Statistical Theory of Energy Levels*, (Academic Press, San Diego, 1991).

[Mey 70] K. R. Meyer, *Trans. Am. Math. Soc.*, **149** (1970) 95.

[Moi 98] N. Moiseyev, *Phys. Rep.* **302** (1998) 211.

[Nol 92] W. Nolting, *Grundkurs: Theoretische Physik Band 5*, (Zimmermann-Neufang, Ulmen, 1992).

[Ozo 87] A. M. Ozorio de Almeida and J. H. Hannay, *J. Phys. A: Math. Gen.* **20** (1987) 5873.

[Ozo 88] A. M. Ozorio de Almeida, *Hamiltonian Systems: Chaos and Quantization* (Cambridge University Press, Cambridge, 1988).

[Plet 03] M. Pletyukhov and M. Brack, *J. Phys. A: Math. Gen.* **36** (2003) 9449.

[Pom 74] N. Pomphrey, *J. Phys. B* **7** (1974) 1909.

[Pos 78] T. Poston and I. N. Stewart, *Catastrophe Theory and its Applications* (Pitman, London, 1978).

[Rao 01] J. Rao, D. Delande and K.T. Taylor, *J. Phys. B.* **34** (2001) 391.

[Rei 82] W. P. Reinhardt, *Ann. Rev. Phys. Chem.* **1982**, 223.

[Ric 01] A. Richter, *Physikalische Blätter* **57** (2001) Nr. 7/8.

[Ros 72] C. K. Ross and R. K. Bhaduri, *Nucl. Phys.* **A188** (1972) 566.

[Sch 97a] H. Schomerus, Ph.D thesis, University of Essen, 1997.

[Sch 97b] H. Schomerus, *Europhys. Lett.* **38** (1997) 423.

[Sch 97c] H. Schomerus and M. Sieber, *J. Phys. A: Math. Gen.* **30** (1997) 4537.

[Sch 98] H. Schomerus, *J. Phys. A: Math. Gen.* **31** (1998) 4167.

[Sch 94] H. G. Schuster, *Deterministic Chaos*, (VCH, Weinheim, 1994).

[Sie 96] M. Sieber, *J. Phys. A: Math. Gen.* **29** (1996) 4715.

[Sie 98a] M. Sieber, *Semiclassics in two-dimensional systems, Workshop University of Regensburg* (1998).

[Sie 98b] M. Sieber and H. Schomerus, *J. Phys. A: Math. Gen.* **31** (1998) 165.

[Sim 73] B. Simon, *Ann. Math.* **97** (1973) 247.

[Str 66] V. M. Strutinsky, *Sov. J. Nucl. Phys.* **3** (1966) 449.

[Str 67] V. M. Strutinsky, *Nucl. Phys.* **A95** (1967) 420.

[Str 68] V. M. Strutinsky, *Nucl. Phys.* **A122** (1968) 1.

[Sug 00] A. Sugita, *Phys. Lett. A* **266** (2000) 321; *Ann. Phys.* (N. Y.) **288** (2001) 277.

[The 99] H. Then, Diploma thesis, University of Ulm, 1999.

[Tho 75] R. Thom, *Structural Stability and Morphogenesis* (Benjamin, Reading, Mass., 1975).

[Tic 48] E. C. Tichmarsh: *Introduction to the theory of Fourier Integrals* (Clarendon Press, Oxford, 1948).

[Tom 95] S. Tomsovic, M. Grinberg and D. Ullmo, *Phys. Rev. Lett.* **75** (1995) 4346.

[Ull 96] D. Ullmo, S. Tomsovic and M. Grinberg, *Phys. Rev. E* **54** (1996) 136.

[Yar 78] R. Yaris, J. Bendler and R. A. Lovett, *Phys. Rev. A* **18** (1978) 1816.

[Yar 78b] R. Yaris and P. Winkler, *J. Phys. B.* **11** (1978) 1475.

[Van 01] J. Vanicek and E. J. Heller, *Phys. Rev. E* **64** (2001) 026215.

[Vie 96] W. M. Vieira and A. M. Ozorio de Almeida, *Physica D* **90** (1996) 9.

[Wai 81] B. A. Waite and W. H. Miller, J. Chem. Phys. **74** (1981) 7.

[Win 92] D. Wintgen, K. Richter and G. Tanner, *Chaos* **2** (1992) 19.

Dank

Für das Zustandekommen dieser Dissertation bedanke ich mich herzlichst bei:

- Prof. Dr. Matthias Brack für die optimale Betreuung und eine Zusammenarbeit, die intensiver nicht hätte sein können. Ausserdem für seine Offenheit für neue Ansichten, nicht nur auf physikalischer Ebene.
- Andreas Jung, für die vielen Diskussionen, Kaffees, Pizzen, ...
  Insbesondere auch dafür, daß er mich auf das Programm **matlab** aufmerksam machte ohne welches ich heute noch rumgurken würde.
- Dr. Peter Schlagheck dafür, dass er sich immer Zeit nahm mit mir über Geister und ähnlich Komplexem auf konstruktive Weise nachzudenken.
- Dr. Thomas Bartsch und Dr. Jörg Main, die mir viele Aspekte der Uniformen Näherungen in einem neuen Licht erscheinen liessen.
- Dr. Christian Amann, welcher mich zu Beginn meiner Semiklassik-Zeit in die Problematik einführte.
- Dr. Mikhail Pletyukhov für die Beantwortung etlicher, mathematischer Fragen.
- Prof. Peter Winkler (University of Reno, Nevada), Dr. Henning Schomerus (Max-Planck-Institut für die Physik komplexer Systeme, Dresden), für die konstruktive Zusammenarbeit und angenehme Gastfreundschaft während meiner Besuche.
- Bei der DFG welche diese Doktorarbeit im Rahmen des Graduiertenkollegs GRK 638 “Nichlinearität und Nichtgleichgewicht in kondensierter Materie” finanziell unterstützte. Innerhalb des Graduiertenkollegs möchte ich mich besonders für die freundliche Unterstützung bei Prof. Karl F. Renk, Ulla Turba und Prof. Klaus Richter bedanken.
- Bei den vielen Wegbegleitern während meiner Promotionszeit, vorallem Dr. Benedikt Lehmann-Dronke, Dr. Holger Hehl, Juan Diego Urbina, Michael Berner, Wolfgang Feil, ...
- Bei meinen Bad Kissinger Freunden, Uli, Frank und Till für die vielen spassigen Treffen und erfrischenden Email-Konversationen.
- Vorallem aber bei meinen Eltern und meiner Familie.

"In Nature's infinite book of secrecy, a little I can read."
(Soothsayer, Antony and Cleopatra)